Experimental study of cluster effects in binary and ternary decays of low excited actinides

by

Vusi David Malaza

Dissertation presented in partial fulfilment of the requirements for the degree of

Doctor of Philosophy

(Physics)

at the University of Stellenbosch

Supervisors:
Prof N.M. Mkaza
Prof S.M. Wyngaardt

Co-Supervisors:
Prof Yu V. Pyatkov
Dr D.V. Kamanin

December 2018

Declaration

By submitting this dissertation electronically, I declare that the entirety of the work contained therein is my own, original work, that I am the sole author thereof (save to the extent explicitly otherwise stated), that reproduction and publication thereof by Stellenbosch University will not infringe any third party rights and that I have not previously in its entirety or in part submitted it for obtaining any qualification.

December 2018

Abstract

The experimental study of rare decay modes of ternary fission performed by the FOBOS group at the Joint Institute for Nuclear Research (JINR) in Dubna, Russia, revealed a new ternary decay mode of low excited heavy nuclei. This new ternary decay mode is referred to as Collinear Cluster Tri-partition (CCT). The distinct features of the CCT include the centre of mass of one of the decay fragments and the centre of mass of the two other decay fragments moving in opposite directions relative to each other. Another experimental signature for identifying the CCT is that one of the three decay fragments have a magic nucleon number configuration.

The first experimental observation of the CCT was revealed in a study of spontaneous decay of ^{252}Cf performed using a so-called modified-FOBOS spectrometer facility installed at the JINR. This phenomenon was observed using the missing-mass method, where two fragments were detected, the third one being missing. The missing mass was accounted for by the difference in the masses of the detected fragments and the mass of the initial nucleus. The CCT manifested itself through a bump in the mass-mass distribution of fission fragments from the decay of ^{252}Cf. Further confirmation of the CCT using the same missing-mass method was obtained from the reaction $^{235}U(n_{th}, f)$ where an experiment was performed using a spectrometer referred to as mini-FOBOS. This experiment made use of a neutron beam delivered by the IBR-2 Reactor from the Frank Laboratory of Neutron Physics at the JINR. In both experiments the CCT was revealed as a bump in the mass-mass distribution which was linked to the magic nickel cluster. The bump was referred to as the Ni-bump.

It quickly became clear from the early experiments that a direct detection of all the decay products of the CCT will be a more convincing experimental approach. In an effort to detect all decay products, a new

double arm time-of-flight (TOF) spectrometer, based on a mosaic detection system, aimed at detecting all the CCT products was designed and is presented in this work. This spectrometer is referred to as COMETA (Correlation Mosaic Energy – Time Array). The COMETA spectrometer registers the energy and time signals of heavy ions using mosaics of PIN diode detectors in each arm.

This new spectrometer required a new parametrization procedure to calculate the masses of the registered fragments of the CCT. The parametrization procedure also forms part of this work. This procedure takes into consideration the well-known experimental challenges when registering heavy ions using semiconductor-based detectors such as PIN diodes. The first challenge is the so-called pulse-height defect, which is manifested when registering the energy of heavy ions. The other challenge is the so-called plasma delay, which occurs when registering the time signal for the heavy ions.

To test this procedure a special experimental setup called Light Ion Spectrometer for South Africa (LIS-SA) was put together. In this work, an experiment performed with the LIS-SA setup, that tested this procedure in the mass reconstruction of the fission fragments of the CCT, is also presented.

The results from the COMETA spectrometer that confirmed the existence of the CCT are also presented. In the mass-mass distribution of fission fragments from the COMETA, the CCT reveals itself as rectangular structures bounded by known deformed magic clusters such as ^{108}Mo, ^{98}Sr and also magic clusters such as ^{128}Sn. These structures appeared in the same vicinity where the Ni-bump was observed earlier. Further analysis of these structures revealed that they are linked to the Ni-bump.

This work did not only provide a more convincing approach in the study of multi-body decay of low excited nuclei (the CCT), the existence of the CCT phenomenon was successfully confirmed through the direct

detection of all the decay products of the CCT. The CCT has been confirmed as a decay process that takes place as a two-stage break-up of the initial three body chain-like nuclear configuration with an elongated central cluster.

Samevatting

Die eksperimentele studie van rare verval modus van drieledige splyting wat uitgevoer is deur die FOBOS groep by die Joint Institute for Nuclear Research (JINR) in Dubna, Rusland, wys ’n nuwe drieledige verval mode uit vir lae opgewekte swaar kerne. Hierdie nuwe drieledige verval mode word verwys na as ’n ko-liniêere bondel Tri-partisie (CCT). Die onderskeie kenmerke van die CCT sluit in die massa middelpunte van een van die verval fragmente wat in ’n teenoorgestelde rigting beweeg, relatief tot die massa middelpunt van die twee ander verval fragmente. ’n Ander eksperimentele kenmerk wat die CCT uitwys is dat een van die verval fragmente ‘n voorkeurgetal (Magic number) konfigurasie het.

Die eerste eksperimentele waarneming van die CCT het te voorskyn gekom in ’n studie van spontane verval van ^{252}Cf en is uitgevoer deur gebruik te maak van die sogenaamde gemodifiseerde-FOBOS spektrometer wat installeer is by die JINR. Hierdie verskynsel was waargeneem onder die verlore massa metode, waar twee fragmente waargeneem was, en die derde deeltjie die verlore deeltjie is. Hierdie verlore massa was bepaal deur die verskil tussen die massas van die waargenome fragmente en massa van die oorspronklike kern te bereken. Die CCT word deur ’n piek in die massa-massa distribusie van die splytings fragmente van die verval van ^{252}Cf gemanifesteer. Verdere bevestiging van die CCT onder dieselfde verlore massa metode was verkry vanaf die reaksie $^{235}U(n_{\mathrm{th}},f)$ waar ’n eksperiment gedoen is met ’n spektrometer wat verwys word na as mini-FOBOS. Hierdie eksperiment maak gebruik van ’n neutronbundel wat verskaf word deur die IBR-2 Reaktor by die Frank Laboratorium vir Neutron Fisika by die JINR. In beide eksperimente was die CCT uitgelig as ’n piek in die massa-massa distribusie wat gekoppel is aan die voorkeur (“magic”) nikkel bondel. Die piek word na verwys as die *Ni-piek*.

Dit het vinnig duidelik geword vanaf vroeër eksperimente dat ’n direkte waarneming van al die vervalprodukte van die CCT, ’n meer geloofwaardige eksperimentele benadering sal wees. In ’n poging om al die verval produkte waar te neem, was ’n dubbele arm vlugtyd (TOF) spektrometer, gebaseer op ’n mosaïek detektor sisteem, wat gefokus is op die waarneming van al die CCT produkte, ontwerp en word dit in hierdie werk voorgelê. Hierdie spektrometer word verwys na as die COMETA (Correlation Mosaic Energy – Time Array). Die COMETA registreer die energie en tydseine van swaar ione deur gebruik te maak van ’n mosaïek PIN diode detektore in elke arm.

Hierdie nuwe spektrometer benodig ’n nuwe parameteriserings prosedure om die massa van die geregistreerde fragmente van die CCT te bereken. Die parameteriserings prosedure vorm ook deel van hierdie tesis. Hierdie prosedure neem in ag die welbekende eksperimentele uitdagings wanneer die swaar ione geregistreer word deur gebruik te maak van semigeleier-gebaseerde detektore soos die PIN diodes. Hierdie uitdagings is die sogenaamde pulshoogte afwyking wat ’n negatiewe effekt het wanneer die energie van die swaar ione geregistreer word en ook die plasmavertraging wanneer die tydsein vir swaar ione geregistreer word.

Om hierdie prosedure te toets is ’n spesiale eksperimentele opstelling genoem die Ligte Ion Spektrometer vir Suid Afrika (LIS-SA) aanmekaar gesit. In hierdie werk is ’n eksperiment uitgevoer met die LIS-SA opstelling, wat die prosedure toets vir die massa her-konstruksie van die splytsingsfragmente van die CCT.

Die resultate van die COMETA spektrometer wat bevestig dat die CCT teenwoordig is word ook voorgelê. In die massa-massa distribusie van die splytings fragmente vanaf die COMETA eksperiment, word die CCT geopenbaar as ’n reghoekige struktuur wat begrens word deur die bekende vervormde voorkeurbondel kerne soos ^{123}Mo, ^{63}Sr asook voorkeurbondel kerne soos ^{128}Sn. Hierdie strukture kom te voorskyn in

dieselfde gebied waar die *Ni-piek* waargeneem was. Verdere analiese van hierdie strukture wys uit dat hulle gekoppel is aan die *Ni-piek*.

Nie net gee hierdie werk ’n meer gerieflike benadering tot die studie van veeldeeltjie verval van lae opgewekte kerne (die CCT) nie, maar die bestaan van die CCT verskynsel was suksesvol bevestig deur die direkte waarneming van al die verval produkte van die CCT. Die CCT was ook hier bevestig as ’n verval proses wat plaasvind in ’n tweestap opbreek van die oorspronklike drie deeltjie ketting kern konfigurasie met ’n verlengde sentrale bondel.

Acknowledgements

Firstly I would like to express my sincere gratitude to my supervisors:

- Prof N.M. Mkaza – for the continued support and guidance throughout my entire academic career. As far as I could remember the relationship goes back to when I was an undergraduate and you have overseen my entire academic development from junior degrees to PhD. Thank you for your support, mentorship and continued believing in me, not only academically but as a young man growing up, thanks for your guidance.
- Prof S.M. Wyngaardt – for your patience, understanding and support you gave me throughout my PhD. Your guidance helped me especially during the time for the research and writing up of this dissertation. Mostly thank you for believing in me and providing the opportunity and the best relaxed environment for me to finish my PhD.

A special thanks goes to my supervisors from the Joint Institute for Nuclear Research in Dubna, Russia.

- Dr D.V. Kamanin - thank you for allowing me to be part of such a wonderful team of well experienced scientists. Thank you for your support and mostly for all the opportunities you have provided me in and around the JINR. Thank you for the support financially and for always being there for me when I am in Russia.
- Prof Yu V. Pyatkov – thank you for all your guidance, especially in terms of the research-related work. Thank you for sharing your immense knowledge and continued assistance throughout my project. Most of all thank you for believing in me and giving me the opportunity to be one of your products.

I would also like to acknowledge my colleagues from the Flerov Laboratory for Nuclear Reactions at the JINR: A.A. Aleksandrov, I.A. Aleksandrova, Z. I. Goryainova, E.A. Kuznetsova, O.V. Strekalovsky, A.O. Strekalovsky , V.E. Zhuchko and others that I might have missed to mention. A special thanks to Sasha (A.O. Strekalovsky) for not only being my colleague but also a good friend and a brother when I am in Russia.

Let me acknowledge the Department of Science and Technology, the National Research Foundation, SA-JINR Collaboration for the financial and administration support for this project.

To the Department of Physics, Faculty of Science at Stellenbosch University and the entire staff, colleagues and friends, thank you for the support and for the opportunity for me to undertake my studies.

To the Dean of Faculty of Military Science at Stellenbosch University, Prof M.S. Tshehla for the motivation and support for my studies.

To my colleagues from the Department of Physics (Mil) for assisting with the work load and for the support from the School of Science and Technology under the leadership of Cdr (Dr) J. Bezuidenhout.

To my friends and colleagues, thank you for the support.

To my daughter, Olebogeng, thanks for being my best motivator and a disturbance at the same time. I love you baby girl.

To God, am humbled.

List of Publications

Some of the results presented in this work have been reported in different conferences and published in several scientific papers. Conference presentations and publications that constitutes some of the results of this work are listed below:

1. *S. Yamaletdinov*,
   "STUDIES OF EXOTIC DECAY MODES IN FISSION OF HEAVY ELEMENTS,"
   University of Jyväskylä, Jyväskylä, Finland, 2007
2. *D. V. Kamanin and Y. V. Pyatkov*,
   "Clusterization in ternary fission,"
   Clusters in Nuclei Volume 3 B. Christian, Ed., Springer, 2014, pp. 2-69.
3. *V. D. Malaza*,
   "Multi-detector Registration System for the Study of Multi-body Decay of Heavy Body Nuclei."
   Master's thesis, Stellenbosch University, Stellenbosch, 2012
4. *D.V. Kamanin, Yu.V. Pyatkov, W. von Oertzen, A. A. Alexandrov, I. A. Alexandrova, O. V. Falomkina, N. Jacobs, N. A. Kondratjev, Yu. N. Kopatch, E. A. Kuznetsova, Yu. E. Lavrova,* ***V. Malaza****, S. Mullins, A. N. Tyukavkin, W. Trzaska and V. E. Zhuchko*
   "Multi-cluster decays of heavy nuclei - studies in progress"
   Proceedings of the 2nd SOUTH AFRICA - JINR Symposium "Models and Methods in Few- and Many-Body Systems", Dubna, Russia, 8-10 September 2010. Dubna 2010, pp. 179-193.
5. *D.V. Kamanin, Yu.V. Pyatkov, A.A. Alexandrov, I.A. Alexandrova, N. Jacobs, N.A. Kondratyev, E.A. Kuznetsova,* ***V. Malaza****, O.V. Strekalovsky,*
   "Status of studies of collinear cluster tri-partition of ^{252}Cf (sf)"

Presented at the 7th International Conference on Dynamical Aspects of Nuclear Fission "DANF2011", Smolenice Castle, Slovak Republic, 17-21 October 2011.

6. *D.V. Kamanin, Yu.V. Pyatkov, N.A. Kondratyev, V.E. Zhuchko, A.A. Alexandrov, I.A. Alexandrova, N.M. Jacobs, E.A. Kuznetsova,* ***V. Malaza****, S.I. Mulgin, O.V. Strekalovsky*
"Mosaic time-of-flight COMETA spectrometer for studying of multi-body decays of heavy nuclei"
Presented at the 7th International Conference on Dynamical Aspects of Nuclear Fission "DANF2011", Smolenice Castle, Slovak Republic, 17-21 October 2011.

7. *D.V. Kamanin, Yu.V. Pyatkov, A.A. Alexandrov, I.A. Alexandrova, S.B. Borzakov, N. Jacobs, N.A. Kondratyev, Yu.N. Kopach, E.A. Kuznetsova,* ***V. Malaza****, Ts. Panteleev, D. Pham Minh, V.E. Zhuchko*
"Collinear cluster tri-partition of ^{252}Cf (sf) – evidences in neutron gated data"
Proceedings of the 18th International Seminar on Interaction of Neutrons with Nuclei: "Neutron Spectroscopy, Nuclear Structure, Related Topics". Dubna, 26-29 May 2010. Dubna 2011, pp. 102-107.

8. *Yu.V. Pyatkov, D.V. Kamanin, A.A. Aleksandrov, I.A. Aleksandrova, N.A. Kondratyev, E.A. Kuznetsova, N. Jacobs,* ***V. Malaza****, D. Pham Minh, V.E. Zhuchko*
"Presumable scenario of one of the collinear cluster tri-partition modes"
Proceedings of the International Workshop on State of the Art in Nuclear Cluster Physics "SOTANCP 2010" Brussels, Belgium, 25–28 May 2010. Int. Journal of Modern Physics E. 2011. V. 20, No. 4. pp. 1008-1011.

9. *Yu.V. Pyatkov, D.V. Kamanin, W. von Oertzen, A.A. Alexandrov, I.A. Alexandrova, O.V. Falomkina, N. Jacobs, N.A. Kondratjev,*

E.A. Kuznetsova, Yu.E. Lavrova, ***V. Malaza****, Yu.V. Ryabov, O.V. Strekalovsky, A.N. Tyukavkin and V.E. Zhuchko*

"The collinear cluster tri-partition (CCT) of ^{252}Cf (sf): New aspects from neutron gated data"

Eur. Phys. J. A: Hadrons and Nuclei. 2012. V. 48, No. 7. pp. 94–109.

10. *D.V. Kamanin, Yu.V. Pyatkov, A.A. Alexandrov, I.A. Alexandrova, N. Jacobs, N.A. Kondratyev, E.A. Kuznetsova,* ***V. Malaza****, Yu.V. Ryabov, O.V. Strekalovsky, V.E. Zhuchko*

"Summary of experimental results on collinear cluster tri-partition studies"

Presented at the 20th International Seminar on Interaction of Neutrons with Nuclei, Alushta, Ukraine, 21-26 May 2012.

11. *D.V. Kamanin, Yu.V. Pyatkov, A.A. Alexandrov, I.A. Alexandrova, N. Jacobs, N.A. Kondratyev, E.A. Kuznetsova,* ***V. Malaza****, O.V. Strekalovsky, V.E. Zhuchko*

"Collinear Cluster Tri-partition: current status of studies"

Proceedings of the 19th International Seminar on Interaction of Neutrons with Nuclei, Dubna, Russia, 25-28 May 2011. Dubna 2012, pp. 48-55.

12. *D.V. Kamanin, Yu.V. Pyatkov,* ***V. Malaza****, A.A. Alexandrov, I.A. Alexandrova, N. Jacobs, N.A. Kondratyev, E.A. Kuznetsova, O.V. Strekalovsky, A.O. Strekalovsky, V.E. Zhuchko*

"Study of rare modes of "Collinear Cluster Tri-partition" of ^{252}Cf (sf)"

Proceedings of the 19th International Seminar on Interaction of Neutrons with Nuclei, Dubna, Russia, 25-28 May 2011. Dubna, 2012, pp. 56-61.

13. *D.V. Kamanin, Yu. V. Pyatkov, W. von Oertzen A.A. Alexandrov, I.A. Alexandrova, O.V. Falomkina, N. Jacobs, N.A. Kondratjev, E.A. Kuznetsova, Yu. E. Lavrova,* ***V. Malaza****, O.V. Strekalovsky,*

A.N. Tyukavkin, and V.E. Zhuchko

"Collinear cluster tri-partition as a probe of clustering in heavy nuclei"

Exciting Interdisciplinary Physics. FIAS Interdisciplinary Science Series. 2013. pp.119-128.

14. *Yu.V. Pyatkov, D.V. Kamanin, A.A. Alexandrov, I.A. Alexandrova, N. Jacobs, N.A. Kondratyev, E.A. Kuznetsova,* ***V. Malaza****, Yu.V. Ryabov, A.O. Strekalovsky, O.V. Strekalovsky, V.E. Zhuchko*

"Status and prospects of collinear cluster tri-partition experimental studies"

International Symposium on Exotic Nuclei "EXON-2012", Vladivostok, Russia, 01-06 October 2012. Conference proceedings, Editors: Yu.E. Penionzhkevich, and Yu.G. Sobolev. Published by World Scientific Publishing Co. Pte. Ltd., 2013. pp. 407-410.

15. *D.V. Kamanin, Yu.V. Pyatkov, V.E. Zhuchko, N.A. Kondratyev, A.A. Alexandrov, I.A. Alexandrova, N. Jacobs, E.A. Kuznetsova,* ***V. Malaza****, S.I. Mulgin, A.O. Strekalovsky, O.V. Strekalovsky*

"Methodical base of experimental studies of collinear multibody decays"

International Symposium on Exotic Nuclei "EXON-2012", Vladivostok, Russia, 01-06 October 2012. Conference proceedings, Editors: Yu.E. Penionzhkevich, and Yu.G. Sobolev. Published by World Scientific Publishing Co. Pte. Ltd., 2013. pp. 411-416

16. *D.V. Kamanin, Yu.V. Pyatkov, V.E. Zhuchko, N.A. Kondratyev, A.A. Alexandrov, I.A. Alexandrova, N. Jacobs, E.A. Kuznetsova,* ***V. Malaza****, S.I. Mulgin, A.O. Strekalovsky, O.V. Strekalovsky*

"The COMETA spectrometer for study of multi-body decays of heavy nuclei"

Proceedings of the 20th International Seminar on Interaction of

Neutrons with Nuclei, Alushta, Ukraine, 21-26 May 2012. Dubna 2013, pp. 117-123.

17. *Yu.V. Pyatkov, D.V. Kamanin, A.A. Alexandrov, I.A. Alexandrova, N. Mkaza, V.E. Zhuchko, N.A. Kondratyev, E.A. Kuznetsova, G.V. Mishinsky,* ***V. Malaza****, A.O. Strekalovsky, and O.V. Strekalovsky*
"Status and prospects of investigations into the collinear cluster decay of heavy nuclei"
Physics of Atomic Nuclei. Vol. 77, No. 12, 2014, pp. 1518-1524. From Yadernaya Fizika. Vol. 77, No. 12, 2014, pp. 1591-1597.

18. *Yu.V. Pyatkov, D.V. Kamanin, A.A. Alexandrov, I.A. Alexandrova, N.A. Kondratyev, E.A. Kuznetsova, A.O. Strekalovsky, O.V. Strekalovsky, V.E. Zhuchko, N. Mkaza,* ***V. Malaza***
"Observation of light shape isomers in the multi-body decay of ^{252}Cf (sf)"
Proceedings of the First International African Symposium on Exotic Nuclei "IASEN-2013", Cape Town, South Africa, 2-6 December 2013. World Scientific 2014, pp. 277-284.

19. *D.V. Kamanin, Yu.V. Pyatkov, A.A. Alexandrov, I.A. Alexandrova, N. Jacobs, N.A. Kondratyev, E.A. Kuznetsova, G.V. Mishinsky,* ***V. Malaza****, A.O. Strekalovsky, O.V. Strekalovsky, V.E. Zhuchko*
"New kind of nuclear multi-body decay (CCT) - status and perspectives of studies"
FIAS Interdisciplinary Science Series. Nuclear Physics: Present and Future. 2014. pp.141-150.

20. *D.V. Kamanin, Yu.V. Pyatkov, A.A. Alexandrov, I.A. Alexandrova, N. Jacobs, N.A. Kondratyev, E.A. Kuznetsova, G.V. Mishinsky,* ***V. Malaza****, A.O. Strekalovsky, O.V. Strekalovsky, V.E. Zhuchko*
"Perspectives of the study of collinear cluster tri-

partition of heavy nuclei"
Proceedings of the 21st International Seminar on Interaction of Neutrons with Nuclei, Alushta, Ukraine, 20-25 May 2013. Dubna 2014, pp. 99-106.

21. *D.V. Kamanin, Yu.V. Pyatkov, A.A. Alexandrov, I.A. Alexandrova, N.A. Kondratyev, E.A. Kuznetsova, V.N. Shvetsov, A.O. Strekalovsky, O.V. Strekalovsky, V.E. Zhuchko, N. Jacobs,* ***V. Malaza***
"Status of the VEGA project"
International Symposium on Exotic Nuclei "EXON-2014", Kalaningrad, Russia, 08-13 September 2014. Conference proceedings, Editors: Yu.E. Penionzhkevich, and Yu.G. Sobolev. Published by World Scientific Publishing Co. Pte. Ltd., 2015. pp. 659-667.

22. *D.V. Kamanin, Yu.V. Pyatkov, A.A. Alexandrov, I.A. Alexandrova, N.A. Kondratyev, E.A. Kuznetsova, V.N. Shvetsov, A.O. Strekalovsky, O.V. Strekalovsky, V.E. Zhuchko, N. Jacobs,* ***V. Malaza***
"Searching for new long-lived shape isomers"
International Symposium on Exotic Nuclei "EXON-2014", Kalaningrad, Russia, 08-13 September 2014. Conference proceedings, Editors: Yu.E. Penionzhkevich, and Yu.G. Sobolev. Published by World Scientific Publishing Co. Pte. Ltd., 2015. pp. 401-405.

23. *Yu.V. Pyatkov, D.V. Kamanin, A.A. Alexandrov, I.A. Alexandrova, N.A. Kondratyev, E.A. Kuznetsova,* ***V. Malaza****, N. Mkaza, A.O. Strekalovsky, O.V. Strekalovsky, V.E. Zhuchko*
"Study of shape isomeric states in fission fragments"
Proceedings of the 22nd International Seminar on Interaction of Neutrons with Nuclei, Dubna, Russia, 27-30 May 2014. Dubna 2015, pp. 83-90.

24. *D.V. Kamanin, Yu.V. Pyatkov, A.A. Alexandrov, I.A. Alexandrova, N.A. Kondratyev, E.A. Kuznetsova,* ***V. Malaza****, N. Mkaza, G.V. Mishinsky, V.N. Shvetsov, A.O. Strekalovsky, O.V. Strekalovsky, V.E. Zhuchko*
"Searching for shape isomeric states leading to ternary decay of heavy nucleus"
Proceedings of the 22nd International Seminar on Interaction of Neutrons with Nuclei, Dubna, Russia, 27-30 May 2014. Dubna 2015, pp. 77-82.

25. *D.V. Kamanin, Yu.V. Pyatkov, A.A. Alexandrov, I.A. Alexandrova, N.A. Kondratyev, E.A. Kuznetsova,* ***V. Malaza****, N. Mkaza, V.N. Shvetsov, A.O. Strekalovsky, O.V. Strekalovsky, V.E. Zhuchko*
"Physical program and status of the VEGA project"
Proceedings of the 22nd International Seminar on Interaction of Neutrons with Nuclei, Dubna, Russia, 27-30 May 2014. Dubna 2015, pp. 70-76.

26. *Yu.V. Pyatkov, D.V. Kamanin, A.A. Alexandrov, I.A. Alexandrova,* ***V. Malaza****, N. Mkaza, E.A. Kuznetsova, A.O. Strekalovsky, O.V. Strekalovsky, V.E. Zhuchko*
"New results in studies of the shape isomer states in fission fragments"
Proceedings of the 23nd International Seminar on Interaction of Neutrons with Nuclei, Dubna, Russia, 25-29 May 2015. Dubna 2016, pp. 97-101.

27. *Yu.V. Pyatkov, D.V. Kamanin, N.A. Kondratyev, A.O. Strekalovsky, S. Ilić, A.A. Alexandrov, I.A. Alexandrova, N. Mkaza, E.A. Kuznetsova,* ***V. Malaza****, G.V. Mishinsky, O.V. Strekalovsky and V.E. Zhuchko*
"Experimental testing of heavy ions mass search procedure in the measurements with PIN diodes"
International Conference on Particle Physics and Astrophysics

(ICPPA-2015), 5-10 October 2015, Moscow. Journal of Physics: Conference Series 675, 2016, art. 042018.

28. *Yu V Pyatkov, D V Kamanin, J E Lavrova, N Mkaza,* ***V Malaza****, A O Strekalovsky,*
"Collinear cluster tri-partition – the brightest observations and their treating",
Journal of Physics: Conference Series, v.863 (2017) 012046

29. *D V Kamanin, Yu V Pyatkov, A Alexandrov, I A Alexandrova, N Mkaza,* ***V Malaza****, E A Kuznetsova, A O Strekalovsky, O V Strekalovsky, V E Zhuchko,*
"Observation of shape isomers states in fission fragments"
Journal of Physics: Conference Series, v.863 (2017) 012045

30. *D.V. Kamanin, A.A. Alexandrov, I.A. Alexandrova, E.A. Kuznetsova, A.O. Strekalovsky, O.V. Strekalovsky, V.E. Zhuchko Yu.V. Pyatkov, N. Mkaza,* ***V. Malaza***
"Evidences of true ternary and quaternary fission of low excited actinides",
Int. Symposium on Exotic Nuclei "EXON-2016", Kazan, Russia, 04-10 September 2016. Conference proceedings, Editors: Yu.E. Penionzhkevich, and Yu.G. Sobolev. Published by World Scientific Publishing Co. Pte. Ltd., 2017. pp. 243-248.

31. *Yu.V. Pyatkov, D.V. Kamanin, N.A. Kondratyev, A.O. Strekalovsky, S. Ilić, A.A. Alexandrov, I.A. Alexandrova, N. Mkaza, E.A. Kuznetsova,* ***V. Malaza****, G.V. Mishinsky, O.V. Strekalovsky and V.E. Zhuchko*
"New results in study of shape isomer states in fission fragments",
Int. Symposium on Exotic Nuclei "EXON-2016", Kazan, Russia, 04-10 September 2016. Conference proceedings, Editors: Yu.E. Penionzhkevich, and Yu.G. Sobolev. Published by World Scientific Publishing Co. Pte. Ltd., 2017.

32. *Yu. V. Pyatkov, D. V. Kamanin, A. A. Alexandrov, I. A. Alexandrova, Z. I. Goryainova, J. E. Lavrova, N. Mkaza,* ***V. Malaza,*** *E. A. Kuznetsova, A. O. Strekalovsky, O. V. Strekalovsky, V. E. Zhuchko*,
"Analysis of some modes of multibody decays of low excited actinide nuclei",
International Conference on Particle Physics and Astrophysics (ICPPA-2016), 10-14 October 2016, Moscow. Journal of Physics: Conference Series 798, 2017, art. 012078.

33. *Yu.V. Pyatkov, D. V. Kamanin, A. A. Alexandrov, I. A. Alexandrova, Z. I. Goryainova,* ***V. Malaza****, N. Mkaza, E. A. Kuznetsova, A. O. Strekalovsky, O. V. Strekalovsky, and V. E. Zhuchko*
"On the question of verification of collinear cluster tri-partition(CCT)",
Proceedings of the 25th International Seminar on Interaction of Neutrons with Nuclei, Dubna, Russia, 22-26 May 2017. Dubna 2018, p. 409-414.

Table of Contents

List of Figures

List of Tables

Chapter 1

Introduction

1.1. General Introduction

The existence of an atom has been hypothesized since the time of *Democritus* (400 BC), who suggested that any matter can be broken down to a fundamental structure that can no longer be taken apart. This fundamental structure suggested at that time was found to be an atom in the late 19th century. The development of atomic theories gained momentum soon after J.J. Thomson discovered the electron in 1890 [1].

From Thomson's discovery, Ernest Rutherford [2] suggested that the atom is similar to the solar system. His discovery suggested that there is a nucleus at the centre of an atom with electrons orbiting around it. Rutherford made this conclusion from his famous scattering experiment and mathematical modelling of scattering reactions [2]. According to the laws of electrodynamics, a charged particle undergoing a rotational motion is continuously accelerating and would eventually radiate all its kinetic energy and fall into the nucleus. This implies that according to the Rutherford atomic model, the electrons were supposed to lose energy and fall into the nucleus. This phenomenon was not observed in experiments; thus, it became a phenomenon that the Rutherford Atomic Model could not explain.

This phenomenon was explained by Niels Bohr in 1913 [3]. Bohr's understanding of quantum physics suggested that the electrons orbit the

nucleus in orbits that have a set size and energy. This indicates that the orbits are closed and are quantized. There is no energy that is lost. This was a remarkable achievement in understanding the structure of the atom. The Atomic Model that is used today was completed by Erwin Schrödinger [4]. Schrödinger used the famous Heisenberg Uncertainty Principle and the ideas of Louis de Broglie to show that atomic particles are also wave-like in nature. Schrödinger in his work came up with a wave equation that explains the behaviour of atomic particles.

It is well understood now that the smallest part of an element is called an atom. Each atom is different in structure from other atoms. An atom is divided into subatomic particles called electrons, protons and neutrons. The centre of an atom is made up of a nucleus with constituent protons and neutrons. Electrons are negatively charged, protons are positively charged and neutrons are neutral, thus the nucleus of an atom is positively charged.

Understanding the properties of a nucleus and the interaction of different nuclear systems is the main focus of nuclear science. When two or more nuclei interact with each other, another or new element is formed. The interaction between different nuclei is studied using nuclear reactions. Nuclear reactions are widely classified but the most notable ones are nuclear fission and nuclear fusion. Nuclear fission is a process where a heavy nucleus splits into two or more lighter nuclei and nuclear fusion, in general, is when two (or more) lighter nuclei combine to form a heavy nucleus.

This dissertation focuses on nuclear fission reactions. It presents a new type of nuclear decay which is referred to as a rare decay mode. This mode is a specific type of ternary fission. Ternary fission is when a nucleus disintegrates into three lighter nuclei. In the specific ternary fission mode to be presented here, the three fragments are observed to fly apart collinearly at the scission point and one of the decay partners is a known nuclear magic cluster. The nuclear magic cluster in the

context of this work means that one of the detected fragments has a magic nucleon composition. Therefore, this phenomenon was given the name Collinear Cluster Tri-partition (CCT). At the beginning of this work, this mode was considered to be undiscovered. This work presents a detailed report of the first experimental confirmation of the existence of the CCT decay mode.

1.2. Terminology

In general, a nuclear fission process is characterised by the splitting of a nucleus into two or more lighter nuclei. If a nucleus splits into only two primary fission fragments, the process is called *binary fission*. During the break up or at scission point, the primary fragments will obtain their full energy of motion after a duration of $10^{-18}s$ while they are separated by a distance of $2 \times 10^{-11}\ m$ from each other [5]. If three particles are formed within the $10^{-18}\ s$ time interval, the fission event is called *ternary fission*. This definition holds for the whole spectrum of three-particle fission events, that is, from one extreme mode where a neutron will accompany the two primary fragments to the other extreme mode where three primary fragments of almost equal masses are produced. It is worth mentioning the so-called conventional ternary fission, defined as the decay where a binary fission is accompanied by an alpha particle emitted in the plane perpendicular to the fission axis. The fission event where three primary fragments of almost equal masses are observed is called *true ternary fission*. When a light charged particle (LCP) is observed together with the two heavy fragments, the process is called the *light charged particle accompanied fission* (*LCP-fission*). In a case when fission into three fragments takes place, but the mass ratio and other parameters are not of interest, the process is called *tri-partition* [5].

1.3. Nuclear Fission

1.3.1. Types of Fission Reactions

The interest in nuclear reactions, nuclear fission to be specific, came just after Fermi and his collaborators discovered that when a heavy nucleus absorbs neutrons, new radioactive isotopes are formed [6]. Fermi discovered that when a heavy element, such as uranium in his case, absorbs neutrons, new elements are produced with an atomic mass heavier than that of the uranium. Furthermore, other scientists such as Meitner and Frisch, Hahn and Strassman, Curie and Savitch [7], [8], developed more interest in this work and their research led Hahn and Strassman to discover that new radioactive elements of smaller atomic numbers are formed when uranium is bombarded with neutrons [7].

Meitner and Frisch, from their experimental work, discovered that the uranium nucleus splits into two almost equal pieces, after absorbing a neutron [8]. This is a phenomenon referred to as nuclear fission. Its existence was further confirmed through quantitative calculations performed by Niels Bohr and John Wheeler using their *Liquid Drop Model* [9]. The resulting nuclei from the fission reaction are called fission fragments.

Fission reactions can be further classified as induced fission reactions and spontaneous fission reactions. The fission process discussed above is the induced fission reaction. This means that a very low energy neutron enters a nucleus such as uranium and causes it to be excited. The excited nucleus is unstable; therefore, it breaks apart due to the excess energy obtained after absorbing the neutron, thus undergoing a fission reaction.

Spontaneous fission was first discovered by G.N. Flerov and K.A. Petrzhak in 1940 as a fission process where a nucleus can break into other nuclei without being induced by neutrons or any other processes [10]. Only a few isotopes can be used in experiments involving

spontaneous fission with reasonable half-lives. In most isotopes the dominant decay is the alpha decay as compared to the spontaneous fission. The commonly used spontaneous fission sources includes ^{252}Cf ($T_{1/2} = 2.65\ y$) and ^{248}Cm ($T_{1/2} = 3.47 \times 10^5\ y$).

The above-mentioned fission sources received more interest when compared to the neutron-induced fission of uranium due to the difference in the mass distributions of the fission fragments. The mass peaks of the fission fragments in the mass distribution of ^{252}Cf and ^{248}Cm are wider than the one of uranium and are more shifted towards the higher mass distribution. This is shown in Figure 1.1 where the fission fragments of ^{252}Cf are compared to the fission fragments of ^{235}U [11].

It is known that the mass distribution of fission fragments for a particular element will peak at the neutron-rich isotopes. ^{252}Cf is more neutron-rich than ^{235}U. This means that there are more possibilities to discover new isotopes with spontaneous fission than with neutron-induced fission [11].

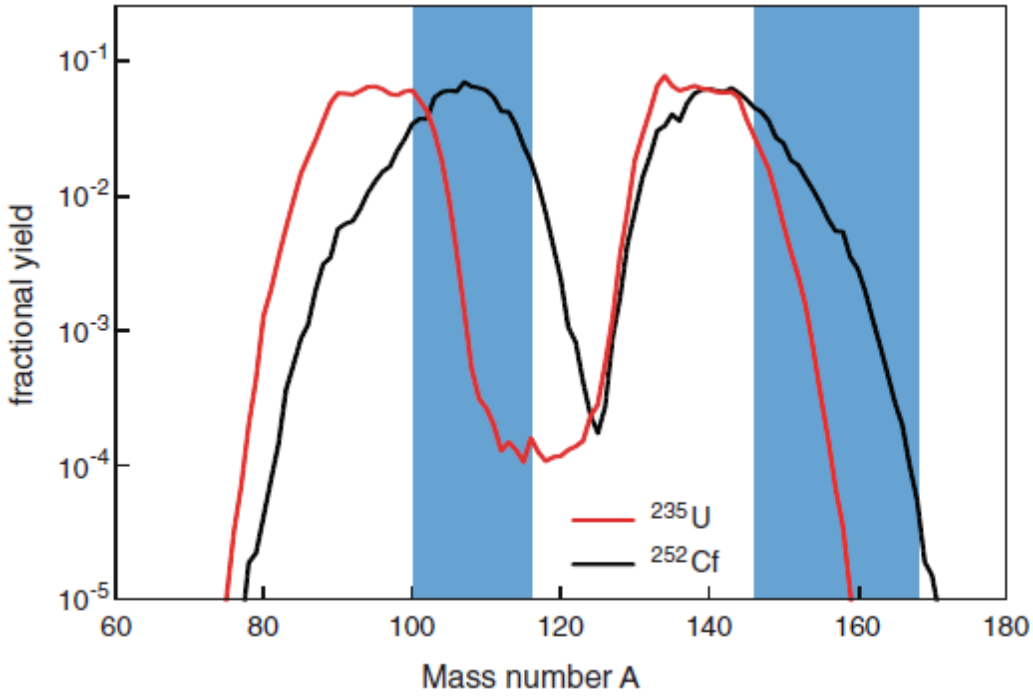

Figure 1.1: Fission fragment yield of neutron induced fission of ^{235}U and spontaneous fission of ^{242}Cf [11], [12]. The blue shaded area shows a mass region where new isotopes were discovered in spontaneous fission of ^{252}Cf and ^{248}Cm.

1.3.2. Ternary Fission

Ternary fission was discovered by L.L. Green and D.L. Liversy in 1946 [13]. It was later pointed out that ternary fission of low and middle excited nuclei, found to exist at that time, can be classified as *conventional ternary fission* and *polar emission* [14]. The conventional ternary fission is the process where an LCP accompanies the binary fission products and is emitted perpendicular to the fission axis due to the focusing effect of the Coulomb field. The characteristics of the LCP is influenced by the Coulomb field. This form of fission was intensively studied in experiments involving spontaneous fission and neutron-induced fission. In most cases He isotopes were observed but particles with masses of up to 36 amu were detected [15].

Polar emission occurs when the LCP is found to be moving almost along the fission axis. This type of ternary fission was discovered by Piasecki and his colleagues in their work on polar emission and evaporation from fission fragments [16]. Polar emission was best explained by a so-called *Evaporation Model* which was based on the hypothesis that polar particles are evaporated from the fission fragments [17] and [18]. At that time this was the only model that could explain polar emission and attempts to verify polar emission were performed in [19]. The authors compared experimental data with the theoretical predictions from the *Evaporation Model*.

Further work on ternary fission carried out by Ronen proved that the strong similarity that exists between ternary fission and cluster decay suggests that other ternary decay processes can be considered to be cluster-decay processes [20]. This is analogous to the ternary alpha emission that is classified as alpha decay. In this case, cluster decay or cluster radioactivity is defined as a spontaneous emission of light fragments that is heavier than alpha particle ($A = 4\ amu$) and lighter than fission fragment ($A \approx 60\ amu$). Ronen also indicated that the clusters associated with cluster radioactivity are related to the clusters

with high yield obtained in ternary fission. This suggests that the ternary fission is a cluster decay of a nucleus that is undergoing fission, especially in its last stage of scission.

It is outlined in [21] that ternary fission is energetically more favourable than binary fission as already suggested in [5]. Evidence of this was provided by Swiatecki when he calculated the amount of energy that is released when a nucleus disintegrates into a number of fragments based on the *Liquid Drop Model* [22]. These results demonstrated that fission of heavy nuclei into three fragments releases more energy than binary fission. This is only applicable for nuclei with a fission parameter between $30.5 < Z^2/A < 43.3$. This includes elements from Bi to Fm. Swiatecki suggested that for the purpose of experimental detection of ternary fission, nuclei with maximum available value of the fission parameter Z^2/A should be used. It was further suggested that despite all the theoretical and experimental work, knowledge and understanding of ternary fission are far from complete and should be investigated further [22].

1.4. Rare Decay Modes

Strutinsky's discovery in 1968 showed that along with the one neck configuration at the scission point, there exists more complicated configurations with two and even three necks [23]. Before this discovery, the fission process was thought to involve a configuration with only one neck at scission. Following this idea, there were more experimental attempts to find true ternary fission in low energy fission processes. From these experiments, especially from the work of Diehl and Greiner [24], [25], it was clear that ternary fission is a very rare phenomenon, therefore it is regarded as one of the rare radioactive decay modes.

The rare decay modes (specifically the ones to be discussed in this work) were first reported in [26] as fine structures observed in the fission fragments mass-energy distribution for the reaction $^{233}U(n_{th}, f)$ where

n_{th} represents the incident thermal neutron and f the fission products. The recognised fine structures were linked to the manifestation of the rare decay modes in fission. This was a very complex process in fine structure identification and different methods were used to reveal these fine structures. The methods that were used include the second derivative method, low-pass filtering, high-pass filtering and band-pass filtering [26].

Cluster radioactivity, is already defined in the above sections as a binary fission process. The fact that one of the decay partners in the rare decay modes have a magic constituent brings along the ideas of cluster radioactivity. The question that arises is whether the decay of a heavy nucleus into magic constituents occurs naturally. Searching for such decays is one of the motivations to undertake this work.

In one of the experiments performed with the FOBOS Spectrometer, mentioned in [5], [21] and also outlined in chapter 2, a specific group of events linked to the rare decay modes were revealed for the first time. The total mass of the two registered fragments which fly apart almost collinearly was significantly less than the initial mass of the ^{252}Cf nucleus. The mass of at least one of the registered fragments corresponded to the mass of one of the known magic nuclei. It has been mentioned already in sections 1.2 that in a case when fission into three fragments takes place but the mass ratio and other parameters are not of interest, the process is called tri-partition. Taking all this into consideration, the observed rare decay modes were referred to as Collinear Cluster Tri-partition (CCT).

1.5. Collinear Cluster Tri-partition

The Collinear Cluster Tri-partition (CCT) was identified as a new type of ternary decay of low excited heavy nuclei. It was observed experimentally together with conventional and binary fission [27]. Vijayaraghavan and his colleagues on their study of sequential decay

processes calculated potential energies of different pre-scission configurations which lead to ternary decays and kinetic energies of the CCT partners [28]. The results obtained were depended on the specific models used to calculate the potential energies and only treated as a first step in describing the CCT [27].

Diehl and Greiner worked on the theory of ternary fission using the *Liquid Drop Model* and showed that in the direct ternary fission modes, prolate ternary fission configuration is more energetically favoured than oblate fission configuration [25]. This constrains the CCT decay to a collinear separation of the fission fragments. It is mentioned in [27] that there is a strong link between CCT decay mode, cluster radioactivity and cold fission. Cluster radioactivity has also been studied as a rare spontaneous decay mode of heavy nuclei. The heavy fragments in cluster radioactivity are grouped in the vicinity of the ^{208}Pb nucleus. Therefore, this is usually referred to as "lead radioactivity". Cold fission is when fragments of comparable masses are emitted in the lead radioactivity process. It is important to note that cluster radioactivity is closer to alpha decay than it is to spontaneous fission. The difference between alpha decay and spontaneous fission is that in alpha decay products are formed in their ground states whereas in spontaneous fission both fragments are deformed and strongly excited.

During the early stages of the work reported in this dissertation, true ternary fission, together with a so-called three-body cluster radioactivity was considered to be undiscovered for low-excited heavy nuclei. The process closer to CCT at that time was a so-called polar emission (discussed in section 1.3.2). Experimentally only very light ions were observed close to polar emission. It was concluded that CCT could not be described using the ideas of polar emission. Therefore, the CCT decay was treated as a separate process from the polar emission [27].

From one of the first experiments outlined in [29] and [30], some indications of the CCT process were observed and one of the decay

partners detected was a double magic cluster. Based on these findings and the discussions in [27] it can be concluded that the collinear tri-partition of low-excited heavy nuclear systems is a promising field of research. Some of the important experimental results leading to the discovery and confirmation of the CCT are discussed in section 1.6. The details of the experiments leading to these results will be discussed in chapter 2 of this dissertation.

1.6. Results of previous experiments in the study of the Collinear Cluster Tri-partition

The first manifestation of the CCT was observed towards the end of the 20th century [5]. Intense experimental work was supported by theoretical work done by a group of scientists from the Flerov Laboratory of Nuclear Reactions (FLNR) at the Joint Institute for Nuclear Research (JINR) in Dubna, Russia. Important results obtained from these experiments, where the CCT phenomenon was revealed for the first time are reported below. These results were obtained mainly from the experiments where the spontaneous fission source ^{252}Cf and the $^{235}U(n_{th}, f)$ reaction were used. Later in this section neutron-gated data that showed strong evidence of the CCT will be discussed.

1.6.1. CCT from Spontaneous ^{252}Cf fission

The first results were obtained from an experiment performed using the FOBOS spectrometer [31] at the FLNR at JINR. The experimentation linked to CCT using the FOBOS spectrometer, and the FOBOS spectrometer itself, are discussed in section 2.2.1 of this dissertation. The main results obtained from this experiment are displayed in Figure 1.2 as a contour map using a logarithmic scale showing the mass-mass

distribution of the collinear fragments detected in coincidence from the two arms of the FOBOS spectrometer [21], [27], [32].

In Figure 1.2, M_1 is defined as the mass of the fragment that is detected from arm 1 of the FOBOS spectrometer. This arm is facing the side that includes an additional dispersive (scattering) material on the ^{252}Cf source. This material is referred to as a source backing and it is made of 50 $\mu g/cm^2$ of Al_2O_3. The M_2 is defined as the mass of the fragment that is detected in arm 2 of the spectrometer which is free from the source backing. The regions 1 and 2 in the figure depicts the events of the conventional binary fission. The tails marked 3, 4, 5, and 6 extending from region 1 and 2 shows events scattered from the source backing and the grid edges that was inserted on the "stop" detectors (Figure 2.6). The diagonal line $M_s = M_1 + M_2 = 225\ amu$ is shown and it separates the interesting events (tails 3,4,5,6) from the conventional binary events located above this line.

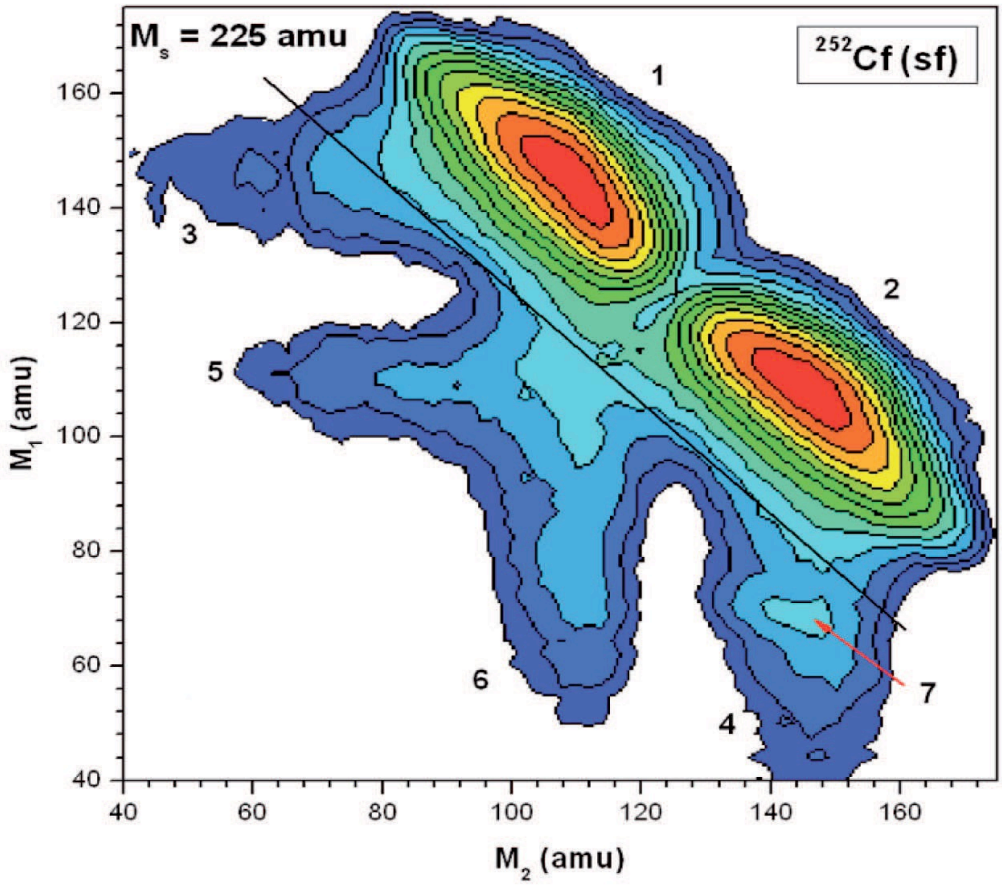

Figure 1.2: Contour map of the mass-mass distribution of the collinear fragments detected in coincidence from the two opposite arms of the FOBOS spectrometer setup [21], [27], [32].

The region marked by arrow 7 in tail 4 of Figure 1.2 was found to be the main breakthrough in revealing the CCT. This has been seen as the significant difference in the counting rates and the shapes of tail 3 and 4. This shows an additional distinct bump marked by arrow 7 in the figure. The formation of this bump can be explained by considering the trajectory of the CCT shown in Figure 2.5. If the ternary fission takes place, two light fragments fly in the same direction and get scattered, with an angle $\sim 1^{o}$ between each other after passing through the source backing. It should be noted that the bump is located on the side where there is a source backing and the grid edges, as shown in Figure 2.6 (arm 1). Therefore, out of the two fragments flying in the same direction towards the first arm of the spectrometer, one will hit the edges of the grid (that is the missing fragment) and the other fragment will hit the Position Sensitive Avalanche Counter and be detected.

The bump shows events where only one light fragment is detected in arm 1 in coincidence with the other fragment detected in arm 2. The third fragment is missing. In a case when the two light fragments flying in the same direction both hit the avalanche counters and get detected, the event is registered as a conventional binary fission, thus the mass will lie in region 1 or 2 of Figure 1.2.

The appearance of the bump in the above data revealed that ternary fission took place. The one fragment was missing due to the grid and scattering in the source backing. Only two fragments were detected. This reveals that there were three fragments from this fission event. Therefore, this was referred to as the "missing mass" method. Only two fragments were detected and the sum of their masses is significantly less than the mass of the initial nucleus. It should be noted that the absence of the grid in previous experiments [33] was the main reason the authors could not detect ternary fission in the past.

To further analyse the bump and confirm that the events responsible for the bump are linked to the CCT, consider the distribution shown in

Figure 1.3. This figure shows the contour map of a two dimensional mass-mass distribution obtained from subtracting tail 3 from tail 4 in Figure 1.2. No additional normalization was applied to these data and the distribution is free from the conventional binary fission fragments. To emphasize the fact that the features shown in Figure 1.3 are linked to real events of the CCT, a second derivative filter method was applied to these data and the results are shown in Figure 1.4. The second derivative filter is the method that is used to find peaks in gamma spectra [26], [33].

The data shown in these figures reveal tilted lines that represents the $M_s = const$ of values 204, 208, 212 and 214, which correspond to the different combinations of two detected fragments where at least one of them has a magic nucleon number. These marked points are related to mass values with known magic subsystem from binary fission listed in [34] and [35]. The well-known magic subsystems corresponding to the detected $M_s = const$ (displayed in the figures) are listed below and the ternary decay $Q-$ values are given in the braces:

$$204 \rightarrow {}^{70}Ni + {}^{134}Te \qquad \{241MeV\}$$

$$204 \rightarrow {}^{72}Ni + {}^{132}Sn \qquad \{251MeV\}$$

$$208 \rightarrow {}^{80}Ge + {}^{128}Sn \qquad \{261MeV\}$$

$$212 \rightarrow {}^{80}Ge + {}^{132}Sn \qquad \{257MeV\}$$

$$212 \rightarrow {}^{78}Ni + {}^{134}Te \qquad \{228MeV\}$$

$$212 \rightarrow {}^{68}Ni + {}^{144}Ba \qquad \{217MeV\}$$

$$214 \rightarrow {}^{82}Ge + {}^{132}Sn \qquad \{226MeV\}$$

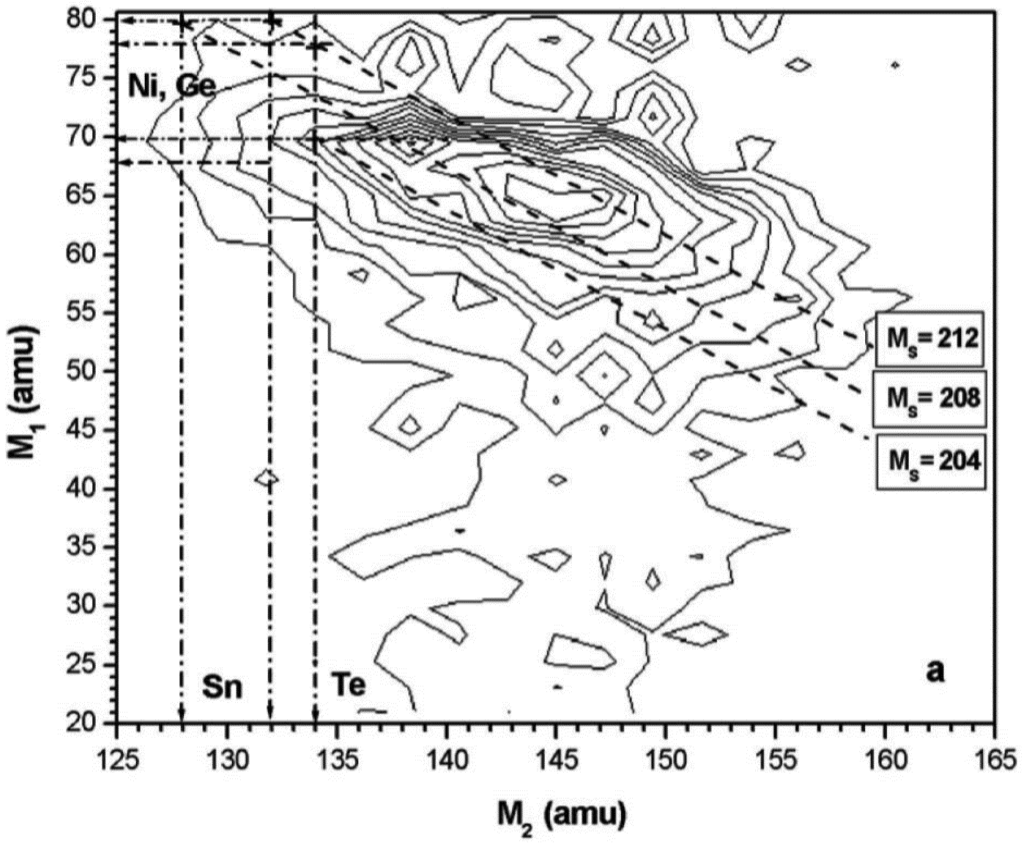

Figure 1.3: Two dimensional mass-mass distribution of the events obtained from subtracting tail 3 from tail 4 of Figure 1.2 [21], [27], [32].

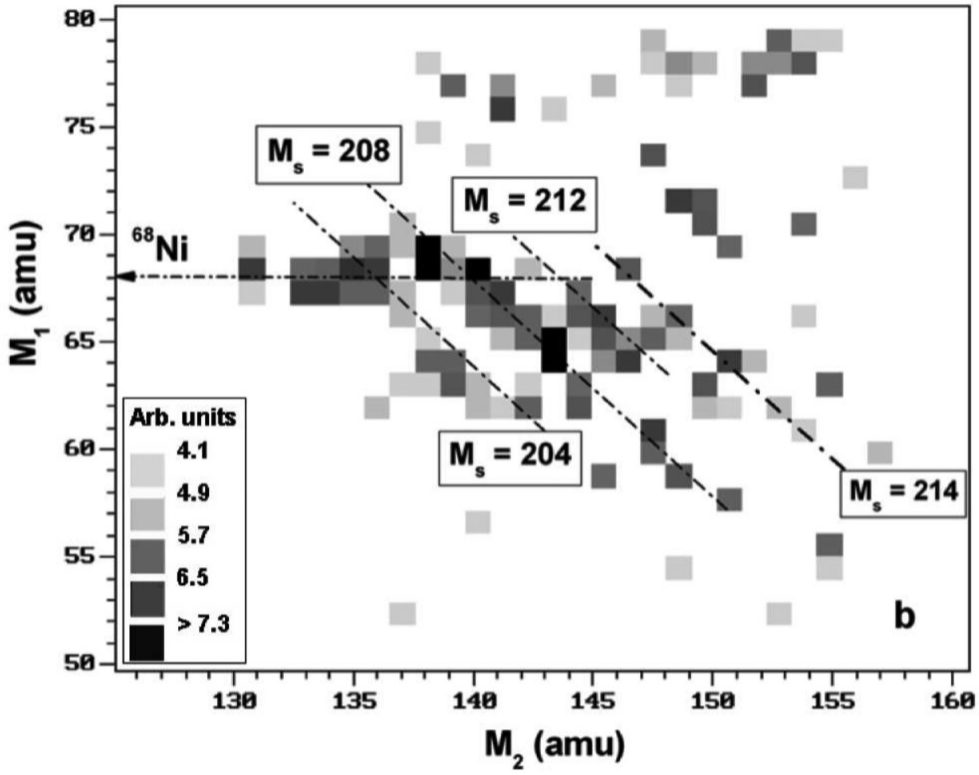

Figure 1.4: The second derivative filter method applied to the data shown in Figure 1.3 to depict the distinct diagonal lines where M_s = const linked to the actual missing masses are shown [21], [27], [32].

In all of the reactions shown above, a light fragment was missing and its mass is obtained when M_s is subtracted from the mass of the original nucleus. The diagonal lines in Figure 1.3 and Figure 1.4 confirm all the events associated with the above possible reactions. The Q-value of each reaction as outlined in [35] and [36] is shown next to each reaction. It should be noted that the Q-value that corresponds to the most probable binary partition of ^{252}Cf is 216 MeV.

Projections of tail 3 and 4 of Figure 1.2 are shown in Figure 1.5. The graph denoted by 'a' in Figure 1.5 shows the events from tail 4 where the bump is seen very clearly in the vicinity of $M_1 + M_2$ between 200 amu and 220 amu. The events from tail 3 are shown by the graph 'b' in Figure 1.5. The subtraction of tail 3 from tail 4 is shown by graph 'c' and the bump is vividly visible. The projection of the bump along M_1 is shown in Figure 1.6. This figure clearly shows that the effect of the bump is linked to the isotopes of $^{68,70}Ni$ which are magic nuclei. This bump in the discussions to follow is referred to as the "Ni bump".

The results discussed above were obtained from the first experiment which was dedicated to the investigation of CCT. In this specific experiment the CCT manifested from the missing-mass method. Further investigation and confirmation of these observations are needed and will be discussed in the following sections.

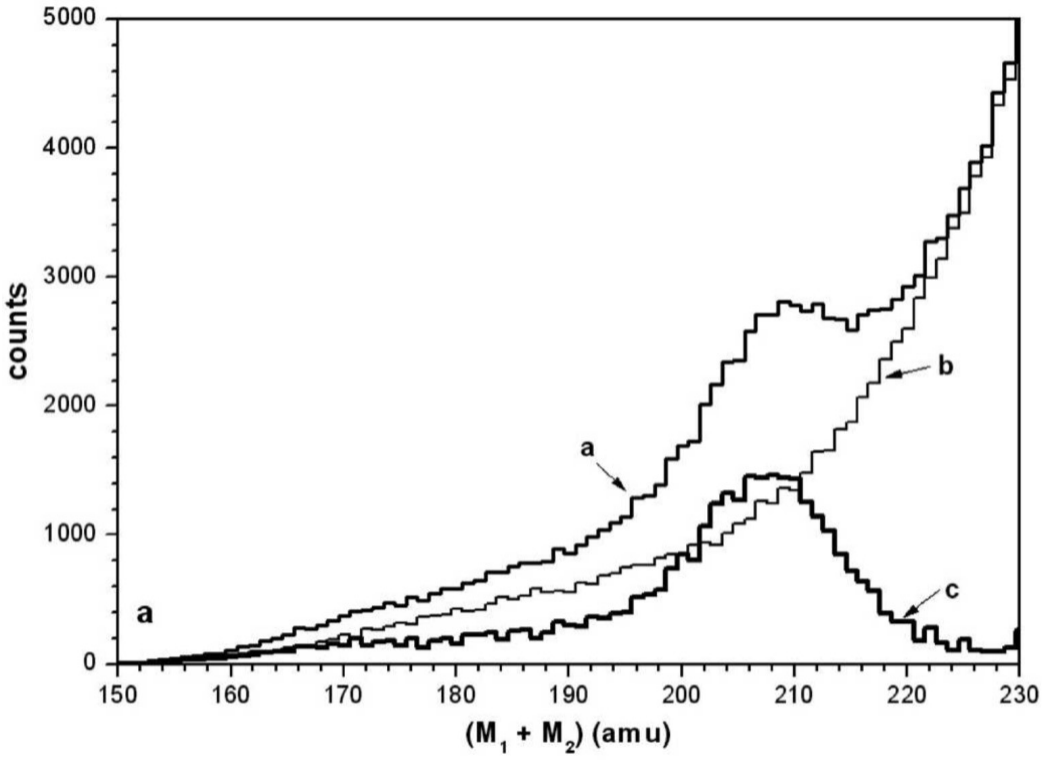

Figure 1.5: The projection Figure 1.2 along tail 3 and 4. The graph 'a' shows tail 4 where the bump was observed, graph 'b' shows tail 3. The subtraction of the two tails is shown by graph 'c' [27], [32].

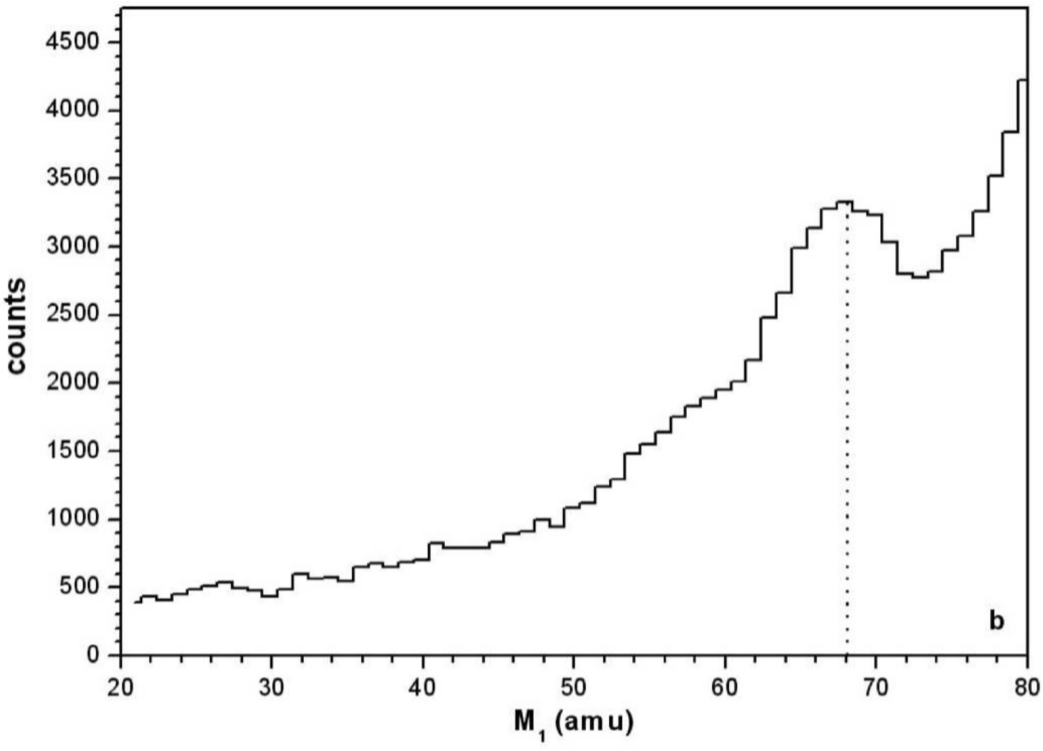

Figure 1.6: The projection of Figure 1.3 along M_1 which shows the bump in the vicinity of $^{68,70}Ni$ [27], [32].

1.6.2. CCT from the neutron induced fission reaction of ^{235}U

Another experiment to confirm the existence of the CCT was performed using the mini-FOBOS spectrometer from the Flerov Laboratory of Nuclear Reaction at the JINR. The mini-FOBOS spectrometer is outlined in section 2.2.2. This experiment investigated the fission induced by thermal neutrons in the $^{235}U(n_{th}, f)$ reaction. The beam of thermal neutrons was delivered by the IBR-2 reactor from Frank Laboratory of Neutron Physics at the JINR. In this experiment two parameters that are sensitive to the charge of the fission fragments were measured. The first parameter is the drift time between the Bragg Ionization Chamber (BIC) and the Position Sensitive Avalanche Counter (PSAC) of the mini-FOBOS detector system. The other parameter is the specific energy loss in the PSAC. These parameters were very useful in the selection of the events that are directly linked to the CCT.

The existence of the "Ni-bump" discussed above and first observed in a plot similar to the one shown in Figure 1.2 from ^{252}Cf study was confirmed by this experiment and is shown in the mass-mass distribution of Figure 1.7. The bump is vividly clear and is pointed out by the arrow in the figure. The yield of the events in the bump is $(5.1 \pm 0.4) \times 10^{-3}$ relative to the total number of fission events detected [27]. Similar to the results discussed above, the bump is observed from the arm of the spectrometer that is facing the scattering medium in the target (target backing).

The projection of the bump against M_1 for both the reaction of ^{252}Cf from Figure 1.2 and $^{235}U(n_{th}, f)$ from Figure 1.7 are shown in Figure 1.8. It can be seen that in both distributions the bump appears in the same vicinity of $^{68,70}Ni$ isotopes. As discussed above, the bump is linked to the CCT events. This means that in both experiments, three fragments were released during the fission event and two of them travelled in the same

direction and one in the opposite direction. The two fragments travelling in the same direction got scattered by an angle of $\sim 1^{o}$ and due to the grid in the 'stop' detectors only, one fragment was detected. One of the fission fragments was linked to one of the known magic nuclei as discussed in the previous sections.

The two additional parameters sensitive to the charge of the fission fragments that were measured in this experiment as compared to the ^{252}Cf study, made it possible to show the distribution of nuclear charge of the fission fragments detected in both arms of the spectrometer. Such a distribution is shown in Figure 1.9. The difference in the yield of the nuclear charge around $Z = 28$, (isotope of Ni) is clearly seen. This is a region where the bump is located and the yield of the bump is shown on an insert in Figure 1.9 on a linear scale and a high yield in the $Z = 28$ is vividly seen.

The results on the charge distribution actually confirm the previous findings on the mass distributions of Figure 1.2 and Figure 1.7 where a bump was observed in the arm facing the scattering media. This confirms the hypothesis that the upper boundary of the bump is connected to the Ni isotopes. As discussed in the previous sections, the tilted ridges of the $M_s = const$ in the ^{252}Cf data were obtained using a special, but complex mathematical process, that is used in peak finding in the gamma spectroscopy [27]. The true meaning of this ridges has now been confirmed using an independent method in the ^{236}U system. This method makes use of the additional parameter that was only recorded in this experiment. This parameter is the specific energy that the fission fragment loses in the 'stop' detector of the mini-FOBOS spectrometer [27].

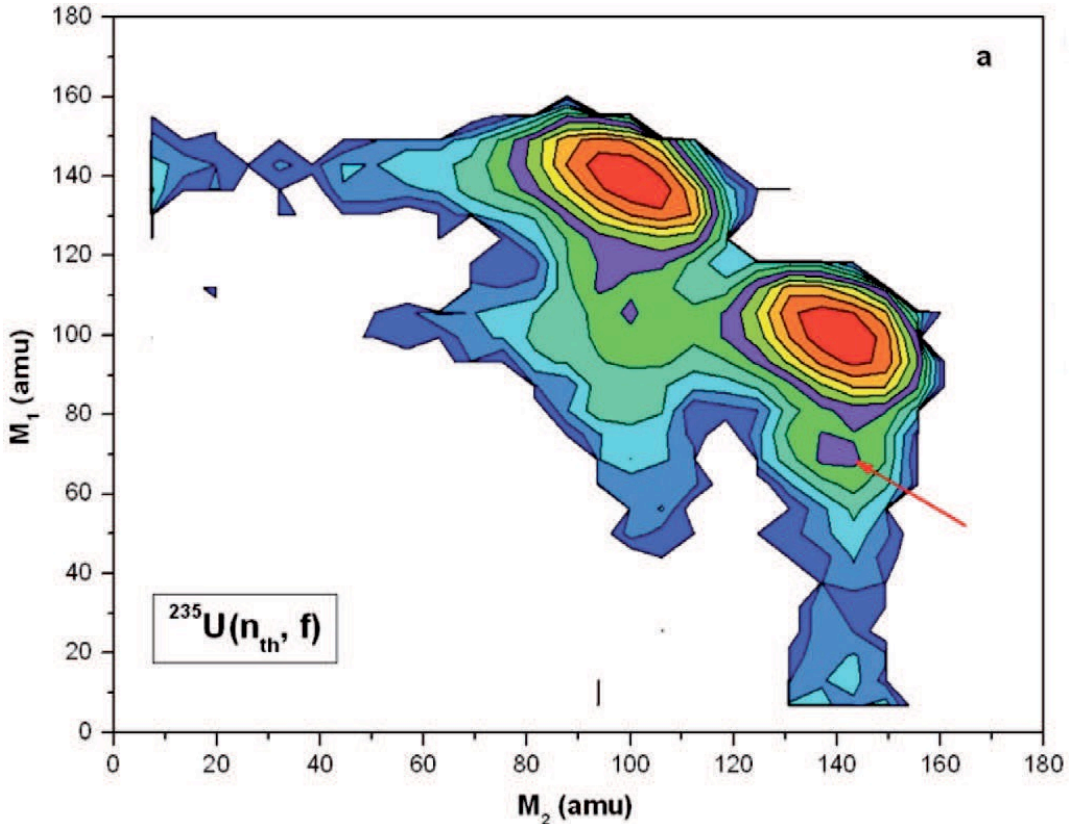

Figure 1.7: Fission Fragment mass-mass distribution obtained from $^{235}U(n_{th}, f)$ *reaction [27], [32].*

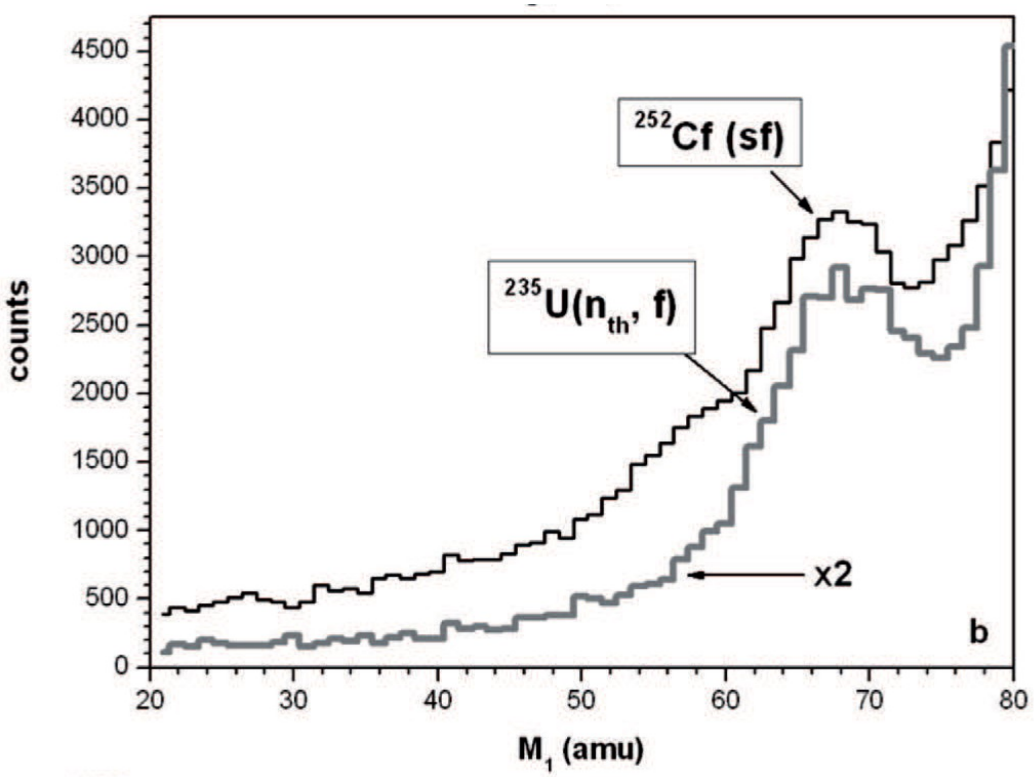

Figure 1.8: Projection of the bump on M_1 for the comparison of both the reactions of ^{252}Cf and $^{235}U(n_{th}, f)$ [27], [32].

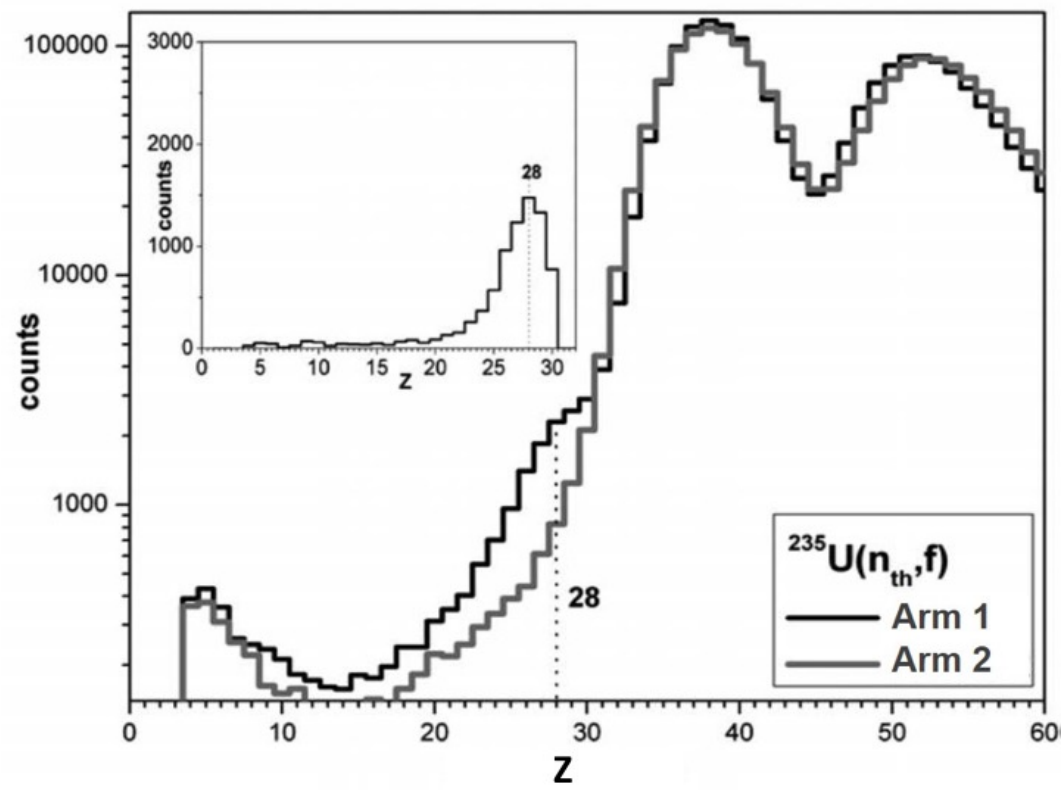

Figure 1.9: Distribution of nuclear charge of the fission fragments detected in both arms of the mini-FOBOS spectrometer from the reaction $^{235}U(n_{th}, f)$ *[27], [32].*

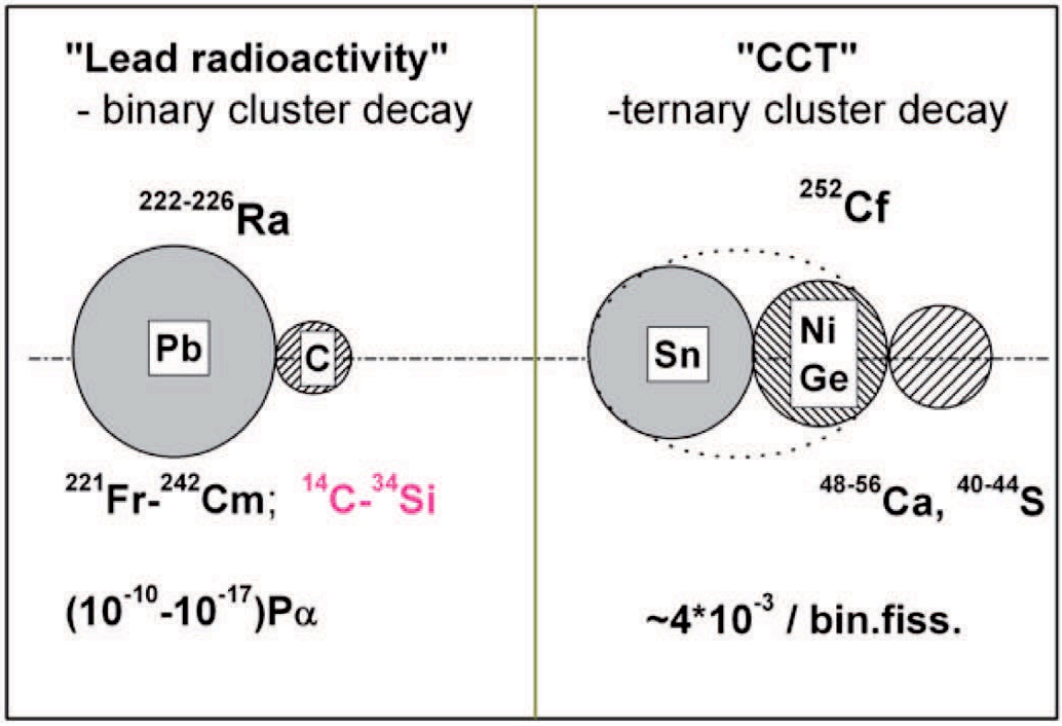

Figure 1.10: : A cluster scheme that compares lead radioactivity with collinear cluster radioactivity [27], [32].

The discussions and the results mentioned above did not only confirm the existence of the bump, but its internal structure was also revealed. Ridges along the $M_s = const$, where the bump occurred, were found to correspond to magic clusters such as Ni/Sn and Ge/Sn clusters. These ridges that were linked to pairs of magic clusters were found to be the same for both fission systems of ^{252}Cf and $^{236}U^*$. In addition, the extra parameters that were measured in the $^{235}U(n_{th}, f)$ reaction, which are linked to the nuclear charge of the fission fragments, gave a clear argument in support of the origin and existence of the bump.

The existence of this new decay mode is further confirmed in [37] as a CCT decay channel. One of the decay modes which was observed amongst the above-mentioned clusters that contributed to the bump can be treated as a new type of cluster decay. This decay mode is treated as a new decay mode because it displays different configurations when compared to the well-known heavy ion decay or lead radioactivity. This idea is shown in Figure 1.10 above.

As mentioned in [27], the observed high yield of CCT can be well understood if a collective motion through a hyper-deformed pre-scission configuration of the mother system is assumed. This is supported by the fact that a three cluster system that is realized through a linear arrangement has the lowest Coulomb potential energy. Therefore, the ternary fission process must be considered as a process that take place in a sequential mode with two neck raptures happening within a short time sequence.

1.6.3. Evidence of the CCT from neutron gated data

At this point, it is clear that there are several decay modes in which the CCT have been observed. In one of these modes a middle fragment of the three-body pre-scission chain has a very low velocity, presumably at rest at scission point. If a nucleus disintegrates, the fission fragments will

emit neutrons. During this mentioned decay mode, the moving binary fission fragments will emit neutrons along the fission axis [38]. The almost stationary fragment will emit neutrons isotropically.

Based on the above-mentioned idea, an experiment was performed to detect CCT together with neutrons emitted from the fission events. The neutrons were detected in such a way that there was a possibility to select fission events based on a certain neutron multiplicity from the neutron detectors. In this case, if the events are selected with the condition that at least three or more neutrons were detected, those events will be linked to the CCT.

The experiment was performed using a mini-FOBOS spectrometer (described in section 2.2.2) and the fission source ^{252}Cf. For this experiment, neutron detectors were installed in the mini-FOBOS spectrometer as a belt around the position of a fission source. The neutron detectors were referred to as a 'neutron belt' and the centre of the belt coincided with the position of the fission source. The detector system (including neutron detectors), the mini-FOBOS spectrometer and the modelling of the neutron belt are discussed in section 2.2.2 and outlined in [39].

The two dimensional mass-mass distribution analogous to Figure 1.2 and Figure 1.7 obtained from this experiment is shown in Figure 1.11. A similar bump that was observed in Figure 1.2 and Figure 1.7 can be seen in Figure 1.11 and is observed from the arm of the spectrometer that is facing the source backing. The bump in Figure 1.11 is less pronounced when compared to the other results. This is because there was poor mass resolution in the stop detectors due to the thicker foil used in the source backing [40]. The bump is generally in an agreement with the previous results, thus confirming the existence of the CCT.

It should be noted that the data relating to the neutrons will not be discussed here. The neutrons were used to only select events that are in coincidence with the fission events, which are linked to the CCT. The

mechanism used with neutrons is that the fission events detected in coincidence with multiplicity three or more of neutrons is directly linked to the CCT.

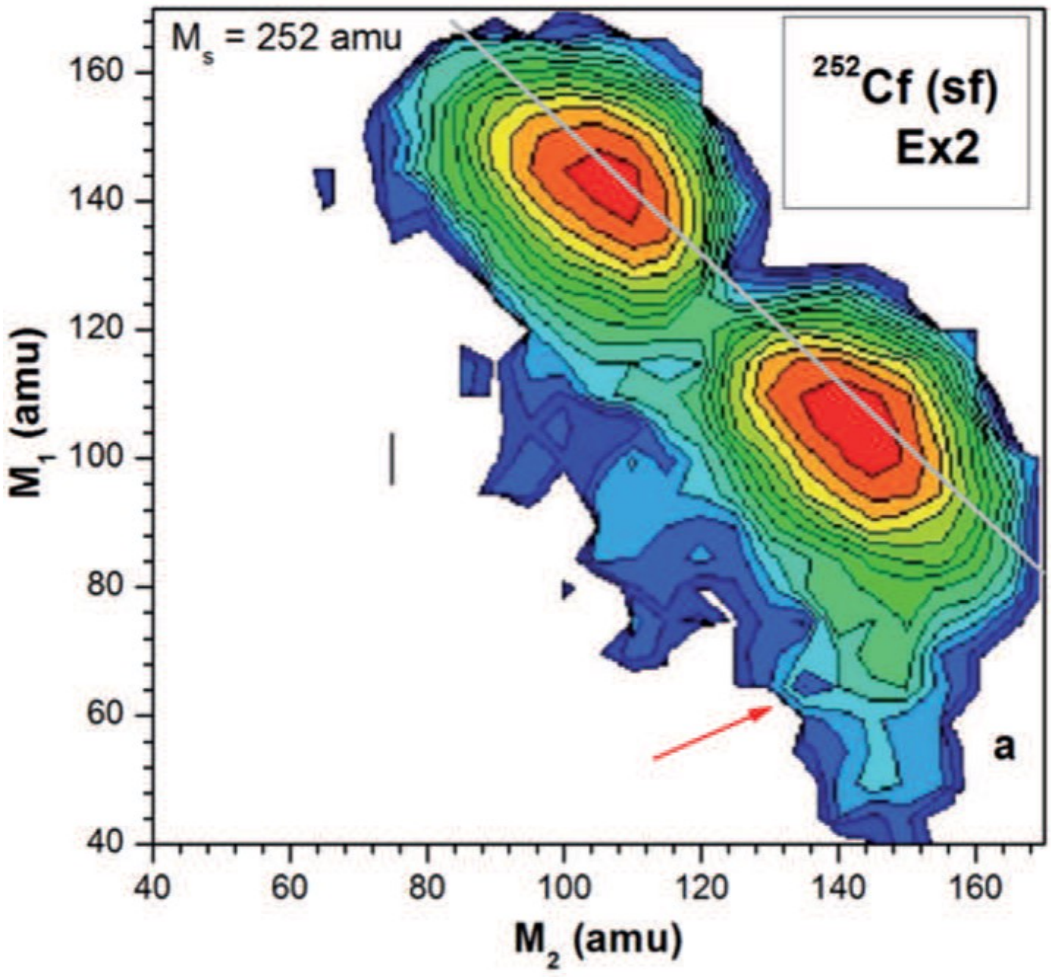

Figure 1.11: Contour map of the mass-mass distribution obtained from the experiment with mini-FOBOS setup using neutrons in coincidence with fission events [27], [40].

1.7. Scope of the Work

A new type of ternary fission decay of low excited heavy nuclei has been discussed above as a new remarkable observation since the discovery of ternary fission. This decay mode is referred to as Collinear Cluster Tri-partition (CCT). It was given this name due to the features observed, that is, the decay partners fly apart almost collinearly, one of the decay partners has a magic nucleon composition and the decay is presumably a ternary process.

The first results where the manifestation of the CCT through a specific bump corresponding to a specific missing mass in the fission fragment mass-mass distribution was observed, have been discussed in this chapter. This bump was observed when the two fragments of the CCT flying towards the same arm of the spectrometer, passes through a dispersive medium, which provided an angular dispersion between them. It is also important to mention that not only the dispersive medium allowed the observation of the bump, but also the blocking structure (grid edges) in the 'stop' detectors of the spectrometers. This deliberately ensured that one of the fragments was blocked. The angular straggling and blocking of one of the fragments allowed the detection of the CCT events.

In chapter 2, different methods of detection in the study of rare decay modes such as the CCT will be discussed. Previous experimental spectrometers that were used in this work will be discussed in the first part of chapter 2. These spectrometers were used to obtain the results discussed earlier and they are based on a double-arm time-of-flight detection system with a radioactive source positioned at the centre of the spectrometer. The first spectrometer to be discussed is the modified-FOBOS spectrometer. This spectrometer produced the first manifestation of CCT shown in Figure 1.2 from the spontaneous fission of ^{252}Cf. The second spectrometer to be discussed is the mini-FOBOS spectrometer. This spectrometer uses the same detector modules as a

modified-FOBOS and it brings a possibility of in-beam measurements. The reaction of $^{235}U(n_{th}, f)$ where the thermal neutrons were delivered by the IBR-2 neutron reactor from the Frank Laboratory of Neutron Physics at the JINR was investigated. The results shown in Figure 1.7 were obtained from this spectrometer.

Until now, the CCT has been revealed using the 'missing mass' approach. It is well understood that the direct detection of all the decay products of the CCT will be a more convincing experimental approach. It is important to note that the direct detection of all three partners brings along its own set of complications as one needs to use a mosaic detection system. Therefore a multi-detector registration system is needed to achieve the direct detection of all the CCT partners.

Such a multi-detector system was first presented in [21], in its design form. This multi-detector system is called COMETA (Correlational Mosaic Energy – Time Array) and will be presented in chapter 2 of this work. It is important to mention that the work presented in this dissertation is a continuation of the work presented in [21]. It was already pointed out in [21] that using a COMETA spectrometer to register heavy ions brings along its own set of experimental challenges. The two major challenges are the known pulse-height defect and plasma delay associated with the registration of energy and time signal respectively. A procedure that takes into account only the pulse-height defect in the calculation of fission fragment's masses was first presented in [21]. An improved data processing procedure that considers both the pulse-height defect and plasma delay in the calculation of fission fragment's masses is presented in chapter 3 of this work. An experiment to test this procedure is also presented in chapter 3. This experiment uses an improved Light Ion Spectrometer for South Africa (LIS-SA) which was first presented in [21].

The COMETA spectrometer to be presented in this work was designed based on similar ideas underpinning the previous spectrometers. A

'neutron belt' was installed around the start detector of the COMETA spectrometer to detect neutrons that are in coincidence with fission events. A special model to determine the optimum configuration of the 'neutron belt' was designed based on the Monte Carlo N-Particle (MCNP) simulation code [41]. This model was first presented in [42] and the experiment to confirm this model and determine the efficiency of the 'neutron belt' is presented in [21]. The results obtained from this model and the best configuration for the 'neutron belt' of the COMETA spectrometer will be discussed in chapter 2 of this work.

The results outlined in the Master's thesis of V.D. Malaza [21] suggested that it is possible to detect all the decay products of the CCT using the COMETA spectrometer. Therefore, the main objective of this work is to use the COMETA spectrometer for the direct detection of all the decay products of the CCT and experimentally confirming the existence of the CCT phenomenon. Improving the data acquisition procedure to include both the pulse-height defect and plasma delay in the calculation of the fission fragment's masses is also one of the objectives of this work.

The main results from the COMETA spectrometer are outlined and discussed in chapter 4. These results include the mass-mass distribution of fission fragments where the CCT is observed as rectangular structures bound by deformed and double magic clusters. These results are compared to the bump presented in chapter 1 and they display a good agreement.

The final chapter presents a conclusion to this work by looking at the few suggested CCT decay scenarios. The study of these scenarios does not form part of this work but it is important to discuss a few of them. Future work where the CCT phenomenon will be confirmed further by using an independent experimental approach which uses a different method of detection will be outlined. This dissertation presents a successful experimental study using a multi-detector registration

system that provides a direct detection of all the CCT products and confirms the existence of the CCT phenomenon.

Chapter 2

Experimental Setups and Techniques

It was mentioned in chapter one that the Collinear Cluster Tri-partition (CCT) phenomenon has been discovered using the missing-mass method. The direct detection of all the decay partners will be a more convincing experimental approach in the investigation of the CCT phenomenon. This chapter outlines a new experimental setup designed to achieve the direct detection of all the three decay partners of the CCT.

The different methods of measurement that can be used to study fission decays of nuclei will be discussed first. The experimental setups that were used to obtain the results discussed in chapter 1 will be fully described in this chapter. A setup referred to as Correlation Mosaic Energy – Time Array (COMETA), which is designed to achieve the direct detection of all the decay products of the CCT will be presented. The main outcome of this work is to present the design, testing and use of the COMETA to confirm the existence of the CCT by achieving the direct detection all the decay products. As mentioned in chapter 1 this spectrometer was first presented in [21].

2.1. Methods of measurements

The important parameters to be determined in the study of fission fragments, amongst others, includes the mass distribution, nuclear charge, kinetic energy and radioactive properties. There are several measurement methods that can be used to measure these parameters. Four of these methods that are commonly used in the double-arm time-of-flight spectrometers to study the CCT are listed below:

2.1.1. The 2E - Method

In the 2E Method, only the energies of the fission fragments that are detected in the two opposite arms of the spectrometer are measured. In this method, a spectrometer should at least have a detector capable of measuring the energy of heavy ions in each arm. This method only achieves the measurement of kinetic energy of fission fragments and cannot be used independently.

2.1.2. The 2V - Method

This method measures the velocities of the two fission fragments that are detected in the two arms of the spectrometer. To achieve such measurement, the spectrometer should have at least two detectors capable of measuring the time-of-flight for the heavy ions in each arm. With the distance between the detectors known, and the time signals being registered accordingly, the velocity of the fission fragments can be calculated. If the mass of the initial nucleus and the velocities of the fission fragments are known, the mass of the detected fission fragments can be calculated from the momentum conversation laws. Thus, this method brings the possibility of calculating the mass of the fission fragments.

2.1.3. The VE - Method

This method measures the velocity and the energy of only one fission fragment. It requires the spectrometer to have at least one detector that can measure time and one detector capable of measuring energy of heavy ions. Only one arm of the spectrometer can be used in this method. When the velocity and the energy of the detected fission fragment is known, its mass can be calculated using the nonrelativistic energy equation

$$m = \frac{kE}{v^2} \tag{2.1}$$

with $k = 1.9297$ (mass dimensions to be a.m.u.). This method provides the possibility of calculating the mass of the fission fragments.

2.1.4. The 2V-2E Method

This is the method mostly used in the double arm time-of-flights spectrometers. This method involves the measurement of the velocity and the energy of both fission fragments that are detected in both arms of the spectrometer. This method requires that the spectrometer should have at least two detectors that measure the time and at least one detector that measures the energy in each arm. This method is the combination of all the other methods mentioned above. It also provides the option of calculating the mass of both the fission fragments detected in the two arms of the spectrometer.

The spectrometers to be discussed below were designed based on the above-mentioned methods of measurement. A choice of a particular spectrometer and its modification is determined by the choice of the measurement method to be used and it determines the experimental procedure. In the spectrometers to be discussed below, all the above methods can be used depending on the main goal of the experiment.

2.2. Previous experimental setup used in the study of CCT

After the realization of the possibility to observe the ternary fission experimentally using the double arm time-of-flight spectrometers, a number of experiments were performed at the Flerov Laboratory of Nuclear Reaction (FLNR) at JINR. Several spectrometers were designed to perform these experiments. These spectrometers include the so-called modified-FOBOS and mini-FOBOS spectrometers. The modified-FOBOS was mainly used to study the spontaneous fission of ^{252}Cf and the mini-FOBOS was mainly for the study of the non-spontaneous fission of ^{235}U. Some results generated by these spectrometers have been discussed in chapter 1.

The main goal of this dissertation is to present a new experimental spectrometer designed to detect all the decay products of the CCT directly. The modified-FOBOS and the mini-FOBOS will be briefly discussed and the COMETA spectrometer which has been designed from the ideas of these spectrometers in order to achieve the direct detection of all the CCT partners, will be outlined.

2.2.1. Modified-FOBOS Spectrometer

The modified-FOBOS spectrometer was constructed from the elements of the 4π spectrometer referred to as FOBOS [31]. The FOBOS setup was installed at the FLNR at JINR in Russia. The FOBOS spectrometer was designed to study the kinematics of nuclear reactions and it can register charged reaction products ranging from protons to heavy ions. The detector system of the FOBOS spectrometer consists of three consecutive shells for the detection of particles. The inner shell consists of 30 Position Sensitive Avalanche Counters (PSAC). The flight path of $50\ cm$ is measured from the front section of the PSAC to the start detector. The PSAC and the flight path provide the possibility to

measure the time-of-flight (TOF) and the (x, y) coordinates for the fragments.

The second detector shell attached to the PSAC from the inner part of the detector is the Bragg Ionization Chamber (BIC). The BIC measures the stopping power of the fission fragments along their path within the gas chamber. From the measured TOF and the residual energy obtained from the stopping power, the mass of the fragments can be calculated. This is achieved when the energy lost by the fission fragment penetrating the detector is taken into consideration. A third scintillation shell of $CsI(TI)$ detectors is positioned behind the BICs. This shell is sensitive to the fast ionizing Light Charged Particles (LCP). For the experiments performed using ^{252}Cf source, the third shell was not used.

The FOBOS spectrometer was designed to be fully flexible for even exclusive measurements. The coordinate information received from the PSAC can be used together with TOF to determine the momentum vector for each fragment, event by event. The general layout of the FOBOS spectrometer is shown in Figure 2.1 and the structure of the detector module is shown in Figure 2.2.

The experimental results discussed in section 1.6.1 from the spontaneous reaction of ^{252}Cf were obtained using a modified-FOBOS spectrometer. This spectrometer includes some modifications that were made to the original FOBOS spectrometer. The main reason for modifying the FOBOS spectrometer was to improve the quality of the data. These modifications include a development of a new start detector with the ^{252}Cf source installed inside the detector. Another modification involves the installation of a "neutron belt" which comprises of neutron detectors positioned as a belt around the start detector. The main aim of the "neutron belt" was to detect neutrons in coincidence with fission events. This was aimed at verifying the high neutron multiplicity in the CCT events. Due to high energy loss in the gas-filled detectors, a special

technique of calibrating the FOBOS gas-filled detectors was also designed.

In general, the modified-FOBOS spectrometer is a double arm TOF-E (time-of-flight - energy) spectrometer. This spectrometer resulted from the modification of the FOBOS spectrometer and each arm consists of five big and one small standard FOBOS detector modules. Each detector module consists of PSAC and BIC. This spectrometer measures both the energy and the velocity of the fission fragments and it covers approximately 29% of the hemisphere in each arm. In order to provide a precise start signal for the TOF measurement, a wide-aperture 'start' detector that can hold the radioactive source inside was used.

The scheme of the experiment that was used in the modified-FOBOS spectrometer to perform the coincidence measurement of the decay products of the ^{252}Cf is shown in Figure 2.4. As discussed in section 1.6.1, this measurement was performed under the missing-mass approach. As illustrated in Figure 2.5, the heavy fragment flies in the opposite direction to the two light fragments. The two light fragments are scattered by an angle of approximately 1^{o} after passing the source backing. One of the fragments will hit the supporting grid (shown in Figure 2.6). That will be the missing fragment and the other one will be detected.

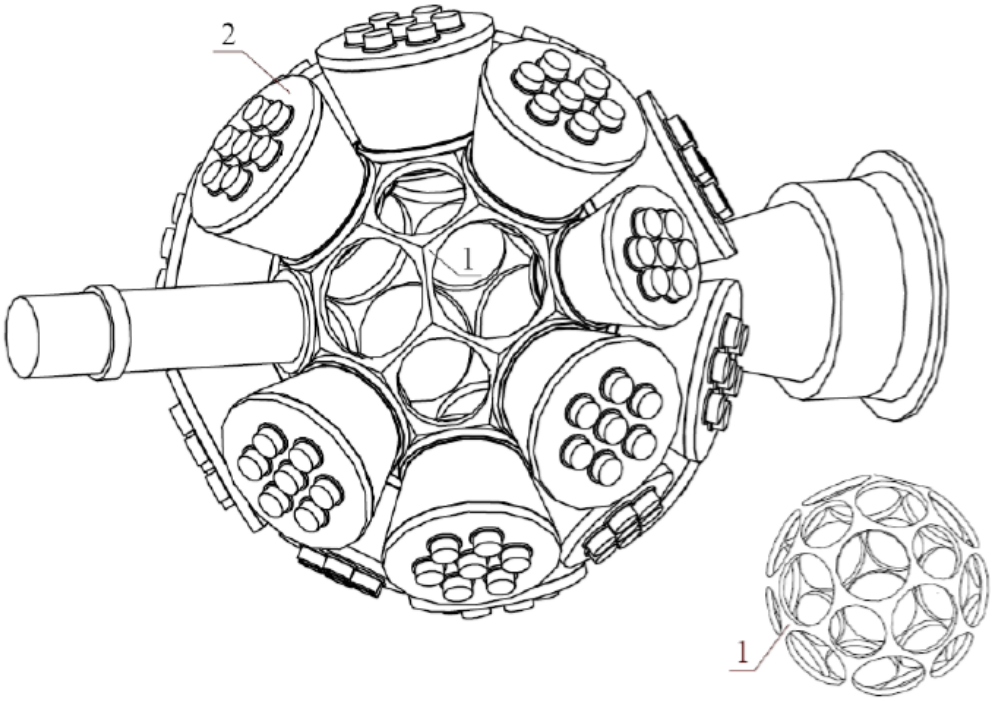

Figure 2.1: General layout of the FOBOS Spectrometer: 1. Monolithic Skeleton, 2. Detection module, [5].

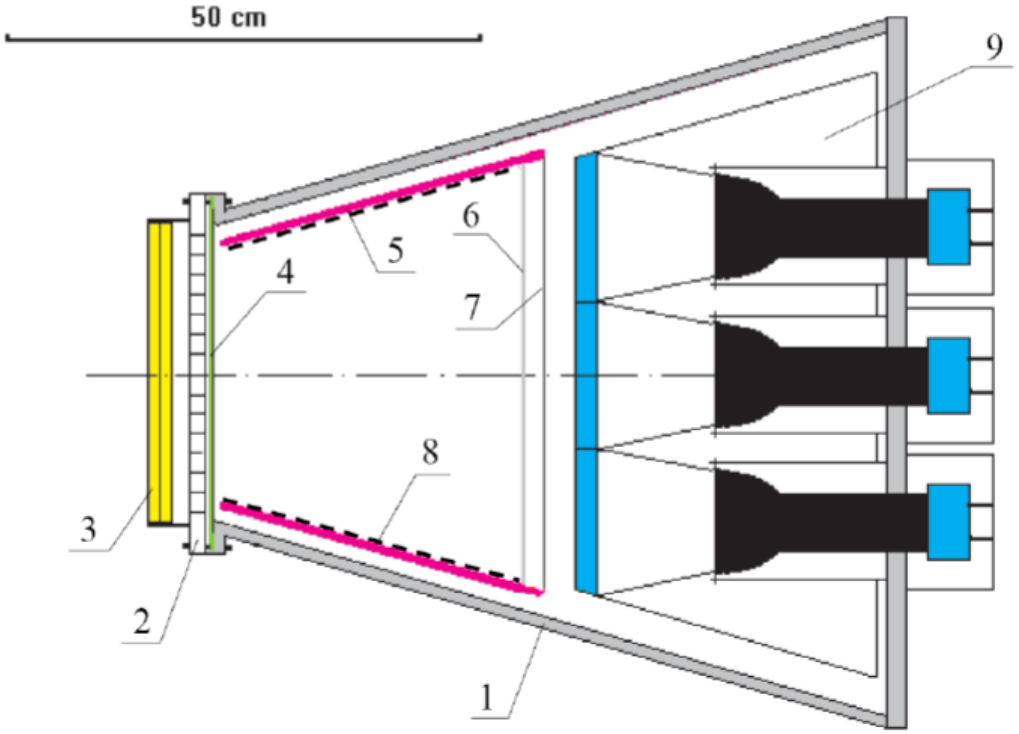

Figure 2.2: Detector module for the FOBOS spectrometer: 1 outer part of the BIC, 2. Supporting grid for the entrance window, 3. PSAC, 4. Thin foil, 5. Teflon cone, 6. Grid, 7. Anode, 8. HV divider, 9. Scintillation shell [5].

The modified-FOBOS spectrometer provided the opportunity to test a specific CCT model. This mode is the three-body chain-like configuration at scission point which was initially suggested in [29]. This means that after scission the two outer fragments fly apart along the chain axis and the third one is presumably at rest. The third fragment is expected to be an isotropic source of post-scission neutrons of high multiplicity (~10) in the laboratory system. The neutrons emitted by the moving fragments are focused along the fission axis. Therefore, a 'neutron belt' was assembled in a plane that is perpendicular to the symmetry of the fission fragments and around the fission source.

The "neutron belt" for the modified-FOBOS spectrometer consists of 140 hexagonal neutron detector modules [43]. The neutron detectors will be discussed in section 2.3.5 of this chapter. The schematic view and the picture of the modified-FOBOS spectrometer with the 'neutron belt' are shown in Figure 2.3 and Figure 2.7 respectively.

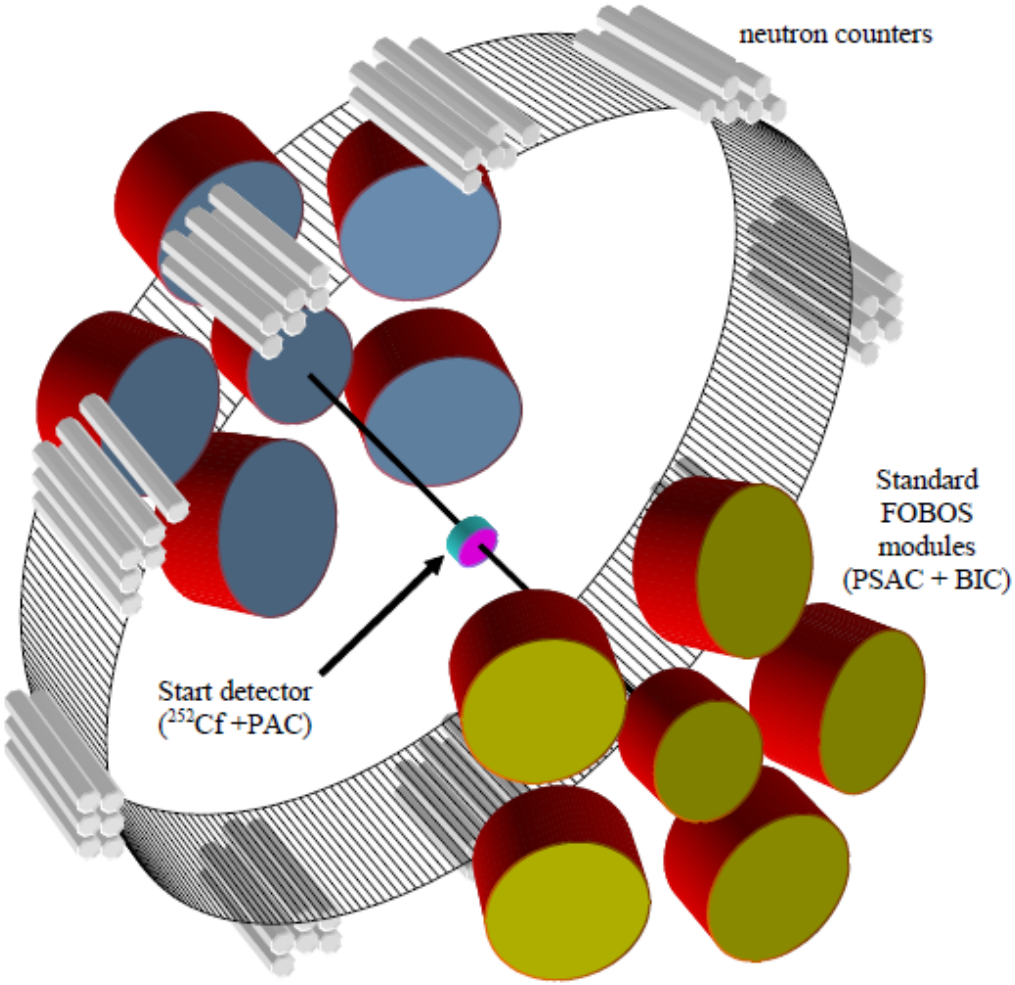

Figure 2.3: Schematic view of the modified-FOBOS spectrometer [5].

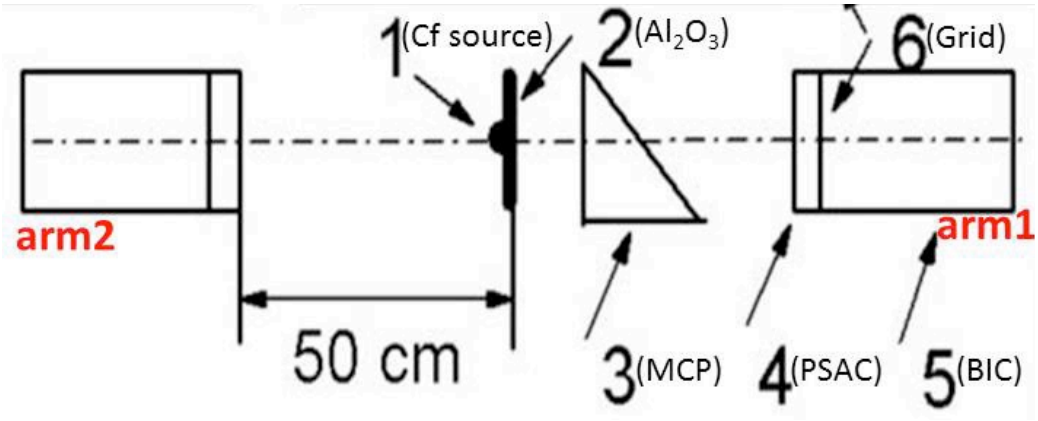

Figure 2.4: A schematic arrangement of the detectors used in the modified-FOBOS Spectrometer [5].

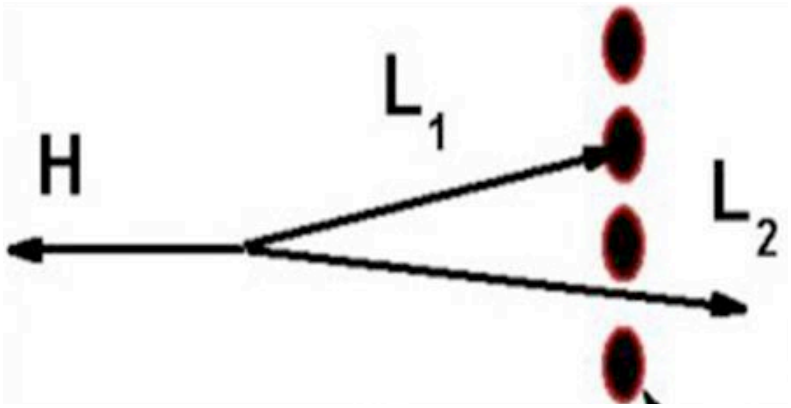

Figure 2.5: The trajectory of the decay products of the CCT. The heavy fragment flies in the opposite direction and two light fragments flying in the same direction undergoes divergence after passing through the source backing. Fragment L_1 hits the grid (Figure 2.6) and hence becomes a missing fragment while L_2 is detected [5].

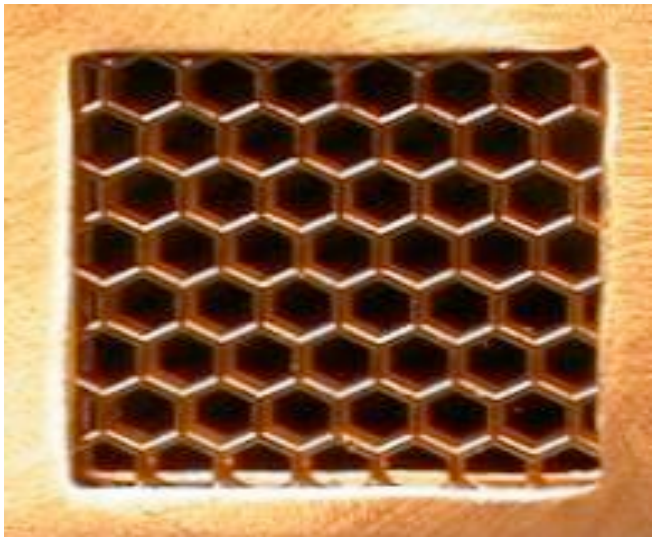

Figure 2.6: Grid that is responsible for the missing mass installed in front of the detectors [5].

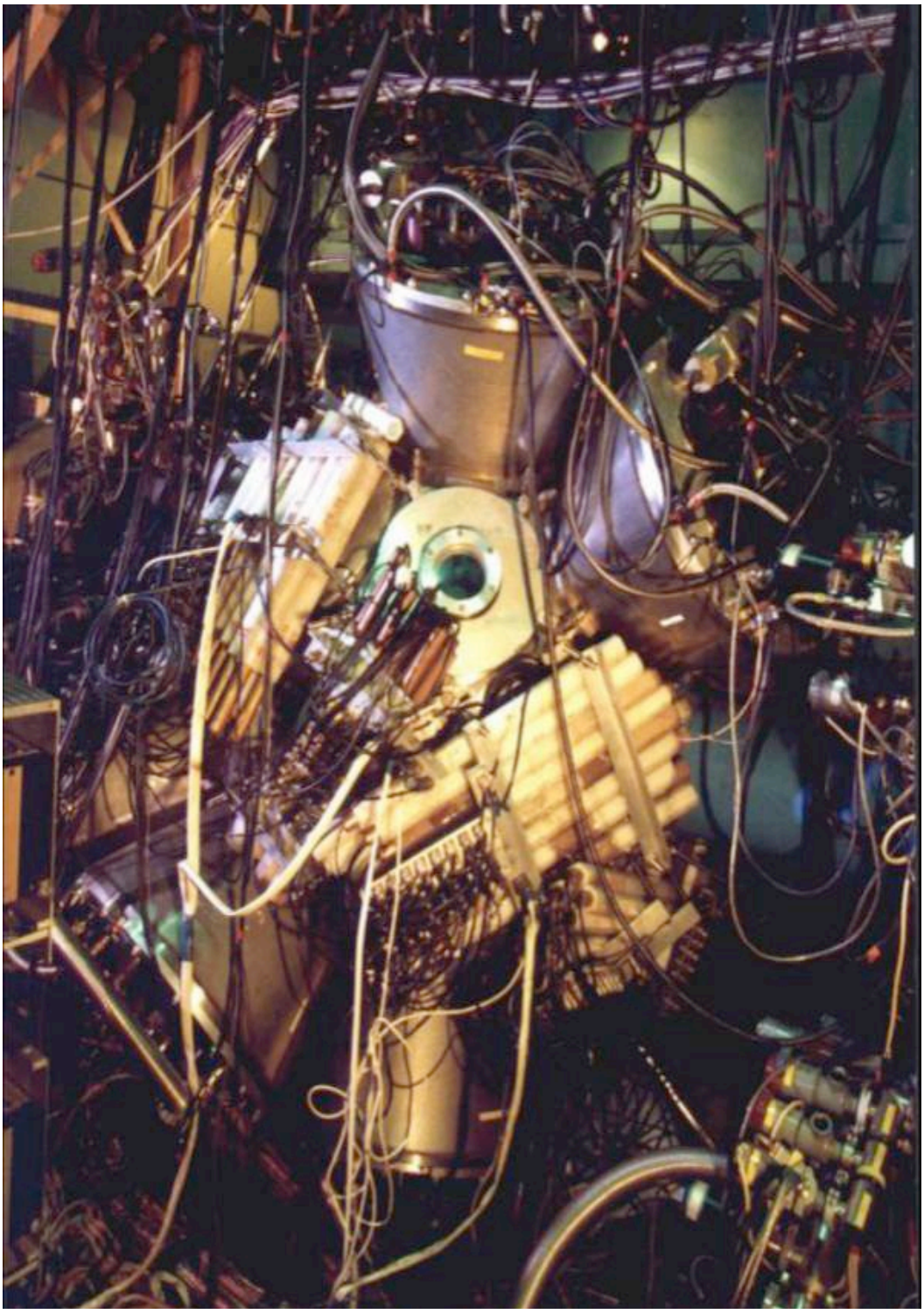

Figure 2.7: Picture showing the modified-FOBOS spectrometer with neutron belt [5].

2.2.2. Mini-FOBOS Spectrometer

After the results were obtained using the modified-FOBOS spectrometer to study the spontaneous decay of ^{252}Cf, another spectrometer was developed to investigate the non-spontaneous decay in nuclear fission. This spectrometer was called the mini-FOBOS because the same ideas and main modules of the FOBOS spectrometer were used on a small scale. The main idea of this setup was to investigate the CCT using in-beam experimental measurements. Specifically for the results discussed in section 1.6.2, the mini-FOBOS was used to investigate the fission induced by thermal neutrons in $^{235}U(n_{th}, f)$ reaction. The beam of thermal neutrons was delivered by the IBR-2 reactor from the Frank Laboratory of Neutron Physics at JINR. The mini-FOBOS spectrometer is flexible enough such that it can also be used for spontaneous fission reactions.

The mini-FOBOS is also a double-arm time-of-flight (TOF) spectrometer. The general idea of the mini-FOBOS is using a small reaction chamber which can be unique for each experiment and still maintain the same detector modules as the modified-FOBOS. The flight path of 50 cm has been kept the same, thus all the resolution parameters of the mini-FOBOS and the modified-FOBOS are the same.

The scheme of the mini-FOBOS spectrometer for the experiment where the reaction of $^{235}U(n_{th}, f)$ was investigated is shown in Figure 2.8. The start detector was modified to be a symmetric avalanche counter with a target installed inside the detector. The target was prepared by evaporating 100 $\mu g/cm^2$ of ^{235}U on a Al_2O_3 backing of 50 $\mu g/cm^2$. The stop detectors used were the normal modified-FOBOS modules which consist of Position Sensitive Avalanche Counters (PSAC) and the Bragg Ionization Chambers (BIC).

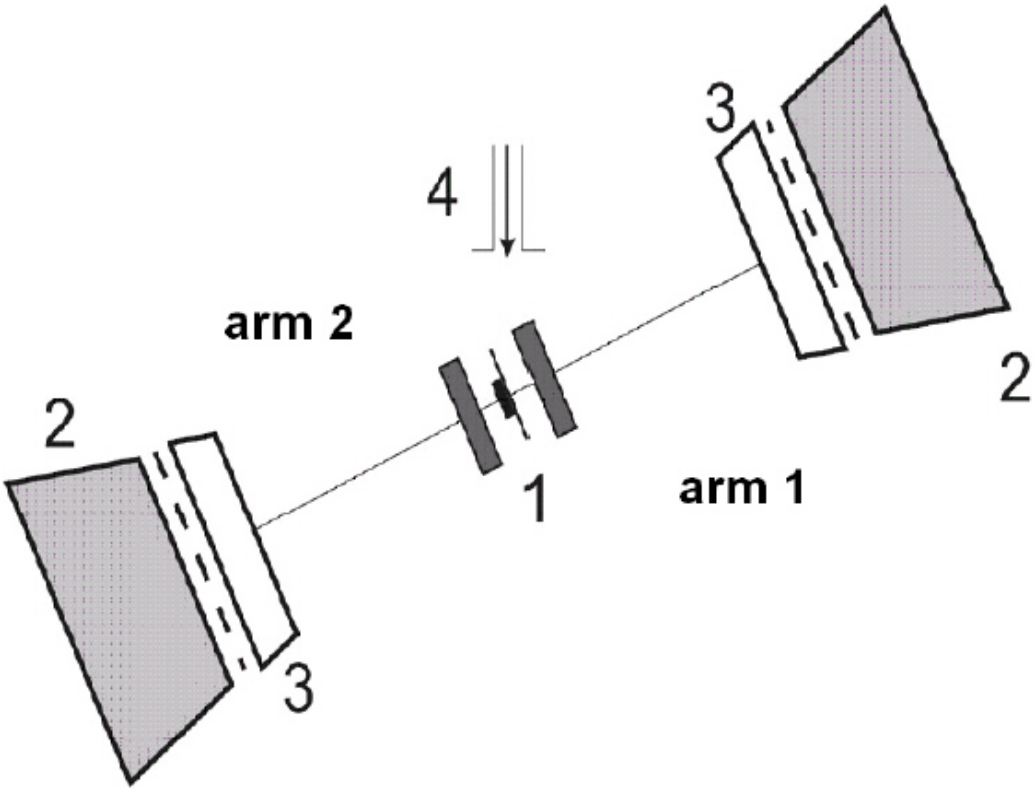

Figure 2.8: Schematic view of the mini-FOBOS spectrometer showing 1-'start' avalanche counter, 2-BIC, 3-PSAC and 4-beam of thermal neutrons [5].

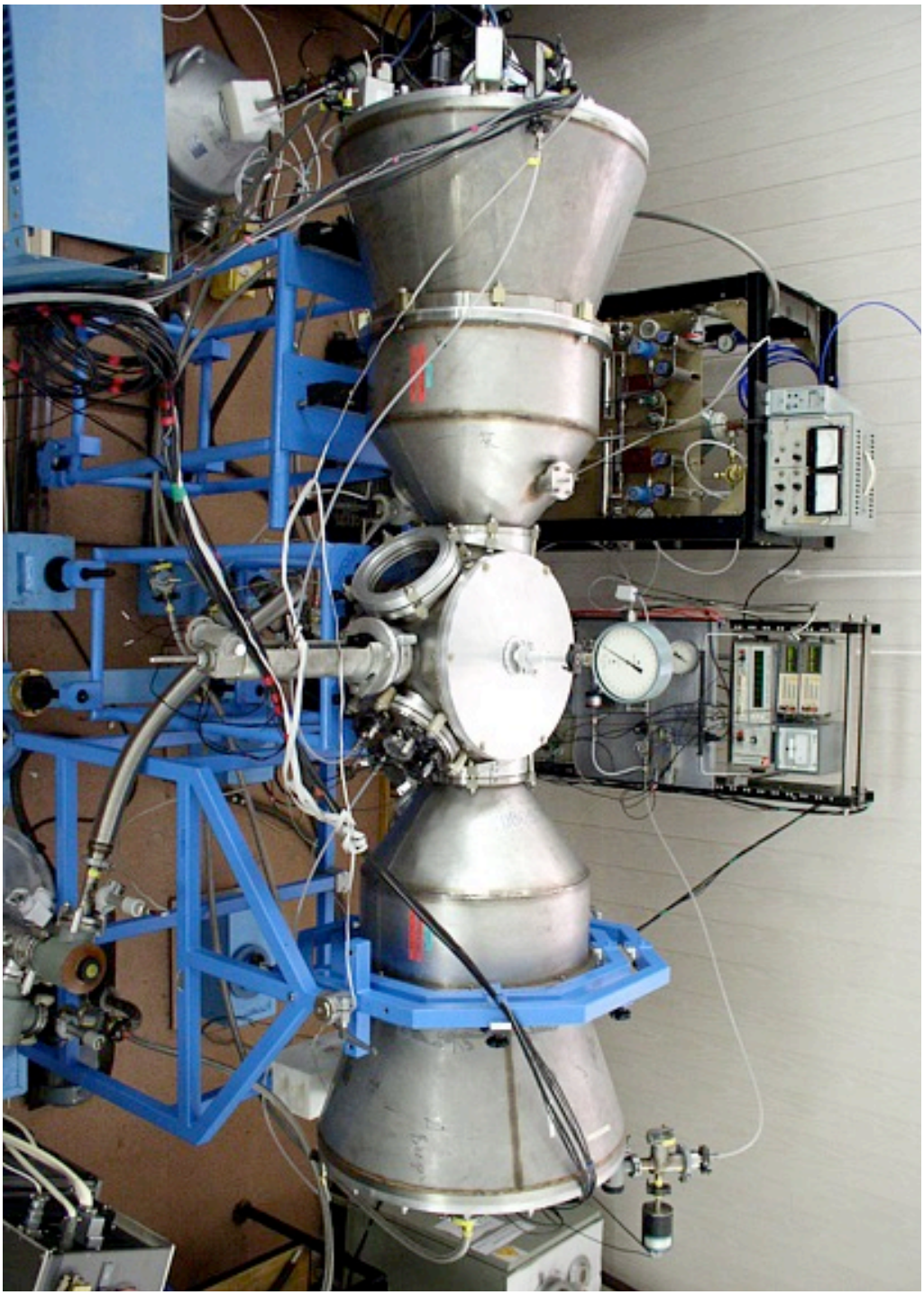

Figure 2.9: Picture of the mini-FOBOS spectrometer.

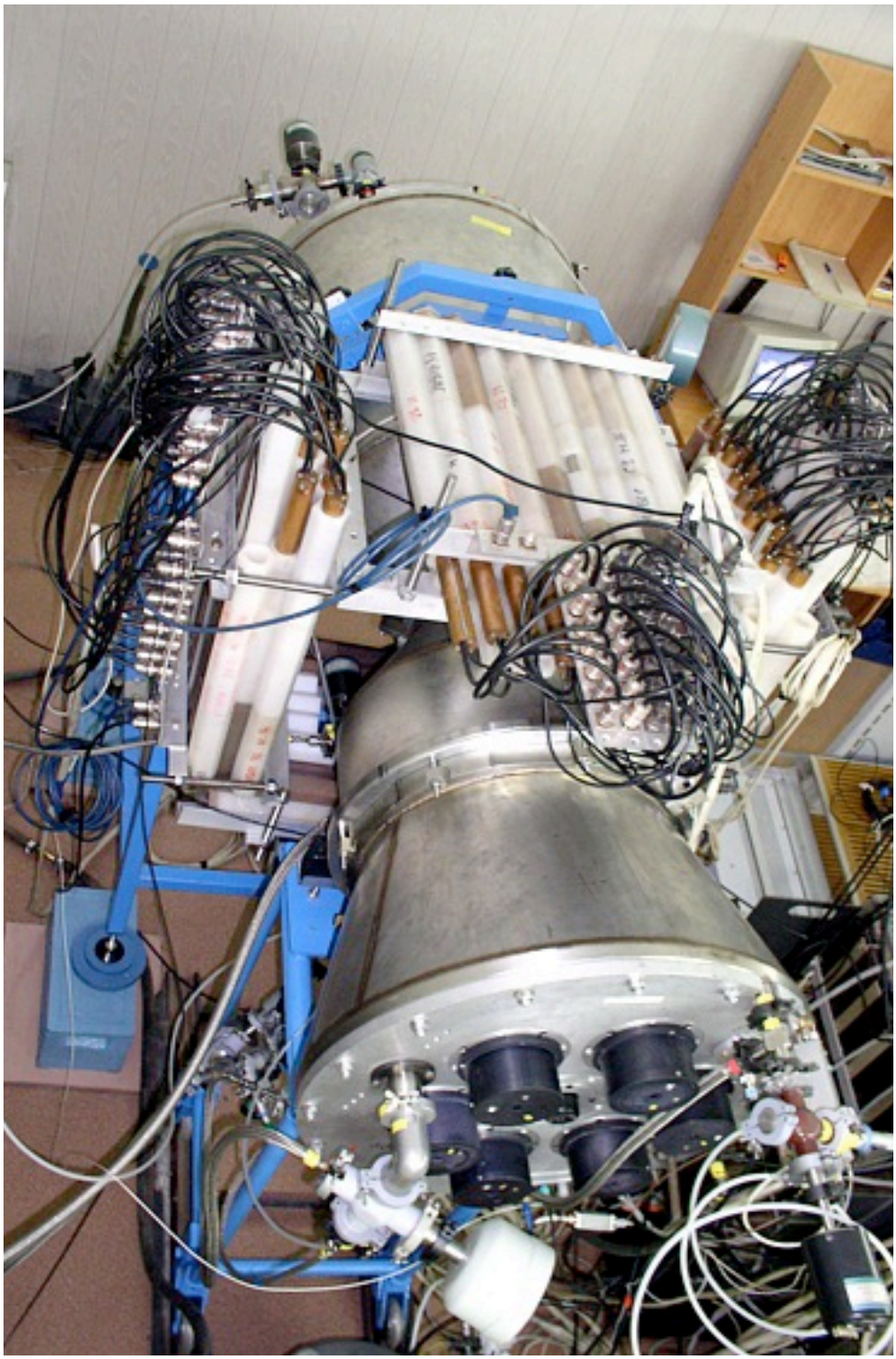

Figure 2.10: Picture of the mini-FOBOS spectrometer with 'neutron belt' installed.

It was mentioned in chapter 1 that apart from measuring the TOF and energy of the fission fragments, two additional parameters that are sensitive to the charge of the fission fragments were measured. These parameters are the drift time between the BIC and the and the specific energy loss in the PSAC. The picture of the mini-FOBOS spectrometer is shown in Figure 2.9.

Depending on the requirement for the experiment, the mini-FOBOS spectrometer provides an opportunity and flexibility to install other detectors. For instance, in order to increase the possibility to detect the CCT events, high-efficiency neutron counters were installed as a belt around the start detector. This was done for the experiment involving a spontaneous fission ^{252}Cf source. The picture of the mini-FOBOS spectrometer with the 'neutron belt' installed is shown in Figure 2.10.

2.3. COMETA Setup

The results that revealed the CCT phenomena discussed in chapter 1 were obtained using the missing-mass method outlined in [44] and [45]. Several other experiments were performed in the past to investigate different nuclear systems over a wide range of excitations. All these experiments showed that a direct detection of all the decay partners of the CCT will be a more convincing experimental approach. It is important to note that the masses defining the CCT mode under investigation differ radically. This means that one of the masses is very light while the other one is very heavy. Therefore, there is a need for a more complex spectrometer with high granularity capable of detecting all the decay partners of the CCT.

To increase the possibility of selecting the CCT events in a more reliable way by means of a direct detection of all the decay products, a spectrometer consisting of a mosaic of PIN-diodes referred to as COMETA (Correlation Mosaic Energy – Time Array) spectrometer was brought into operation at FLNR. The entire process of designing, testing

and using this spectrometer in the study of CCT is presented in this work. In this section, a full description of the COMETA spectrometer is given and the results obtained from experiments performed using the COMETA will be presented in chapter 4.

2.3.1. Description of the COMETA Setup

The COMETA spectrometer was first presented in [21], while it was still in its design stage. The COMETA is a double arm time-of-flight spectrometer that consists of a Micro-Channel Plate (MCP) Time Based Detector, two mosaics of eight PIN diodes detectors each and 28 ^{3}He filled neutron counters that are positioned as a belt around the MCP time based detector. The Micro-Channel Plate time based detector, in this dissertation, will be referred to as MCP detector.

The MCP detector of the COMETA is designed in a way that the ^{252}Cf radioactive source is attached in front of the detector and it provides the 'start' time signal for the fission fragments. Each PIN diode for the COMETA setup provides both the energy and time signals for the detected fission fragments. The distance between the MCP detector and the mosaics in each arm is 15 cm. A schematic view of the COMETA spectrometer is shown in Figure 2.11 and the picture of the COMETA with the 'neutron belt' is shown in Figure 2.12.

2.3.2. PIN Diode Detectors

The PIN diode detector is a diode that is made out of a silicon structure that consist of a p-type diffusion layer, an intrinsic region and an n-type diffusion layer, that is where the acronym PIN originates. The intrinsic region has a high resistivity. The arrangement of the PIN diode is such that the p-type layer is in front of the silicon intrinsic layer which is then followed by the n-type layer. The use of PIN diodes for detecting ionizing radiation such as heavy ions is outlined in [46].

The COMETA spectrometer presented in this dissertation consists of 16 PIN diode detectors. Each arm comprises of 8 PIN diodes installed as an array. The COMETA spectrometer comes with a possibility of using up to 54 PIN diodes depending on the requirement for the experiment. The size of each PIN diode is $20\,mm \times 20\,mm$ but the working area of the PIN diode is $18\,mm \times 18\,mm$ due to the supporting grid that holds the PIN diodes as an array in each arm. The dead layer thickness is $0.01\,\mu m$. The dead layer of the PIN diode is defined as a region where no ionization is produced. The total time taken to deliver an output signal at an operation voltage of $200\,V$ is $5\,ns$. The picture and the schematic view of the PIN diode are shown in Figure 2.13 and Figure 2.14 respectively.

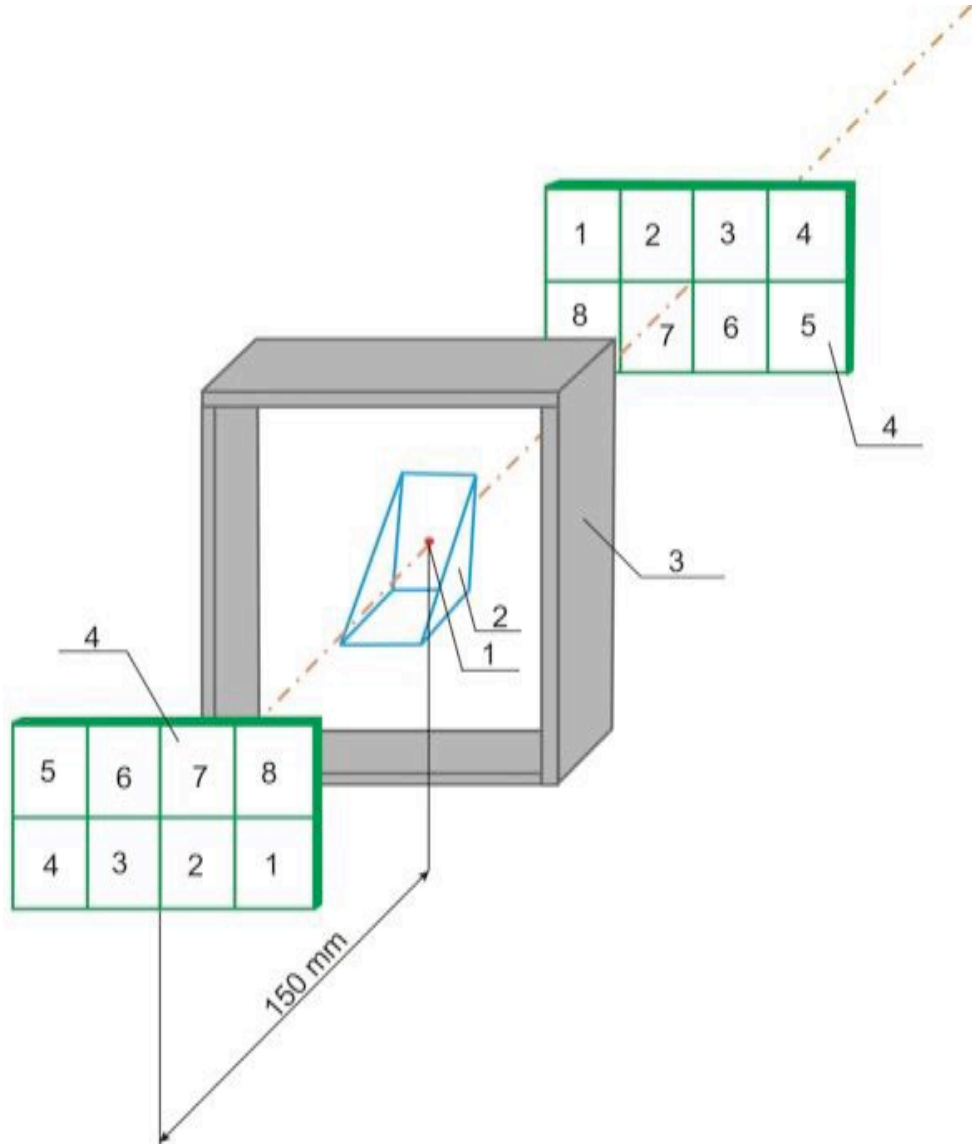

Figure 2.11: Schematic view of the COMETA setup showing the mosaics of PIN diodes (4), MCP Time Based detector (2) with ^{252}Cf source (1) installed inside, and a neutron belt (3) that consists of 28 ^{3}He filled neutron detectors [21].

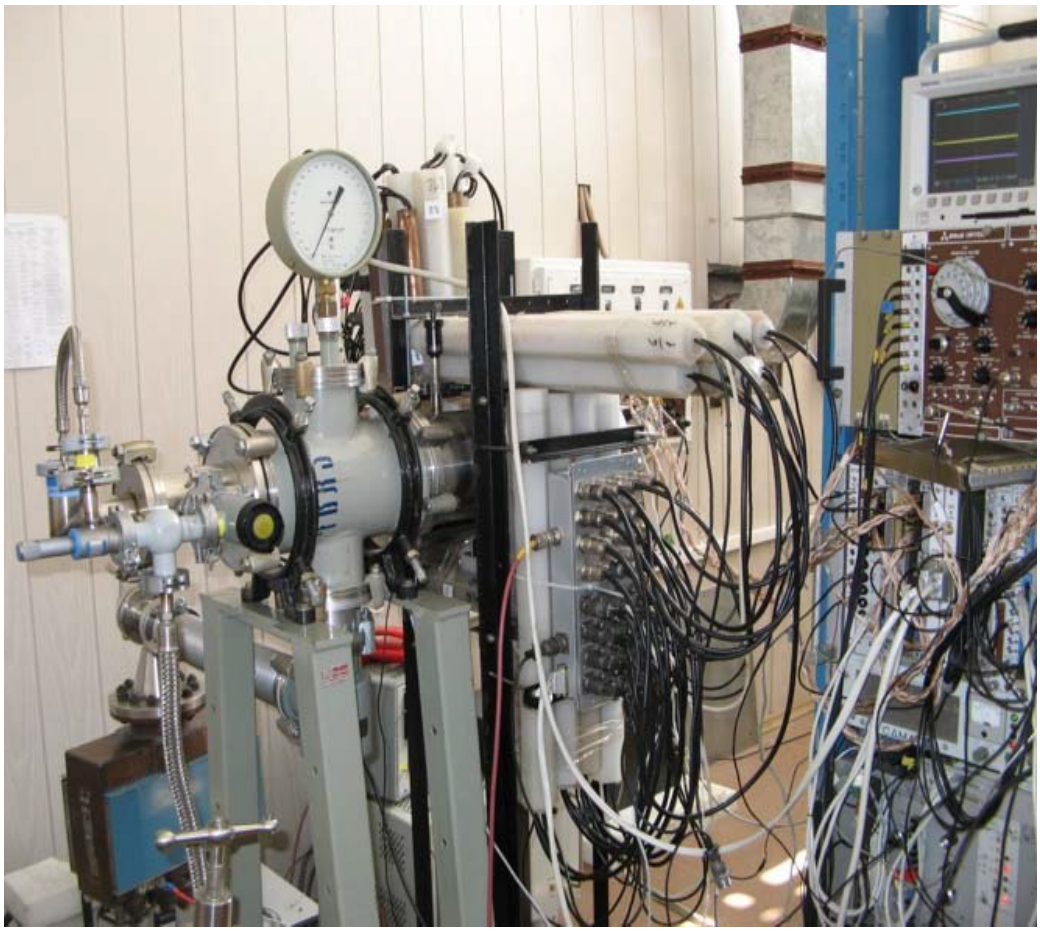

Figure 2.12: Picture of the COMETA setup and the 'neutron belt' installed around the start detector of the COMETA setup [21].

2.3.3. Micro-Channel Plate Time Based Detectors

When the time-of-flight (TOF) and energy measurements are combined in an experiment involving heavy ions, there are two important requirements: (a) a very good time resolution for both "start" and "stop" detector, (b) the start detector must have less influence on the ions. The second point is very important, especially when heavy ions ($A \geq 40$) with low energies ($E/A \leq 1 MeV/amu$) are measured [47].

The above-mentioned conditions can be satisfied by using the Micro-Channel Plate (MCP) electron multipliers [48], referred to, in this work, as MCP detector, to measure the time signal. In the COMETA spectrometer the MCP detector is used only as a start detector. The possibility of using such detectors to measure the TOF is available on the COMETA but this is used in another spectrometer called LIS-SA to be discussed in chapter 3.

The MCP detector consists of a conversion foil, accelerating grid, electrostatic mirror and two Micro-Channel plates (MCP) that are arranged as a chevron configuration assembly. Such a detector was first presented in [49]. The simulated model of the MCP detector is shown in Figure 2.15 and an actual picture of MCP detector is shown in Figure 2.19. The chevron configuration assembly of the two MCPs installed in the MCP based time detector of the COMETA spectrometer is shown in Figure 2.16.

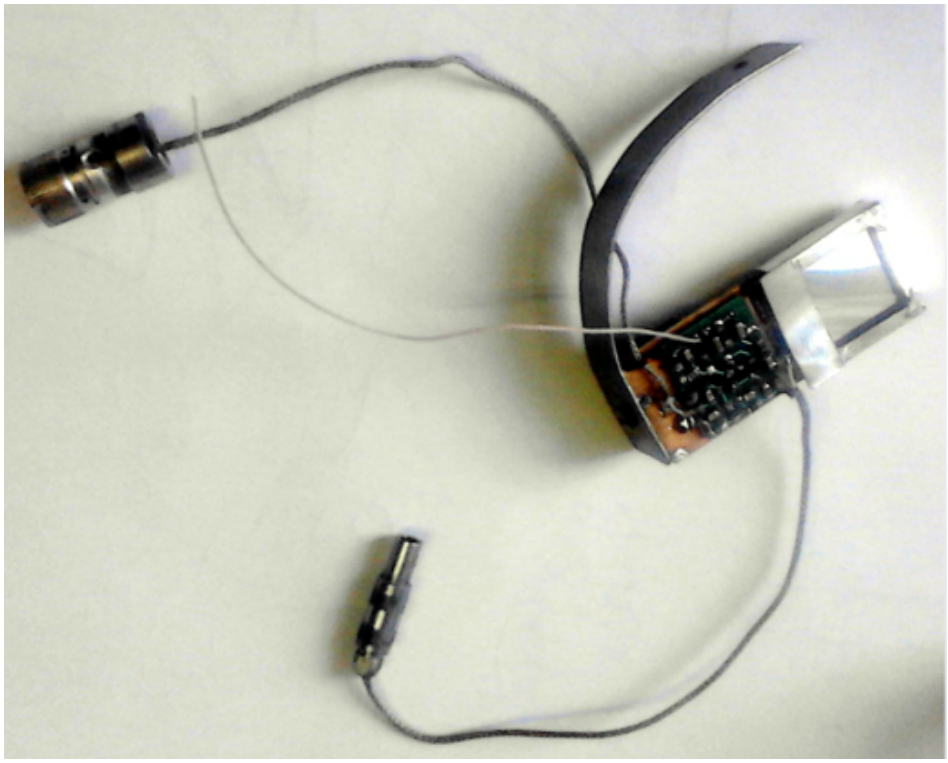

Figure 2.13: Picture of one PIN diode detector.

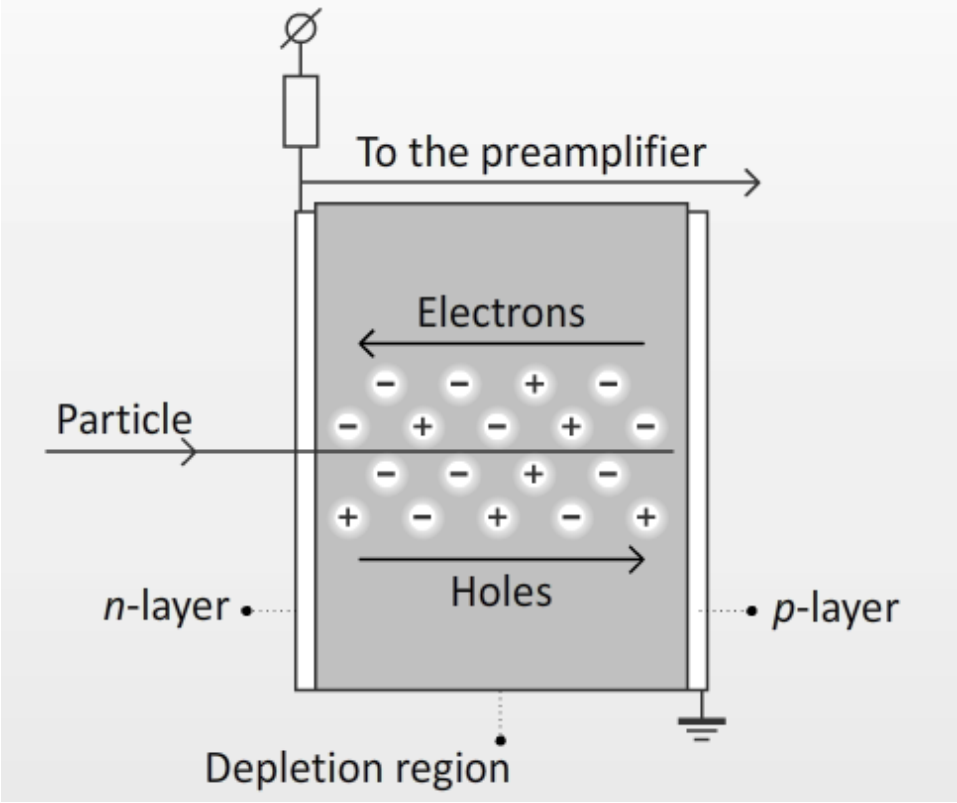

Figure 2.14: Schematic view of the PIN diode detector.

(a) The operation principle of the MCP detector

The detection principle of the MCP detector is based on the registration of secondary electrons that are emitted when the heavy ion (or charged particle) passes through the thin foil. A schematic view that shows how the MCP detector operates is shown in Figure 2.17. The thin foil is mounted perpendicular to the direction of the incoming ion. When the ion passes through the foil, electrons are emitted and scattered away from the foil. The emitted electrons are deflected by an angle of 90^o towards the MCP using an electrostatic mirror.

The electrostatic mirror is made out of thin copper wires to form two parallel grids that are inclined at an angle of 45^o. The emitted electrons are accelerated towards the MCP which is a cellular structure made out of glass tubes (channels) with an inner semi-conductive surface. The inner semi-conductive surface has a resistance of $20 - 1000\ M\Omega$. This means that the MCP is an assembly of a large number of channel electron multipliers.

When an incident electron falls into the channel, more electrons are knocked out by the walls of the channel. The knocked-out electrons are then accelerated by the electric field that is created from the voltage applied to the ends of the channel. These secondary electrons fly in a parabolic path until they hit the wall of the channel and knock out even more secondary electrons. This process goes on repeatedly creating an electron avalanche. A scheme showing the operation of the MCPs installed in the MCP detector is shown in Figure 2.18. Table 2-1 below shows some parameters of the MCP detector that are important for this work [48].

Table 2-1: Parameters of the MCP detector.

Parameter	**Value**
Diameter of a working area	26.0 mm
Thickness of the working area	0.38 mm
Channel diameter	10 μm
Spacing of the grid (channel nodes)	12 μm
Transparency	60 %
Voltage at amplification	1100 V

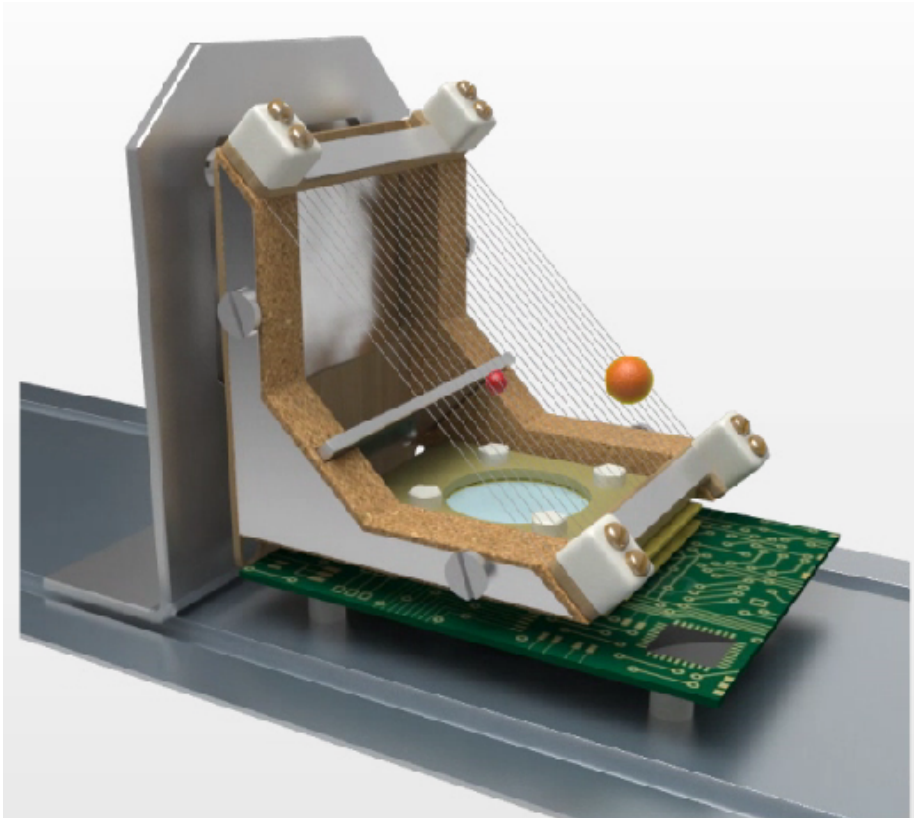

Figure 2.15: Simulated model of the MCP based time detector.

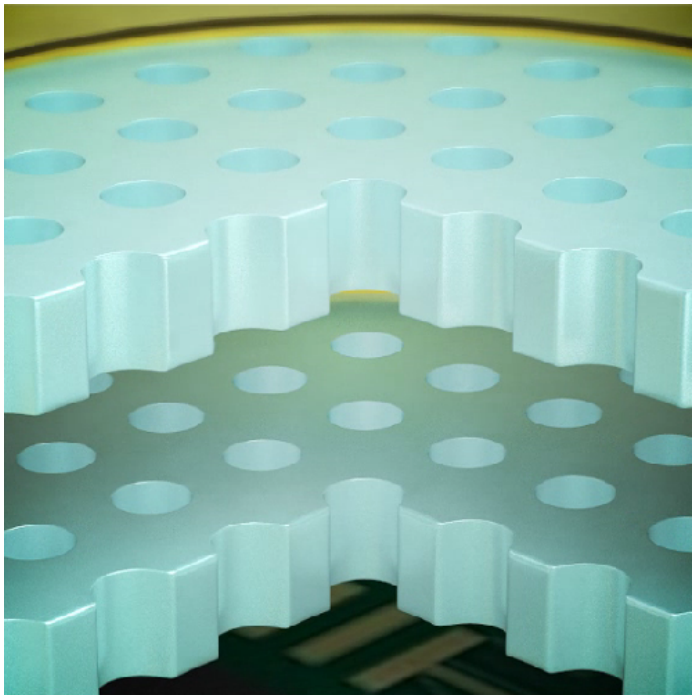

Figure 2.16: Chevron configuration assembly of the two MCPs used in the MCP based time detector.

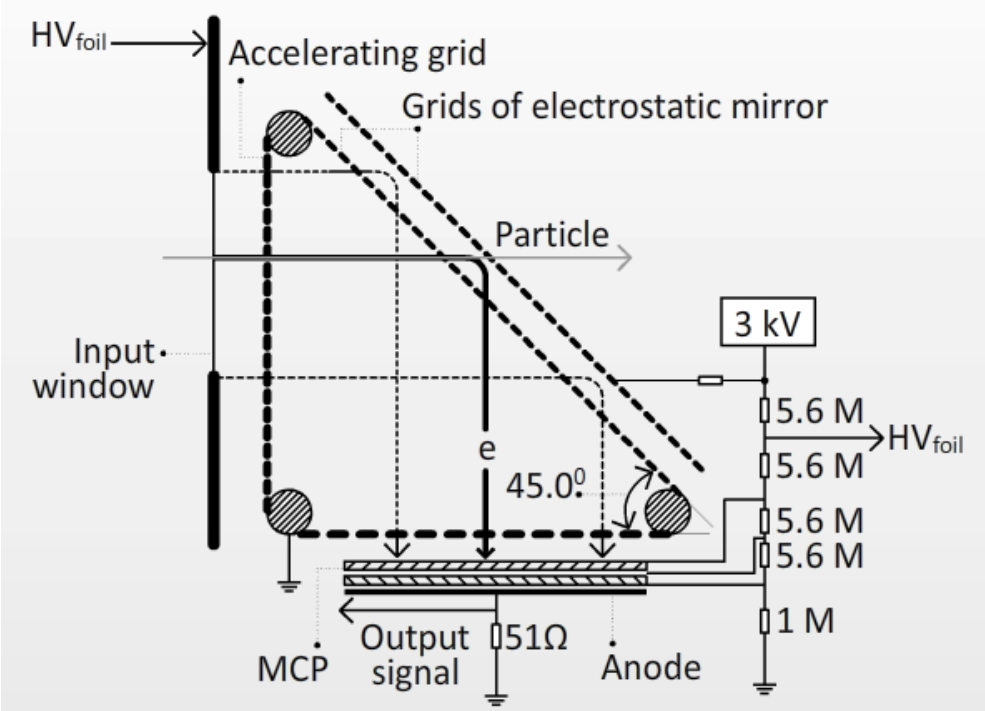

Figure 2.17: The schematic view that shows how the MCP detects the heavy ions passing through via the scattered electrons [48].

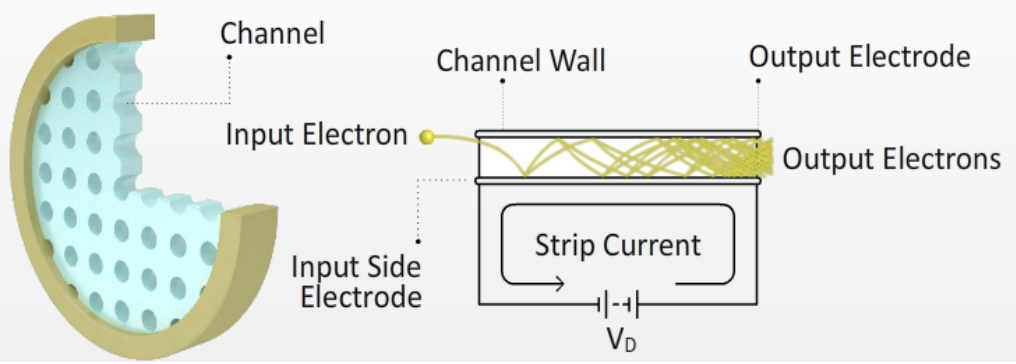

Figure 2.18: The schematic view that shows how the electrons scattered from the heavy ion get detected by the MCP plate of the MCP detector [48].

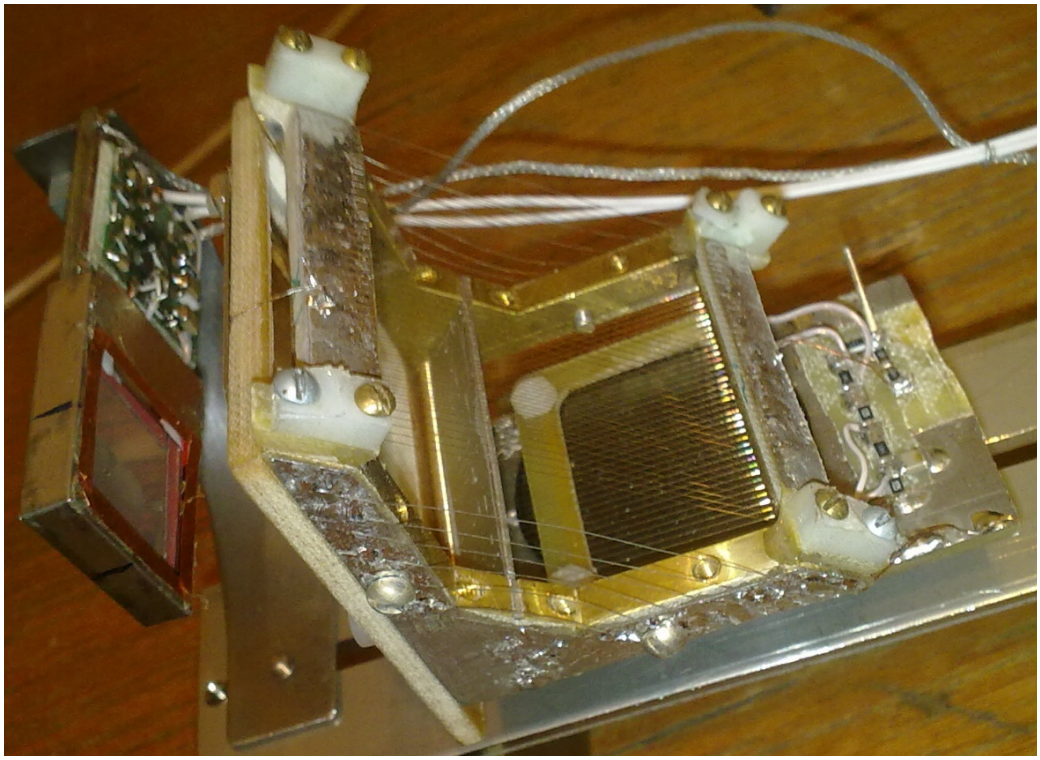

Figure 2.19: Picture of the MCP time-based detector and the PIN diode attached behind the MCP.

2.3.4. Radioactive Source

The COMETA spectrometer can be used to study almost any radioactive source capable to disintegrate into heavy ions, fission fragments or alpha particles. In general, the setup was designed to investigate the spontaneous decay of ^{252}Cf, but recently in-beam experiments using ^{235}U irradiated by thermal neutrons have been carried out. The COMETA spectrometer was mostly used for the investigation of spontaneous fission of ^{252}Cf source. This radioactive source is prepared and attached to the "start" MCP detector for experimentation.

The Californium-252 (^{252}Cf) source decays by alpha emission of about 96.91% probability and spontaneous fission of about 3.09% probability [12]. The half-life for alpha decay is 2.73 years, for spontaneous fission is 85.5 years and the effective half-life is 2.65 years. The most important properties of ^{252}Cf to be considered in this work are given in Table 2-2 below and were obtained from [12].

Table 2-2: Properties of Californium-252 Source [12].

Quantity	**Light Fragment**	**Heavy Fragment**	**Alphas**	**Units**
Energy	103.9	78.54	6.119	*MeV*
Velocity	1.369	1.035	1.718	*cm/ns*
Mass	106.91	141.46	4.002	*Amu*

2.3.5. The 'Neutron Belt' of the COMETA

The COMETA spectrometer comprises of 28 ^{3}He neutron counters that are installed as a belt around the 'start' detector that houses the radioactive source. Figure 2.11 and Figure 2.12 shows the schematic view and the picture of the COMETA spectrometer respectively and the 'neutron belt' is clearly shown. The main idea of including the neutron

counters in the COMETA spectrometer was to enable the selection of events that are directly linked to the CCT. This was achieved by selecting the fission events that are detected in coincidence with a neutron multiplicity of three or more from the neutron counters.

It has been mentioned in chapter 1 that the CCT mode under investigation is based on the three-body chain-like configuration with the third fragment presumably at rest during scission. Similar to the modified-FOBOS and mini-FOBOS spectrometers, the 'neutron belt' was installed in the COMETA spectrometer around the radioactive source with the aim to detect neutrons from the third fragment in coincidence with the fission event.

(a) The neutron counter

Each neutron counter making up the 'neutron belt' of the COMETA consists of a moderator, a high voltage input and a preamplifier. The counter is operated under the gas pressure of 7 bar with an additional 1% of CO_2. The length of each counter is 50 cm and has a diameter of 3.2 cm. The counter is housed in a moderator which is made out of polyethylene material and the moderator has parallel planes that are placed 5cm apart. When a neutron enters a neutron counter it is slowed down for about $1-4\,\mu s$ in the polyethylene material. Thereafter it diffuses into the neutron counter where it gets detected (absorbed by the ^3He counter) or escapes detection. The detection of neutrons inside the counter is by means of the reaction below:

$$^3He + n \rightarrow {}^3H + p + 764keV$$

This reaction shows that the neutrons are completely absorbed in the counter and there are no 'cross talks' taking place. That means one neutron cannot be detected twice or more. This is the main advantage of using the ^3He neutron counters. Unfortunately such neutron counters do not give an energy of the neutron, but that is not a concern in this work because only the number of neutrons is required not their energies.

Pictures of the moderator, the neutron counter with high voltage cable and the neutron counter inside the moderator are shown in Figure 2.20, Figure 2.21 and Figure 2.22 respectively.

(b) Configuration of the 'Neutron Belt'

The optimum configuration for the neutron counters of the 'neutron belt' of the COMETA spectrometer was determined using the Monte Carlo N-Particle (MCNP) simulation code. A detailed account of a study to find a the best way to pack the neutron counters as a belt around the start detector of the COMETA spectrometer is presented in [21]. The MCNP simulation was first presented in [42]. Table 2-3 shows three different configurations that can be used to arrange the neutron counters as a belt. These configurations are obtained based on the probability for the neutron counters to detect neutrons from an isotropic source P_{iso} and from a moving source P_{mov}.

The configuration to be used is the one with the highest ratio of P_{iso}/P_{mov} and the configuration in the first row of Table 2-3 was used for the COMETA. Not only the optimum configuration obtained in this study but also an estimate of the detection efficiency of the counters is given as P_{mov}. From Table 2-3, the estimated detection efficiency for the 'neutron belt' is 5.23%.

(c) 'Neutron Belt' Detection Efficiency

The neutron counters detect neutrons in coincidence with fission events. This means that when the 'stop' detectors of the COMETA spectrometer registers a fission event, the neutron counters are triggered to open a gate to detect neutrons emitted from that particular event. When the gate is opened, not only neutrons from the fission event responsible to open the gate are detected, but neutrons from previous events and from experimental hall are also detected. These neutrons are referred to as background neutrons. To determine the detection efficiency, the background neutrons must be excluded.

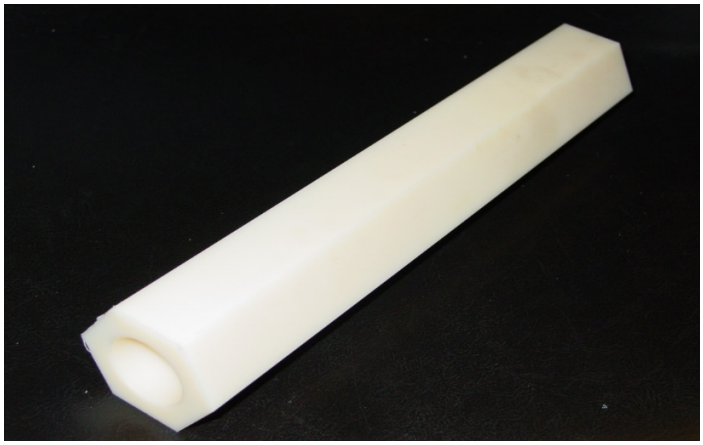

Figure 2.20: Moderator of the neutron counter.

Figure 2.21: The neutron counter with high voltage cables.

Figure 2.22: Neutron counter inside the moderator.

Table 2-3: Different configurations to arrange neutron counters in the belt used in COMETA spectrometer [21].

Configuration	P_{iso}	P_{mov}	P_{iso}/P_{mov}
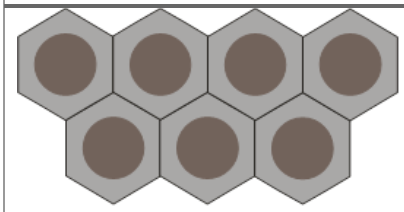	11.8%	5.23%	2.26
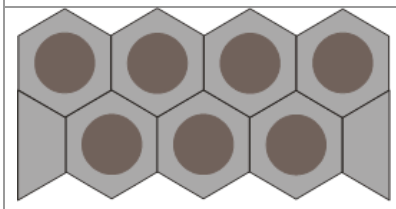	16.17%	7.77%	2.08
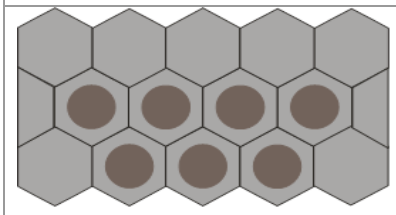	25%	13%	1.9

A precise algorithm to determine the correct detection efficiency of the 'neutron belt' taking into consideration the complication of subtracting the background neutrons, was developed in [21]. This procedure uses probability laws and simulates the background neutrons using a generator capable of producing up to four neutrons per fission event. Using experimental data, the detection efficiency reported in [21] was found to be 4.25 %. Figure 2.23 compares the calculated neutron distribution using the detection efficiency of 4.25 % obtained from the algorithm to the experimental data obtained from the neutron counters. There is clear agreement with the experimental data therefore the detection efficiency for the 'neutron belt' is 4.25 % and has a good agreement with the estimation received from the MCNP simulation.

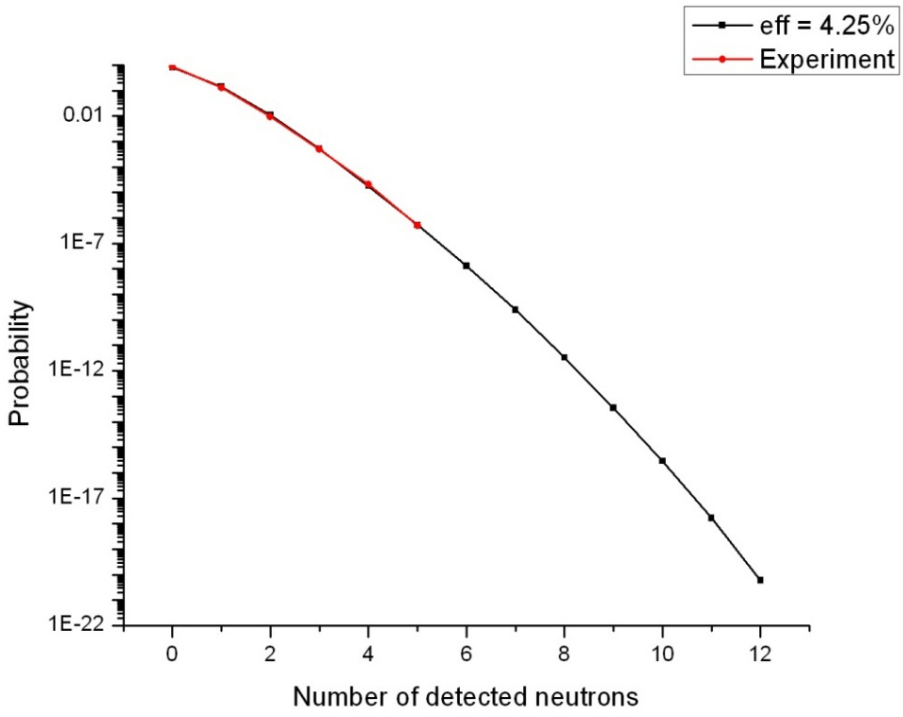

Figure 2.23: Comparing the calculated data from the algorithm used to calculate the detection efficiency of 'neutron belt' to the experimental data obtained from the neutron counters [21].

2.3.6. Electronics System of the COMETA

The method of detection used in the COMETA spectrometer to register fission fragments is the $2V - 2E$ method discussed in section 2.1. This method requires that the velocity and the energy of at least two fission fragments be obtained. The COMETA brings the possibility to detect the third fragment directly. The COMETA uses PIN-diode detectors to register the energy and the time signal for each fragment detected by the detectors. The PIN diode registers the two signals (energy and time) of the fission fragment simultaneously. There are few challenges connected to this process and they are discussed in chapter 3.

The MCP detector delivers a 'start' timing signal whereas the 'stop' timing signal is obtained from the PIN-diodes. The two signals define the time-of-flight (TOF) of the fission fragments. If the flight path of the fission fragment, that is the distance between the MCP detector and the PIN diodes, is known, the velocity of each detected fission fragment can be calculated.

The COMETA spectrometer comprises of 16 PIN diode detectors (8 in each arm) and one MCP detector. The PIN diode detectors are powered by a high voltage power supply (POLON) which delivers $+200\,V$. The MCP detector is powered by a high voltage supply (HT) which delivers a $-2230\,V$. The preamplifiers are powered by a CAMAC crate power supply module that delivers $+5\,V$ to them. In each PIN diode, two cables are connected to register the time and energy signal of each fragment. In the MCP detector only one cable is connected for data acquisition.

The electronic components of the COMETA consist of three Constant Fraction Discriminators (CFD CF 8100), one for each mosaic from the two arms and the third one is used for the start signal from the MCP detector. The time signal from the CFD of the PIN diodes is delayed for 100 ns and then sent to the Time to Digital Converter (TDC Silena 4418). The energy signal from the PIN diode, on the other hand, is delayed for

200 ns and then sent to the Charge to Digital Converter (QDC Phillips Scientific 7166).

The time signal from the MCP detector is delayed for 30ns then sent to the coincidence circuit before being taken to the start TDC. The time signal from the PIN diode is also sent to the coincidence circuit which identifies fission events that take place in coincidence. Three outputs for each event are produced by the coincidence circuit, one is the gate signal that is sent to the QDC, the second one is the start signal that is sent to the TDC, and the third one is the LAM (Look-At-Me) signal that is sent to the Analog Digital Convertor (ADC). The LAM signal is used by the data acquisition system to initiate data acquisition. The QDC, TDC, and ADC signals are sent to the CAMAC BUS which sends signals to the Crate Controller where the computer records the data from. The computer used for data acquisition is a desktop computer with the necessary graphics cards and drivers running on Microsoft Windows. The computer uses a custom-made data acquisition software to save the experimental data on the data network of the JINR for further processiong. The scheme for the electronics of the COMETA is shown in Figure 2.24.

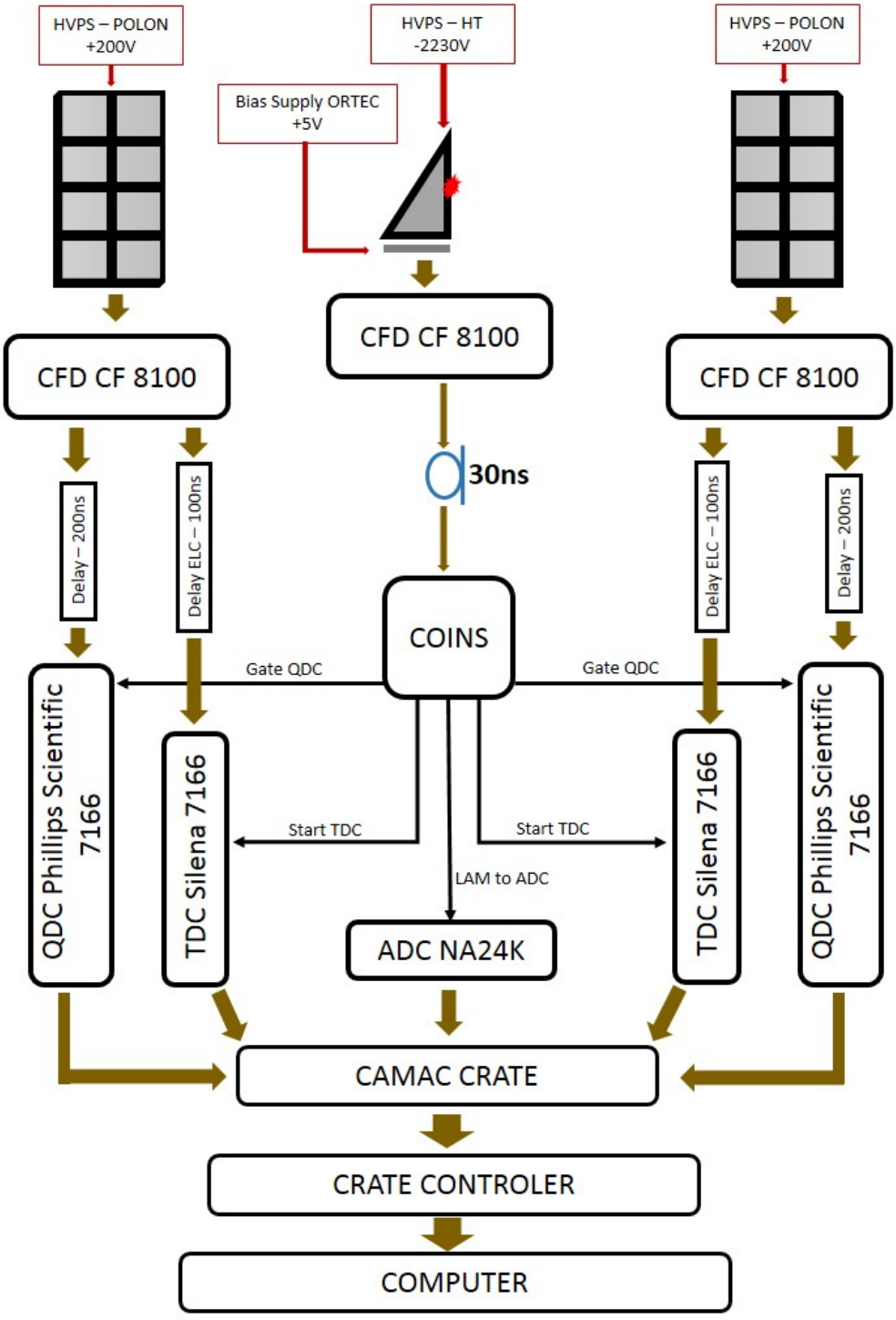

Figure 2.24: Electronics scheme of the COMETA spectrometer.

2.4. Conclusion

The COMETA spectrometer presented in this chapter was designed from the ideas of the modified-FOBOS and mini-FOBOS spectrometer as a double arm time-of-flight spectrometer and was first presented in [21]. The aim of developing such a spectrometer was to achieve the direct detection of all the CCT partners. The COMETA spectrometer was designed to ensure that all the measurement methods outlined in section 2.1 can be achieved. To achieve the direct detection of all the CCT partners, the $2V - 2E$ method was employed in the COMETA and an array of PIN diode detectors was used.

The two fission fragments flying in the same direction that get scattered by an angle of $\sim 1^o$ after passing through the source backing made it possible for the COMETA spectrometer to detect all the three CCT fragments. The missing-mass approach was achieved based on the source backing material and the grid that was introduced in the experiments outlined in section 2.2. As depicted in Figure 2.25, there are three types of events that can be registered by the PIN diodes of the COMETA spectrometer. In all of these events, one fragment flies in the opposite direction to be detected in coincidence with the other one/two fragment(s) in the other arm.

The two fragments flying in the same direction, when their angle of dispersion after passing through the source backing is $0 < \theta < 1^o$, then there is a missing-mass event marked by 1-2-3 in Figure 2.25. This means that only fragment 1 and 2 were detected and fragment 3 is missing. Another scenario is when both the fragments flying in the same direction can hit the same PIN diode that is the event marked by 1-2-4. In this case there is a challenge in determining the correct masses of the fragments (this will further be discussed in chapter 3). Such an event can be regarded as binary fission event. In a case when an angle between the fragments is $\theta > 1^o$, the two fragments can be detected in two

different PIN diodes. Such an event is the desired direct detection of CCT and is marked by 1-2-5 in Figure 2.25.

The COMETA spectrometer presented in this chapter can achieve the direct detection of all the CCT partners. The detailed data acquisition and calibration process will be discussed in chapter 3 and the results obtained from the COMETA spectrometer will be given in chapter 4.

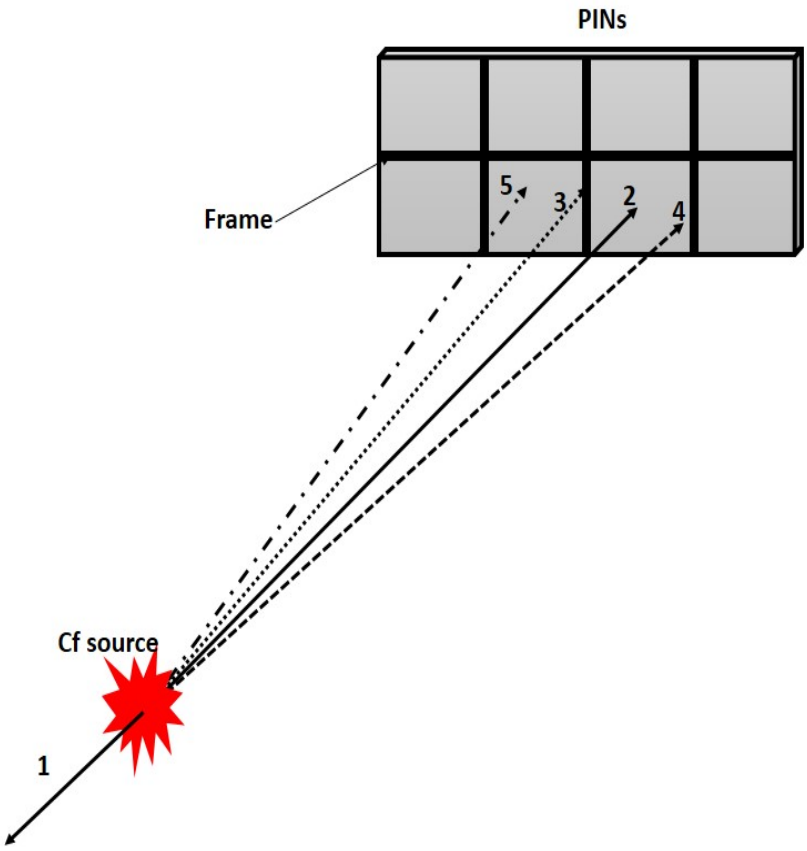

Figure 2.25: The geometric distribution of the fragments hitting the PIN diodes in the COMETA setup and the type of events that can be possible detected.

Chapter 3

Data Acquisition and Processing Procedure

The electronics of the COMETA spectrometer uses the standard CAMAC crate modules to collect the experimental data. As in most experiments, the data is collected in a form of electronics signals. In order to use the $2V-2E$ detection method in the COMETA spectrometer for the registration of fission fragments there are two important signals that are collected for the calculation of fission fragments masses. The first signal is the time-of-flight (TOF). The TOF is the time signal measured from the 'start' time signal delivered by the MCP detector and the 'stop' time signal delivered by the PIN diode detector. This measurement is achieved by the use of the coincidence block shown in the electronics scheme of the COMETA spectrometer (Figure 2.24). The second signal is the energy signal that is registered by the PIN diode detectors. Each fission event is determined by a precise coincidence scheme incorporated into the electronics of the COMETA spectrometer.

The TOF signal is used together with the flight path to calculate the velocity of the fission fragments. The flight path is the distance between the MCP detector and the PIN diode detector. By having the correct velocity and the correct energy of each fission fragment, the $2V-2E$

method can be used to calculate the correct masses of the detected fission fragments.

The general data acquisition process includes firstly; testing the stability of the data and this process is called data stability test. The data stability test is performed to ensure that there are no variations in the time and energy channels due to cables, electronics and actual detectors used on the experiment. The details of this process are outlined in the Master's thesis of V.D. Malaza [21]. The data stability testing is followed by a calibration process where the electronic signals are converted to known units of measurements. The calibration process for the COMETA spectrometer is divided into online time calibration, 3-point energy calibration and the reconstruction of the fission fragment's masses. The online time calibration and 3-point energy calibration were previously referred to as a first approximation calibration. The main factors affecting the correct time and energy detection in the first approximation calibration are only approximated using linear relationships and the output parameters are used on the reconstruction of the fission fragments masses. This chapter will outline all these processes.

3.1. Calibration Process for the COMETA Spectrometer

The COMETA spectrometer detects the TOF signal and the energy signal using the PIN diode detectors simultaneously. This means that when the fission fragment arrives in the PIN diode detector, two signals, namely, the TOF and the energy signal are generated simultaneously from one detector. As discussed in chapter 2, the PIN diode is a semiconductor-based silicon detector. The use of semiconductor- based detectors to register heavy ions has two known experimental challenges when it comes to the registration of time and energy signals in a wide range of masses. This is the case where the mass of one fragment is large

while the other mass is very small. With the COMETA spectrometer this becomes a complex situation because the two signals are registered by the same detector simultaneously.

The first challenge comes from the fact that semiconductor detectors respond differently when detecting heavy ions, such as fission fragments and light ions such as alpha particle and/or protons. This response is observed from the fact that the pulse height of heavy ions is smaller than the pulse height of light ions yielding the same energy. This phenomenon is referred to as Pulse-Height Defect (PHD) [50]. In general, the PHD is defined as the difference between the energy of the heavy ion and that of a light ion yielding the same pulse height. When the PHD is ignored in the registration of fission fragments using PIN diodes, it leads to an incorrect registration of energy.

The second challenge has to do with the correct registration of the TOF signal using the semiconductor detectors and this is called plasma delay. The plasma delay manifests itself with the reduction of the pulse rise time with the decreasing Z (proton number) for lower intermediate mass fragments, for which the generated charge is completely absorbed by the detector. The plasma delay prevents the correct registration of the TOF signal due to the creation of plasma in the detectors, which obstructs the charge collection. This definition of plasma delay is obtained from [51] and is illustrated in Figure 3.1.

Due to the above-mentioned experimental challenges, obtaining the correct masses of the fission fragments from the COMETA spectrometer becomes a very complex task, especially when dealing with heavy ions in the wide range of energies and masses that are far from those of conventional binary fission. This has been the main challenge in the study of the CCT process. A suitable algorithm to take into consideration both the PHD and the plasma delay simultaneously in the calculation of the fission fragments masses was not yet developed in the beginning of this study.

It is worth mentioning that a procedure that only considers the PHD was first presented in the Master's thesis of V.D. Malaza [21], as mentioned in section 1.7. The plasma delay must also be considered. In this work, a mass reconstruction procedure that considers both the PHD and the plasma delay is presented. This is an improved procedure compared to the one presented in [21] and the biggest improvement is the computer programming codes. The first procedure in [21] was coded using FORTRAN programming language. In this work, the C++ programming language was used together with C-Builder to produce a user friendly graphical interface. The procedure presented in this work is therefore a suitable procedure for the calibration process and is one of the main results of the work.

Firstly, the online time calibration and the 3-point energy calibration procedure will be presented. These calibration procedures were referred to as 'first approximation', due to the fact that the PHD and the plasma delay is taken to be a constant and only approximated roughly. The first approximation is very useful for the online data management while the experiment is underway and it provides an indication of whether the data acquisition system is operating correctly. The parameters of the first approximation are used in the reconstruction of fission fragments mass procedure. This is where the correct masses of fission fragments are calculated taking into account the PHD and the plasma delay.

The experimental data used for calibration processes explained below were obtained during the calibration of the COMETA Spectrometer to be used in the IBR-2 Reactor in November 2016. These data are referred to as COMETA-R 16 data. The ^{252}Cf was used as the radioactive source for calibration, its parameters are listed in Table 2-2 and the velocity and mass literature spectra were obtained from [52].

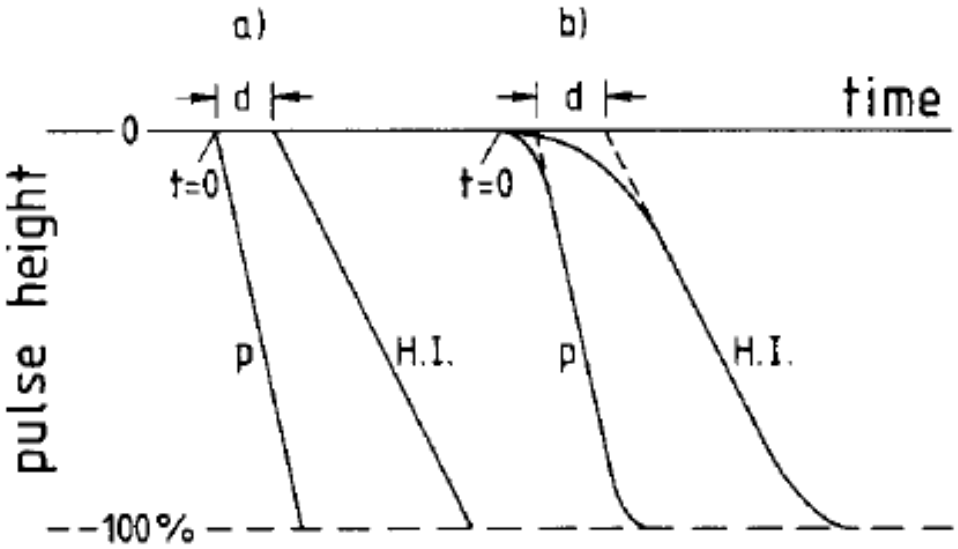

Figure 3.1: Illustration of plasma delay from [51]. a) Shows an unrealistic delay of the beginning of every pulse formation for heavy ions (HI) as compared to protons (p). b) Plasma delay as defined by [53], [54].

3.1.1. Online Time Calibration

The basic calibration process is based on transforming the signals collected by the experimental electronics system into standard units of measurements. For the TOF measurements, the data acquisition software registers the time signal in channels. In the online time calibration, the time signal registered in channels is converted to time in nanoseconds. For this process it is known that time in nanoseconds is linear depended on time in channels. The equation used to convert time from channels to nanoseconds is given by

$$T_{i[ns]} = A \cdot T_{i[ch]} + B \tag{3.2}$$

where $T_{i[ns]}$ is the TOF in nanoseconds and $T_{i[ch]}$ is the TOF in channels. The i subscript in the equation (and the equations to follow) refers to the fact that each registered event is processed individually. The parameters A and B are time calibration parameters and they are determined using the known two peaks of the light fragment and heavy fragment in the velocity distribution of ^{252}Cf obtained from literature [52]. The TOF in nanoseconds for the light, $T_{L[ns]}$ and heavy, $T_{H[ns]}$ fission fragments are given by

$$\begin{aligned} T_{L[ns]} &= \frac{L_{[cm]}}{v_{L[cm/ns]}} \\ T_{H[ns]} &= \frac{L_{[cm]}}{\mathrm{v_{H[cm/ns]}}} \end{aligned} \tag{3.3}$$

where $L_{[\mathrm{cm}]}$ is the flight path for fission fragments measured between the MCP detector and the specific PIN diode where the fission fragment was detected. From the above equations, the value of A can be determined as follows:

$$A = \frac{T_{H[ns]} - T_{L[ns]}}{T_{H[ch]} - T_{L[ch]}} \tag{3.4}$$

Therefore, the values of B for the heavy and the light fragments are respectively obtained as follows:

$$B_H = T_{H[ns]} - A \cdot T_{H[ch]}$$
$$B_L = T_{L[ns]} - A \cdot T_{L[ch]} \quad (3.5)$$

Experimentally the values, B_H and B_L have a significantly small difference, thus the average between the two values is always used

$$B = \frac{B_H + B_L}{2} \quad (3.6)$$

After the values of A and B have been obtained, all the experimental data for the time channel are converted into nanoseconds using equation (3.2) for each PIN diode detector. Having time spectra in nanoseconds, the velocity $v_{i[cm/ns]}$ in centimetres per nanoseconds spectra for each PIN diode detector is obtained as follows:

$$v_{i[cm/ns]} = \frac{L_{[cm]}}{T_{i[ns]}} \quad (3.7)$$

The online time calibration produces the velocity spectra and its parameters will be used together with the energy to calculate the mass of the fission fragments.

3.1.2. The 3 – Point Energy Calibration

The 3-point energy calibration is the process where the detected energy signals of fission fragments are transformed from channel values to their corresponding units of measurement, Mega-Electron Volts (MeV). This process uses the known two energy peaks of fission fragments and the energy peak of the alpha particles from the ^{252}Cf source (see Table 2-2). This process is referred to as a 3-point energy calibration. The energy in channels is converted to the energy in MeV using the following exponential relationship

$$E_{i[MeV]} = C \cdot e^{-E_{i[ch]}/D} + E_0 \quad (3.8)$$

The values C, D and E_0 are energy calibration parameters. To obtain these values, the experimental spectrum containing energy data in channels is exported into a file format readable by a special program called Origin Lab (.dat or .txt format). Using this software, it is possible to perform a Gaussian fit to obtain the three peak positions in channels, namely the alpha peak, light fragment peak and heavy fragment peak. This process is explained in section 3.2. The energy position for the three peaks in MeV is given in Table 2-2. Using the known values of the energy peaks in MeV, the experimental peak position in channels and equation (3.8), the values of C, D and E_0 can be calculated. Each event is processed individually and the energy spectrum for each detector in MeV is obtained. Using equation (3.7) and (3.8), the mass spectra in atomic mass units (amu) for the fission fragments from each PIN diode detector are calculated according to following equation

$$M_{i[amu]} = \frac{1.9297 E_{i[MeV]}}{\left(v_{i[cm/ns]}\right)^2} \tag{3.9}$$

The mass spectra obtained from the above equation are only an approximation since the effect of PHD and plasma delay has been ignored. This procedure is used to determine some of the input parameters that are used in the mass reconstruction procedure for the fission fragments. The mass reconstruction procedure considers the PHD and the plasma delay and calculates the correct masses of the fission fragments. This procedure will be presented in the next section. It is important to mention that the online time calibration and the 3-point energy calibration procedures present a very good approximation for the mass spectra in the vicinity of the loci of the binary fragments. The events far away from the loci of the binary fragments, the PHD and the plasma delay must be considered.

3.1.3. The Reconstruction of Fission Fragment Masses

In order to obtain the correct mass of the fission fragments, energy and TOF should be experimentally measured correctly. This is achieved by considering the PHD and plasma delay when calculating the energy and the velocity of the registered fission fragments to eventually obtain their masses. This section presents a procedure that has been successfully developed to calculate the exact masses of the fission fragments considering the PHD and plasma delay. Developing such a procedure was outlined as one of the main objectives for this study.

The actual energy E in MeV of the registered fission fragment is given by the sum of the detected energy E_{det} in MeV and the pulse-height defect denoted by $R(M,E)$ in MeV:

$$E = E_{det} + R(M,E) \tag{3.10}$$

The detected energy in MeV of the fission fragment is given by

$$E_{det} = E_{[ch]} \cdot E_k + E_0 \tag{3.11}$$

where E_k and E_0 are energy calibration parameters obtained from the first approximation. It is noted that the value of $R(M,E)$ in equation (3.10) has a complicated dependency of energy and mass of the fission fragments. The aim is to calculate the mass using the energy and to obtain the correct energy, the value of $R(M,E)$ must be considered and it also depends on the energy and the mass. This means that a parametrization procedure is required to obtain the correct mass of fission fragments.

Previous studies of the PHD shown that its value consist of three components that can be denoted as follows:

$$R(M,E) = R_w(M,E) + R_n(M,E) + R_{rec}(M,E) \tag{3.12}$$

where $R_w(M,E)$ is associated with the energy lost in the entrance window of the PIN diode, $R_n(M,E)$ is associated with the energy lost

during the collision of heavy ions with atoms of the crystal lattice in the PIN diode and $R_{rec}(M,E)$ is associated with the energy lost during the recombination of the electron-hole pairs in the plasma produced along the tracks of the heavy ions [5].

Determining the value of $R(M,E)$ is quite a challenging task as it depends on many factors that relates to both the detected fragments and the properties of the detectors used. The best method so far is based on calibration procedures which uses empirical formulas for $\mathrm{R(M,E)}$. Parameters of these formulas can either be obtained from measurements of selected masses or from the properties of the radioactive sources used for calibration.

Until now, there are few empirical formulas that have been used to calculate the PHD of silicon detectors by different authors such as [55], [56] and [57]. Unfortunately these formulas only gave satisfactory results for the detector parameters used by the authors and for the heavy ions studied on the original work. The empirical formula that proved to work for the study presented in this dissertation was found to be based on the calculation of both the energy and the TOF of the fission fragments using parametrization procedure derived by Mulgin and his colleagues [50].

The empirical formula for $\mathrm{R(M,E)}$ obtained from [50] to be used in this procedure is given by

$$R(M,E) = \frac{\lambda \cdot E}{1 + \phi \cdot \frac{E}{M^2}} + \alpha \cdot ME + \beta \cdot E \tag{3.13}$$

where $\{\alpha, \beta, \lambda, \phi\}$ are parameters for the calibration process. The mass – energy relation is given by

$$E = \frac{Mv^2}{1.9297} \tag{3.14}$$

The mass in the above equation is in $a.m.u.$ and the velocity v of the fission fragments is given in cm/ns. The velocity in this case is calculated using the parameters obtained from the online time calibration.

Combining equation (3.11), (3.13) and (3.14) into equation (3.10) the equation to calculate the mass of the fission fragments provided that the parameters $\{\alpha, \beta, \lambda, \phi\}$ are known is obtained. It is important to point out that the parameters $\{\alpha, \beta, \lambda, \phi\}$ proposed in [50] are not suitable for calculations in this work due to the characteristics of the PIN diode detectors used.

To obtain the correct parameters $\{\alpha, \beta, \lambda, \phi\}$, a special iteration procedure based on parametrization has been developed. This procedure involves obtaining a numerical solution of the following equation:

$$G(\{\alpha, \beta, \lambda, \phi\}, M, v) = 0 \tag{3.15}$$

where G is an analytical function that depends on the parameters $\{\alpha, \beta, \lambda, \phi\}$, mass M and velocity v. To obtain the solution to equation (3.15) we combine equation (3.11), (3.13) and (3.14) in to equation (3.10) and obtain

$$\frac{Mv^2}{k} = E_{det} + \frac{\lambda \cdot \frac{Mv^2}{k}}{1 + \phi \cdot \frac{v^2}{Mk}} + \alpha \cdot \frac{M^2v^2}{k} + \beta \cdot \frac{Mv^2}{k} \tag{3.16}$$

where $k = 1.9297$ is a constant. The above equation can be simplified to the following cubic function:

$$M^3 + aM^2 + bM + c = 0 \tag{3.17}$$

with

$$a = \frac{\phi v^2}{k} + \frac{\beta + \lambda - 1}{\alpha}$$

$$b = \frac{kE_{det}}{\alpha v^2} + \frac{\phi v^2}{\alpha k}(\beta - 1)$$

$$c = \frac{\phi E_{det}}{\alpha}$$

In order to obtain the correct value of the velocity in equation (3.16), the plasma delay must be considered. The best estimation of plasma delay denoted by t_p produced by heavy ions when entering the PIN diode

detectors is given by the empirical formula of Neidel and Henschel [54] as follows:

$$t_p = 1.33\left(m^{1/6}E^{1/2}\right)/F \tag{3.18}$$

where F is the electric field strength in the diode. Considering the plasma delay, the correct velocity is obtained from the equation

$$v = \frac{L_{[cm]}}{\gamma M^{2/3} + T_{i[ns]}} \tag{3.19}$$

where $T_{i[ns]}$ is the TOF obtained from the first approximation, $L_{[cm]}$ is the length of the flight path of the fission fragments and γ is the new parameter to be calculated together with the parameters $\{\alpha, \beta, \lambda, \phi\}$. This implies that the procedure will now use a vector of parameters $\{\alpha, \beta, \lambda, \phi, \gamma\}$ to find a numerical solution of the set of equation (3.16) and (3.19).

After processing an amount of data using the above-mentioned procedure, a spectrum of quasi-mass is obtained. It is important to note that each event is processed individually. The vector of the parameters is changed by the MINUIT package [58] in order to minimize the following criterion function by changing the parameters $\{\alpha, \beta, \lambda, \phi, \gamma\}$

$$F = [(\langle ML_T\rangle - \langle ML\rangle)^2 + (\langle MH_T\rangle - \langle MH\rangle)^2] + \mu \sum_{M_{TE}} \frac{\left(Y(M_{TE}) - Y_T(M_{TE})\right)^2}{Y(M_{TE})} \tag{3.20}$$

where μ is a free parameter that is chosen by the user and it is used as an input parameter to the MUNUIT minimization procedure. This parameter plays a role of specific relative weight of the second term in the criterion function F. The values $\langle$ML$\rangle$ and $\langle$MH$\rangle$ are average masses of light and heavy fragments calculated from the experimental mass spectrum denoted by $Y(M_{TE})$. In the above equation the known values from literature are denoted by the subscript T. It is worth noting that the first square bracket term in equation (3.20) is sensitive to the difference between the centres of the binary fragment's mass peaks for the fission fragments. The second term is responsible for the agreement

in shapes between the experimental mass spectrum $Y(M_{TE})$ and the mass spectrum from literature $Y_T(M_{TE})$. The MINUIT minimization procedure outlined in [58] and further explained in [21] minimizes the difference between the experimental mass spectrum $Y(M_{TE})$ and the mass spectrum from literature $Y_T(M_{TE})$. When the criterion function in equation (3.20) reaches the value of $F = 10^{-6}$ or below, the parameters $\{\alpha, \beta, \lambda, \phi, \gamma\}$ are extracted and the program exits. This procedure is illustrated in Figure 3.6.

It has been mentioned above that, during the development of this procedure, special computer programming codes to process the data by performing the above-mentioned procedure including MUNUIT minimization header files were first written in FORTRAN 99 language [21]. In this work, these codes were converted to C++ programming language. Recently custom software that incorporates all the codes with a user friendly graphical interface has been designed. This software will be explained in the following section that describe the program package for data processing.

3.2. Program Package for Data Acquisition and Processing

The computers collect data from the electronics of the COMETA spectrometer, using custom designed software. It was discussed earlier that, the data are collected via the crate controller of the CAMAC Bus. The CAMAC modules such as QDC, ADC and TDC are responsible for reading and collecting the experimental signals as data. The experimental data from the COMETA spectrometer are collected by using a custom software (at this point this software is not given a name, it is called 'data collecting software'). This software saves the experimental data in a .tdms file format and these files contain all the information from the experiment. The advantage of this software is that the data can be visualized while the experiment is underway.

A program called TDMS which contain all the experimental configurations such as the number of detectors, distances between detectors and other experimental details, is then used to extract specific files that contain the TOF and energy signals. This program saves the extracted files as text files (.txt or.dat) to be further analysed by other programs.

After the TOF and energy information have been extracted from the .tdms file, it is saved with file names such as T11, T12, T21 T22 and so on for time signals or E11, E12, E21, E22 and so on for energy. The T11 means it is the TOF data from detector 11, which is detector 1 from arm 1 and the E21 means it is energy data from detector 21, which is detector 1 from arm 2. The next step is to perform the first approximation calibration which includes the online time calibration and the 3-point energy calibration. For the first approximation calibration, Microsoft Excel and Origin Lab programs are used. The Origin Lab is used to select the peak positions using Gaussian fits and the peak positions are inserted in a well-designed excel spreadsheet to calculate the calibration parameters for both the online time and 3-point energy calibration.

For the online time calibration parameters, the values of A and B in equation (3.2) are calculated by using the peak positions of the light and heavy fragments in the time channel obtained from the experimental data. Figure 3.2 shows a time channel spectrum from channel T13 that means it is a time channel from detector number 3 of arm 1. In order to obtain the exact peak positions for the light and the heavy fragment in channels, two Gaussian fits are applied in the spectrum as shown in Figure 3.2. These are the values $T_{L[ch]}$ and $T_{H[ch]}$ from equation (3.4). Therefore, using equation (3.3), (3.4) and (3.6), the values of A and B are calculated as discussed in section 3.1.1. After processing all the data from each channel, the online time calibration parameters are obtained. Table 3-1 shows the peak positions for the light $T_{L[ch]}$ and heavy $T_{H[ch]}$ fragment in channels, the flight path $L_{[cm]}$, peak positions for the light

$T_{L[ns]}$ and heavy $T_{H[ns]}$ fragment in nanosecond calculated by equation (3.3) and the values of A and B for each detector.

For the 3-point energy calibration parameters, the energy peak of alpha particles emitted by the ^{252}Cf fission source and the two energy peaks of the heavy and the light fission fragments are used to obtain the three parameters according to equation (3.8) as discussed in section 3.1.2. Firstly, the peak of the alpha particles is extracted from the energy channel and a Gaussian fit is applied to obtain the exact position of the peak. This is shown in Figure 3.3 for the energy channel E13. Thereafter, the fission fragments peaks are extracted and Gaussian fits are applied to both of them to obtain their positions in channels as shown in Figure 3.4. The reason to separate the peak of the alpha particle from the two fission fragments peaks is that the yield of the alpha particles is higher than the yield of the fission fragments. It is a challenge to display all the peaks on the same scale of axes.

Using the three peak positions from the energy channels and the known energy values as discussed in section 3.1.2, three points can be plotted as shown in Figure 3.5. An exponential fit is applied to these points according to equation (3.8), to obtain the calibration parameters, C, D and E_0. The values of this parameters for the channel E13 are displayed on the statistical data shown in Figure 3.5. After processing all the data from each channel, the 3-point calibration parameters for all the detectors are obtained and displayed in Table 3-2. The online time calibration parameters shown in Table 3-1 and the 3-point energy calibration parameters shown in Table 3-2 are used as one of the input files to the procedure for the reconstruction of fission fragment masses.

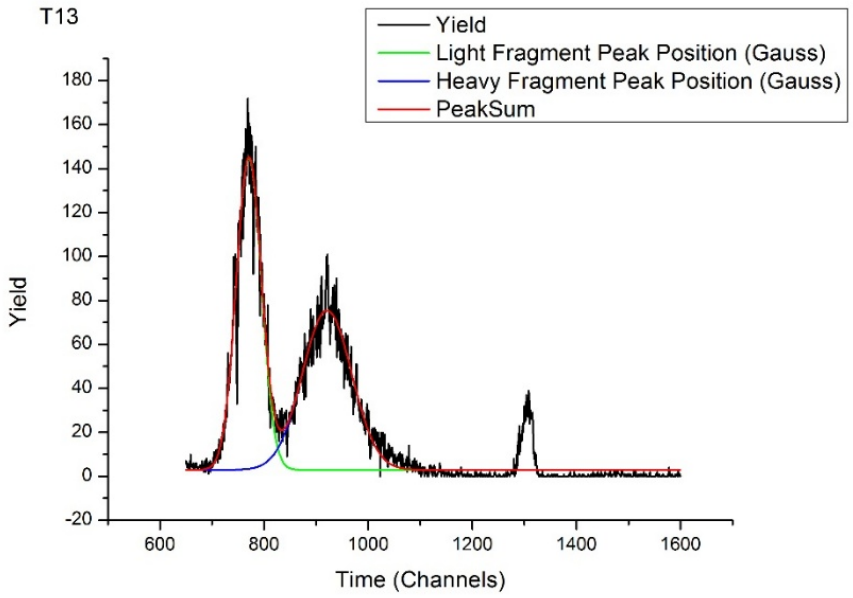

Figure 3.2 : Time spectrum from channel T13 with Gaussian fits for the light and heavy fragment peak positions.

Table 3-1: The online time calibration parameters

Det	$T_{L[ch]}$	$T_{H[ch]}$	$\Delta T_{[ch]}$	$L_{[cm]}$	$T_{L[ns]}$	$T_{H[ns]}$	$\Delta T_{[ns]}$	A	B_L	B_H	B
T11	816,39	969,79	153,40	15,34	11,21	14,82	3,61	0,02	-8,02	-8,02	-8,02
T12	823,82	974,23	150,41	15,07	11,01	14,56	3,55	0,02	-8,43	-8,43	-8,43
T13	770,81	921,10	150,28	15,07	11,01	14,56	3,55	0,02	-7,20	-7,20	-7,20
T14	815,41	966,32	150,92	15,34	11,21	14,82	3,61	0,02	-8,32	-8,32	-8,32
T15	780,45	931,75	151,30	15,34	11,21	14,82	3,61	0,02	-7,43	-7,43	-7,43
T16	799,77	949,58	149,81	15,07	11,01	14,56	3,55	0,02	-7,94	-7,94	-7,94
T17	780,04	931,15	151,11	15,07	11,01	14,56	3,55	0,02	-7,31	-7,31	-7,31
T18	828,62	981,36	152,73	15,34	11,21	14,82	3,61	0,02	-8,40	-8,40	-8,40
T21	826,54	974,43	147,89	15,34	11,21	14,82	3,61	0,02	-8,99	-8,99	-8,99
T22	869,36	1014,86	145,49	15,07	11,01	14,56	3,55	0,02	-10,20	-10,20	-10,20
T23	849,05	996,15	147,10	15,07	11,01	14,56	3,55	0,02	-9,48	-9,48	-9,48
T24	855,21	1005,00	149,79	15,34	11,21	14,82	3,61	0,02	-9,42	-9,42	-9,42
T25	895,81	1044,87	149,05	15,34	11,21	14,82	3,61	0,02	-10,51	-10,51	-10,51
T26	884,38	1033,24	148,86	15,07	11,01	14,56	3,55	0,02	-10,08	-10,08	-10,08
T27	857,01	1002,98	145,97	15,07	11,01	14,56	3,55	0,02	-9,83	-9,83	-9,83
T28	922,41	1074,43	152,02	15,34	11,21	14,82	3,61	0,02	-10,72	-10,72	-10,72

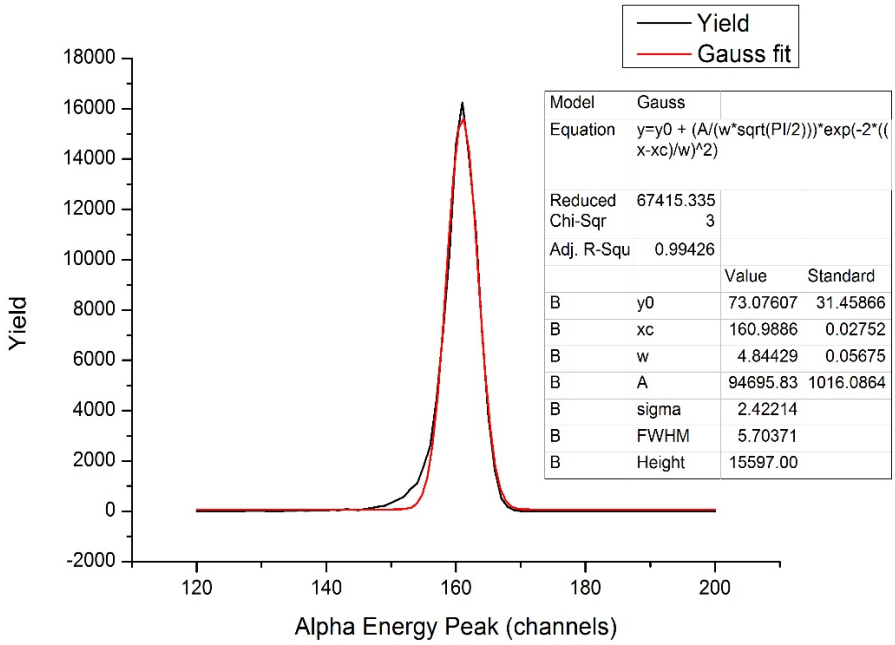

Figure 3.3: Energy peak for the alpha particles from channel E13 with a Gaussian fit. Some statistics extracted from Origin Lab displayed on the figure.

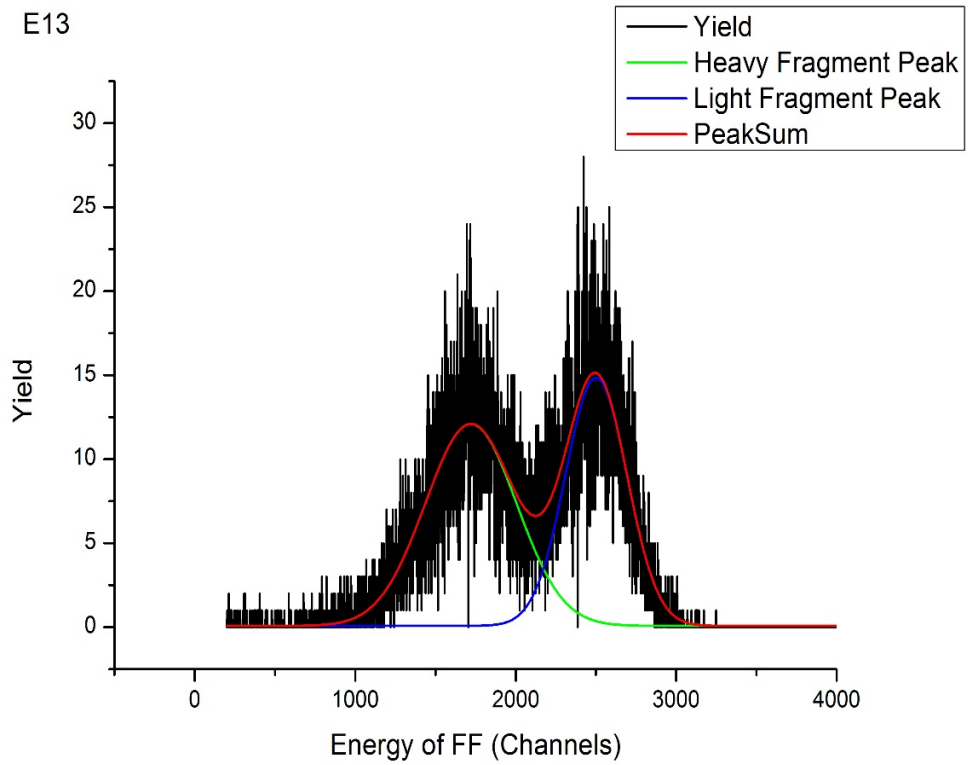

Figure 3.4: Energy peaks of the heavy and the light fission fragment (FF) with Gaussian fits to determine peak positions.

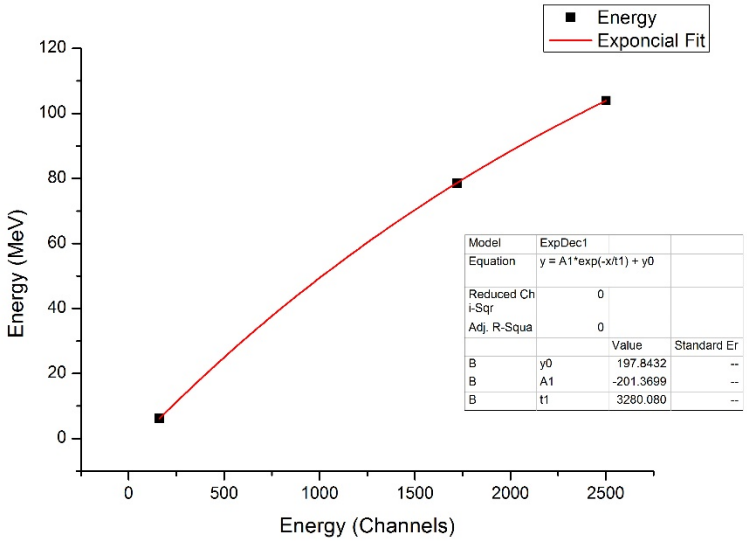

Figure 3.5: The 3-points corresponding to the energy peaks of alpha particles, heavy and light fission fragments with the exponential fit to determine the 3-point energy calibration parameters.

Table 3-2: The 3-point calibration parameters.

Detector	C	D	E_0**(MeV)**
11	-201.37	3280.08	197.8432
12	-207.744	3462.628	204.3936
13	-208.598	3381.609	204.935
14	-207.661	3488.644	204.6692
15	-208.511	3495.198	204.757
16	-210.729	3524.589	207.0392
17	-204.228	3273.095	200.6083
18	-205.326	3328.348	200.9343
21	-205.074	3159.087	201.0444
22	-216.334	3226.708	212.164
23	-215.619	3447.542	212.1698
24	-209.736	3244.021	206.2521
25	-213.651	3433.597	210.5221
26	-209.494	3295.482	206.2897
27	-214.328	3398.99	211.086
28	-208.569	3254.152	205.0988

For the reconstruction of the fission fragment masses, a new program called Minuplaz was designed. This program contains codes with complicated algorithms and calculations to perform the parametrization procedure which considers the PHD and plasma delay. This program performs the algorithms and calculations explained in section 3.1.3 and illustrated in Figure 3.6. It receives a number of input files that contain parameters needed for the minimization procedure. The input files include the experimental raw data that contains the TOF and energy signals for all the events registered from each detector. It also includes files that contain initial values of the parameters $\{\alpha, \beta, \lambda, \phi, \gamma\}$, a distance file that contain distance from the start detector to each PIN diode, the coefficients of the online time and 3-point energy calibration, the mass spectrum from literature and the velocity spectrum from literature [12].

Based on the input files, the Minuplaz program calculates the parameters $\{\alpha, \beta, \lambda, \phi, \gamma\}$, such that the experimental mass spectrum for the binary fission fragments have a good agreement with the mass spectrum from literature [12]. This program runs the MINUIT procedure explained in section 3.1.3. When the criterion function of equation (3.20) reaches the value of $F = 10^{-6}$ or below, the program will exit with correct parameters $\{\alpha, \beta, \lambda, \phi, \gamma\}$. In a case when the criterion function could not be minimized, the user must slightly change the parameters $\{\alpha, \beta, \lambda, \phi, \gamma\}$ as required and input them into the program as new parameters until there is a good agreement in the two mass spectra. The Minuplaz program was designed as part of this work and it contains all the programming codes that perform the iteration outlined in section 3.1.3 and illustrated in Figure 3.6. The MINUIT header file that runs the minimization process is included as a sub-routing in this program.

There are two output files from the Minuplaz program, the first file contains step-by-step results for each iteration the program has performed for that specific detector. This file also contains the output parameters $\{\alpha, \beta, \lambda, \phi, \gamma\}$ for the minimization procedure. The second file

contains the calculated output spectra. These spectra include the mass spectrum and the velocity spectrum for each detector.

The algorithm for the Minuplaz program is illustrated in Figure 3.6. The mass spectra obtained using this program for the November/December 2016 data are shown in Figure 3.7 through to Figure 3.14. It is clearly seen in these results that the calculated mass spectra agree very well with the mass spectrum from literature [12]. This implies that the parameters $\{\alpha, \beta, \lambda, \phi, \gamma\}$ were calculated correctly and these parameters are shown in Table 3-3. The correct parameters $\{\alpha, \beta, \lambda, \phi, \gamma\}$ are then used to calculate the mass of each fragment that was registered by each detector. It is important to note that each detector has its own parameters; therefore, this procedure is performed for each detector. Table 3-4 shows the comparison between the experimental mass value and the expected value as outlined in [12] and [52].

The final program that is used is the Athene program. This is an old program which was designed to treat, visualize and analyse multi-parameter events measurements from the 4π FOBOS Spectrometer at the JINR [31]. Until now, this is still a very useful program in its original form. For the data processing, this program is used to create data matrix and two dimensional spectra. It is further used to sum up all the spectra from each detector of each arm and create two dimensional spectra such as the total mass from arm 1 vs total mass from arm 2. Specific gates for detailed analysis are also created by this program. The input to this program is the spectra calculated from the Minuplaz program. The final results from the COMETA Spectrometer are produced by the Athene program, but other programs that can sketch the graphs and present the spectra in a more modern style such as Origin Lab are used for further visualization.

The data collected during the experiments are saved on a secure computer network hard drive of the JINR. These data are processed by using the TDMS program (explained above) and saved in an easy to use

data format such as .txt or .dat. These files contain the raw data that is processed by using the Minuplaz program. The Minuplaz program runs on a personal computer and therefore the data in a .txt or .dat can be transferred using external hard drives. Initially, processing the data could take more than one week for one detector. This process was time consuming, the Minuplaz program was developed to improve the run time for data processing. Using the Minuplaz program, 16 detectors can be processed in one week. The Minuplaz program requires a computer with a minimum of 8GB of RAM and it must run a 64-bit operating system. A personal laptop, that runs on Microsoft Windows platform, was used to process the data using the Minuplaz program both in Russia (at the JINR) and South African (in Saldanha campus and/or Stellenbosch University).

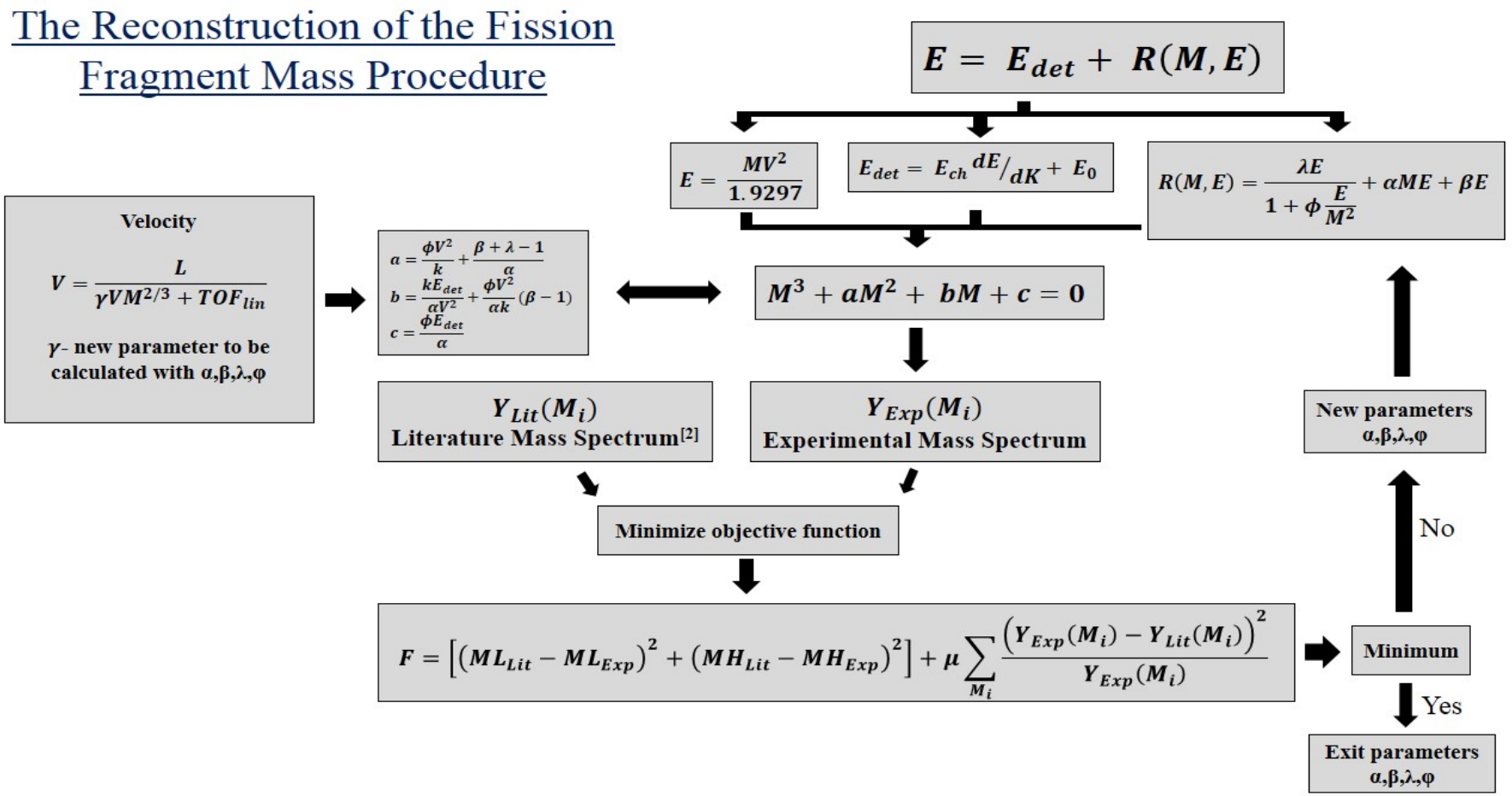

Figure 3.6: The algorithm for the procedure used in the reconstruction of the fission fragments mass.

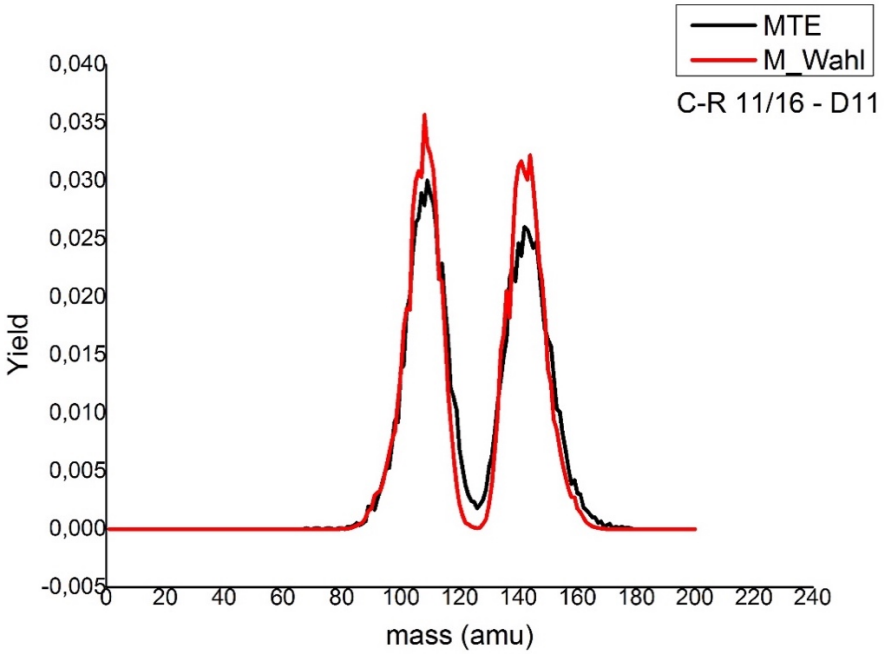

Figure 3.7: The calculated mass spectrum(MTE) of D11 vs the literature mass spectrum (M_Wahl).

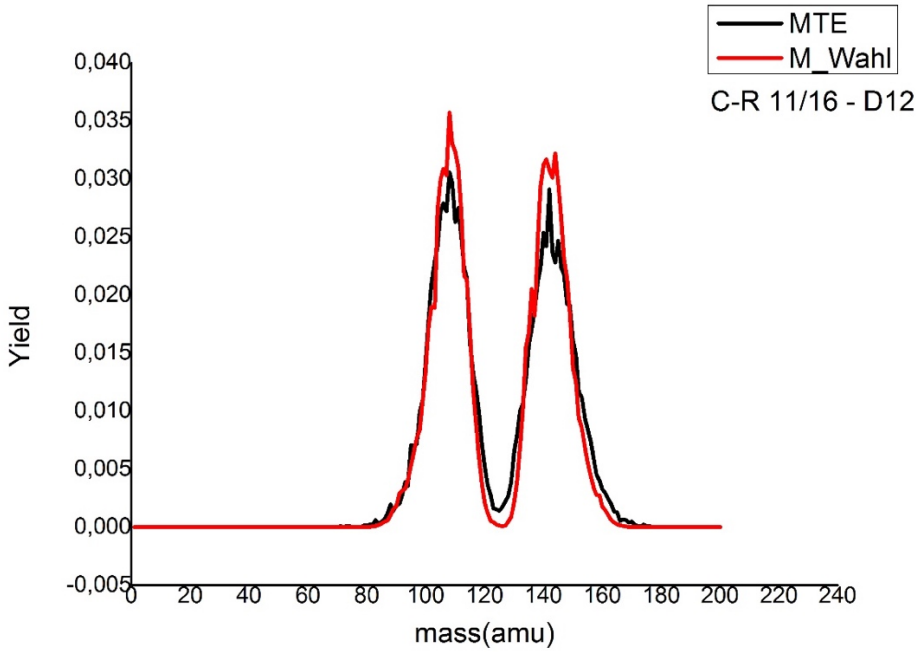

Figure 3.8: The calculated mass spectrum(MTE) of D12 vs the literature mass spectrum (M_Wahl).

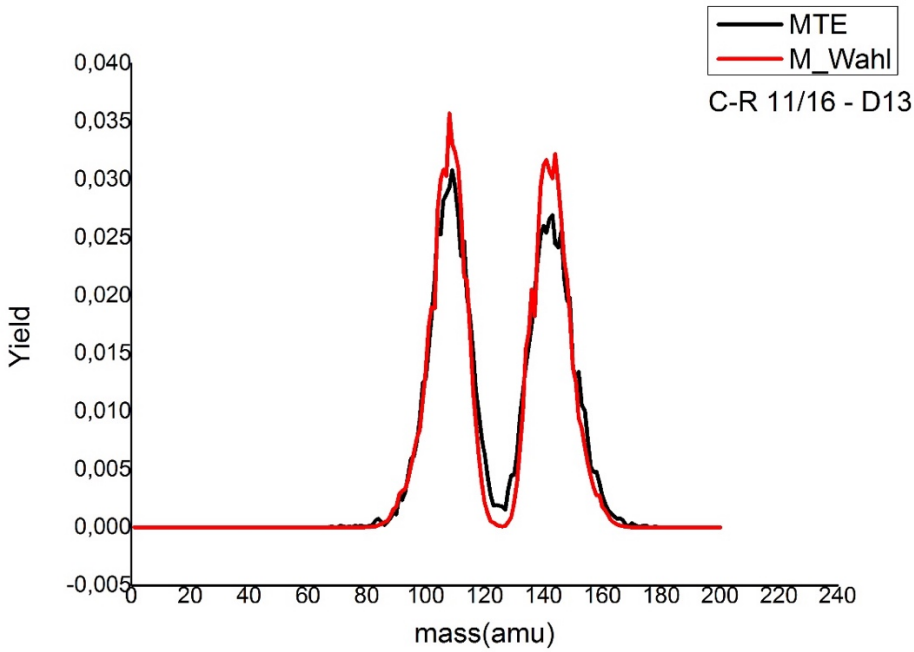

Figure 3.9: The calculated mass spectrum(MTE) of D13 vs the literature mass spectrum (M_Wahl).

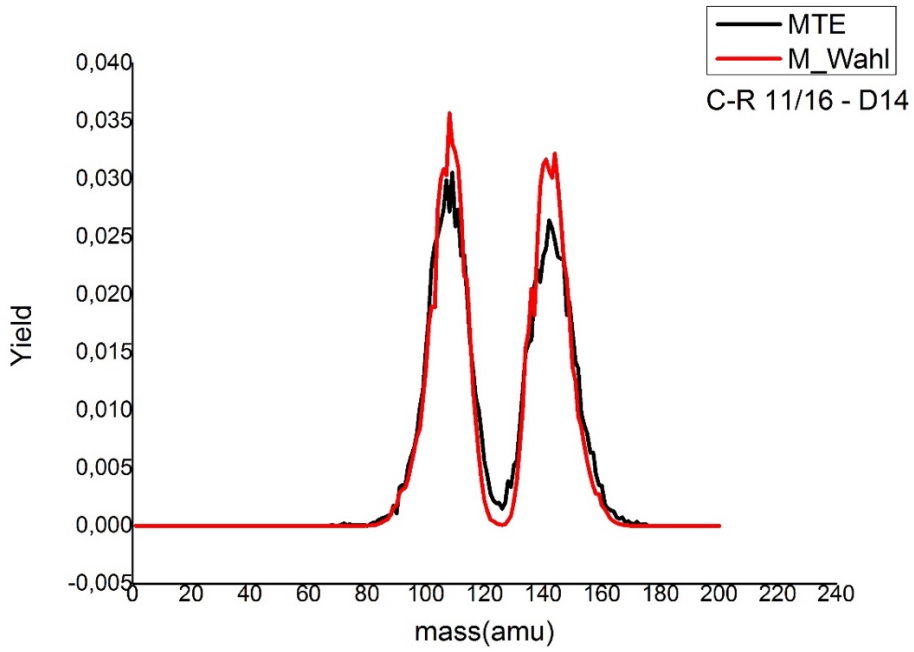

Figure 3.10: The calculated mass spectrum(MTE) of D14 vs the literature mass spectrum (M_Wahl).

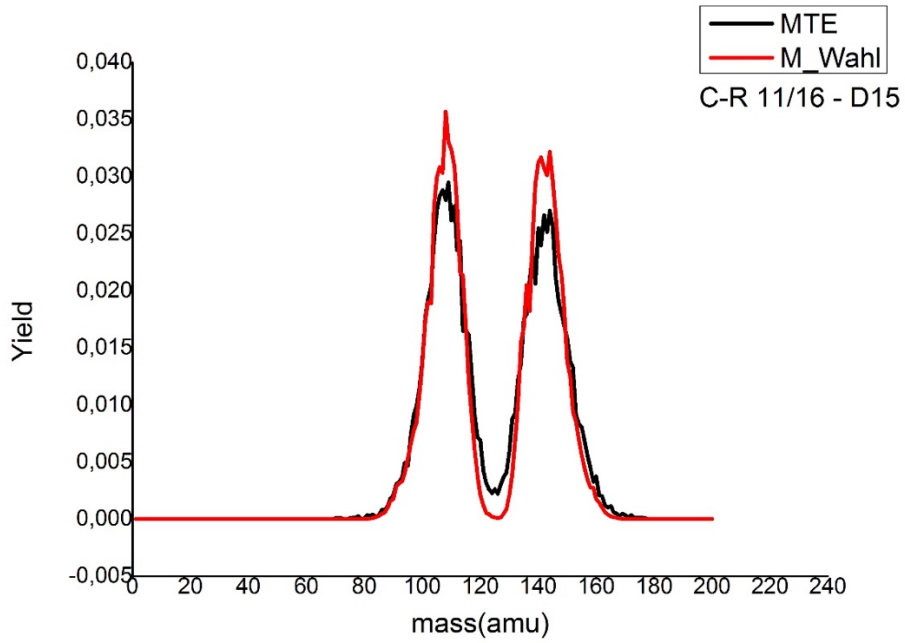

Figure 3.11: The calculated mass spectrum(MTE) of D15 vs the literature mass spectrum (M_Wahl).

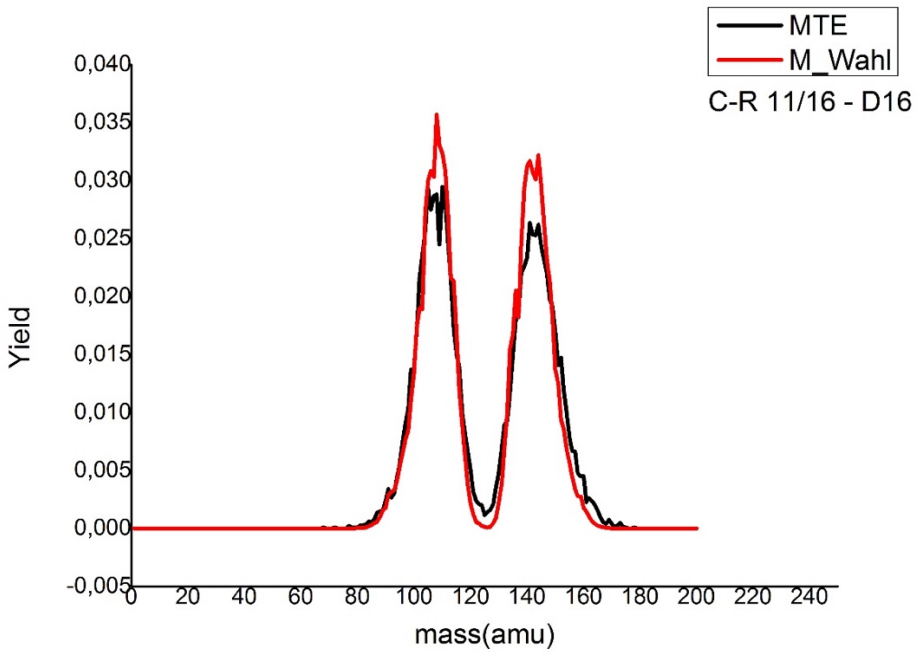

Figure 3.12: The calculated mass spectrum(MTE) of D16 vs the literature mass spectrum (M_Wahl).

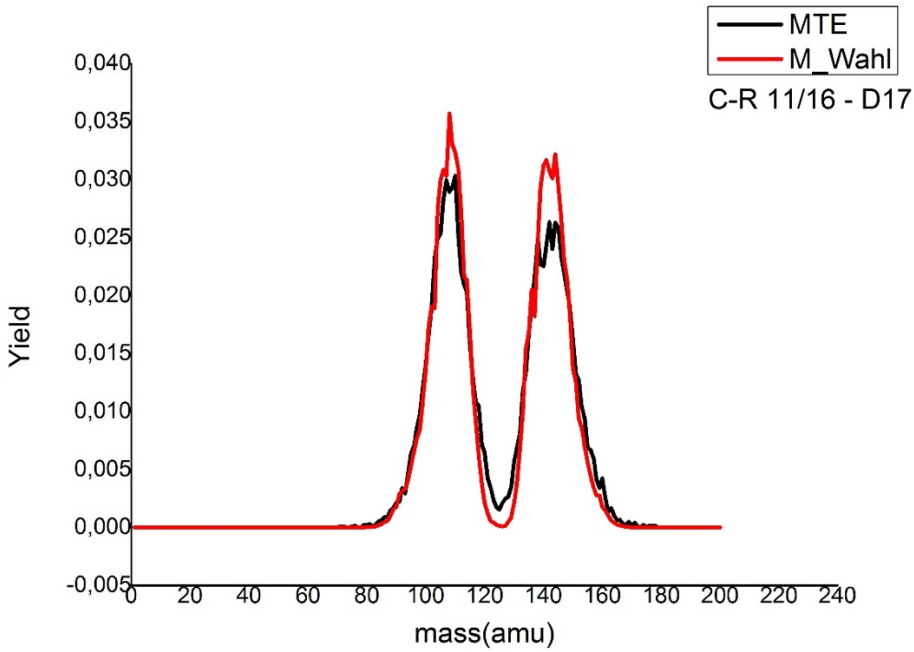

Figure 3.13: The calculated mass spectrum(MTE) of D17 vs the literature mass spectrum (M_Wahl).

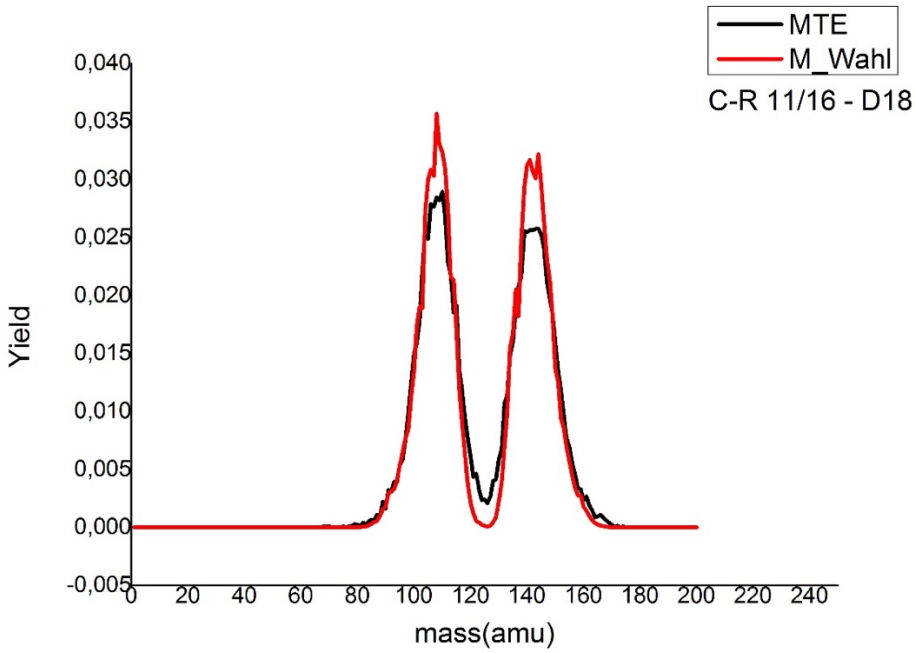

Figure 3.14: The calculated mass spectrum(MTE) of D18 vs the literature mass spectrum (M_Wahl).

Table 3-3: Parameters for the mass reconstruction procedure.

PIN	alpha	beta	lambda	phi	Gamma	kE (MeV/ch)	E0 (MeV)	Ltof (cm)	kT (ns/ch)	T0(ns)	Deg	DegM
11	4.691309e-05	3.844077e-03	4.870000e-01	6.985000e+02	-1.102169e-05	0.000383	0.0000	14.74	0.200000	-1.184921	0.500142	0.166680
12	1.007713e-05	9.091170e-03	4.870000e-01	6.985000e+02	-1.102169e-05	0.000382	0.0000	14.47	0.200000	-1.718613	0.500142	0.166680
13	4.638111e-05	3.357695e-04	4.870000e-01	6.985000e+02	-1.102169e-05	0.000382	0.0000	14.47	0.200000	-1.570166	0.500142	0.166680
14	1.037159e-05	9.969075e-08	4.870000e-01	6.985000e+02	-1.102169e-05	0.000389	0.0000	14.74	0.200000	-1.631770	0.500142	0.166680
15	4.240093e-05	1.023287e-02	4.870000e-01	6.985000e+02	-1.102169e-05	0.000383	0.0000	14.74	0.200000	-1.300374	0.500142	0.166680
16	4.605422e-05	4.902210e-04	4.870000e-01	6.985000e+02	-1.102169e-05	0.000395	0.0000	14.47	0.200000	-2.001545	0.500142	0.166680
17	7.133926e-05	2.462861e-03	4.870000e-01	6.985000e+02	-1.102169e-05	0.000391	0.0000	14.47	0.200000	-2.209370	0.500142	0.166680
18	4.195523e-05	3.398621e-03	4.870000e-01	6.985000e+02	-1.102169e-05	0.000381	0.0000	14.74	0.200000	-3.550003	0.500142	0.166680

Table 3-4: Comparison of the experimental values and expected values from literature [12], [52].

PIN	Mass - Light Fragment (amu)				Mass - Heavy Fragment (amu)				Velocity - Light Fragment (cm/ns)				Velocity - Heavy Fragment (cm/ns)		
	ML_exp	ML_lit	ΔML		MH_exp	MH_lit	ΔMH		VL_exp	VL_lit	ΔVL		VH_exp	VH_lit	ΔVH
11	107,600	107,25	0,35		141,700	141,29	0,415		1,337	1,379	0,042		1,001	1,039	0,038
12	106,900	107,25	0,35		141,600	141,29	0,315		1,344	1,379	0,035		1,003	1,039	0,036
13	107,300	107,25	0,05		141,500	141,29	0,215		1,325	1,379	0,054		0,995	1,039	0,044
14	106,900	107,25	0,35		141,600	141,29	0,315		1,357	1,379	0,054		1,015	1,039	0,024
15	107,100	107,25	0,15		141,400	141,29	0,115		1,337	1,379	0,042		1,000	1,039	0,039
16	106,900	107,25	0,35		141,800	141,29	0,515		1,36	1,379	0,019		1,010	1,039	0,029
17	107,100	107,25	0,15		141,400	141,29	0,115		1,334	1,379	0,045		0,998	1,039	0,041
18	107,200	107,25	0,05		141,400	141,29	0,115		1,329	1,379	0,05		0,993	1,039	0,046

3.3. Experimental testing of the Data Processing Procedure

A special experiment was conducted to test the fission fragment's mass reconstruction procedure presented in section 3.1. This experiment was conducted at the IC-100 Accelerator of the Flerov Laboratory of Nuclear Reactions (FLNR) at the Joint Institute for Nuclear Research (JINR) in Dubna, Russia in November 2015. The IC-100 Accelerator delivered the beam of ^{132}Xe ions of energy of about 1 MeV/A to thin metal targets (foils) of different elements. These elements were aluminium (Al), titanium (Ti), copper (Cu), niobium (Nb), silver (Ag) and gold (Au). Each element was investigated separately and the thickness of each foil was about 1 μm.

Scattered Xe ions and the knock-out ions from the target foils were detected by using a double arm time-of-flight spectrometer referred to as Light Ion Spectrometer for South Africa (LIS-SA). The name of this spectrometer was chosen randomly, it can also be used for heavy ions and was specifically designed to be installed in South Africa at Stellenbosch University. This spectrometer was first presented in [21]. The schematic view of the LIS-SA is shown in Figure 3.15. As shown in this figure, The LIS-SA consist of one PIN diode detector installed in each arm and two MCP detectors installed in each arm. The PIN diodes can be used to measure both the TOF and energy signal of the ions. The two MCP detectors are used to measure the TOF of the ions. In a case of heavy ions, the MCP detectors are free from plasma delay and they produce no distortion to the heavy ion passing through them. The LIS-SA brings along the possibility to measure TOF from MCP – PIN and from MCP – MCP, providing the opportunity to estimate the effect of plasma delay.

For the purpose of this experiment, only one arm of the LIS-SA was used to measure the knocked out ions from the foils. The configuration of this

experiment is shown in Figure 3.16 and Figure 3.17. Figure 3.16 shows the position of the detectors in relation to the beam line. The distance between the target and the start MCP detector is 500 *mm*. The distance between the two MCP detectors is 173 *mm* and the distance between the stop MCP detector and the PIN is 31 *mm*. Therefore, the distance between the start MCP and the PIN is 104 *mm*. Figure 3.17 shows the scheme of the electronics used this experiment.

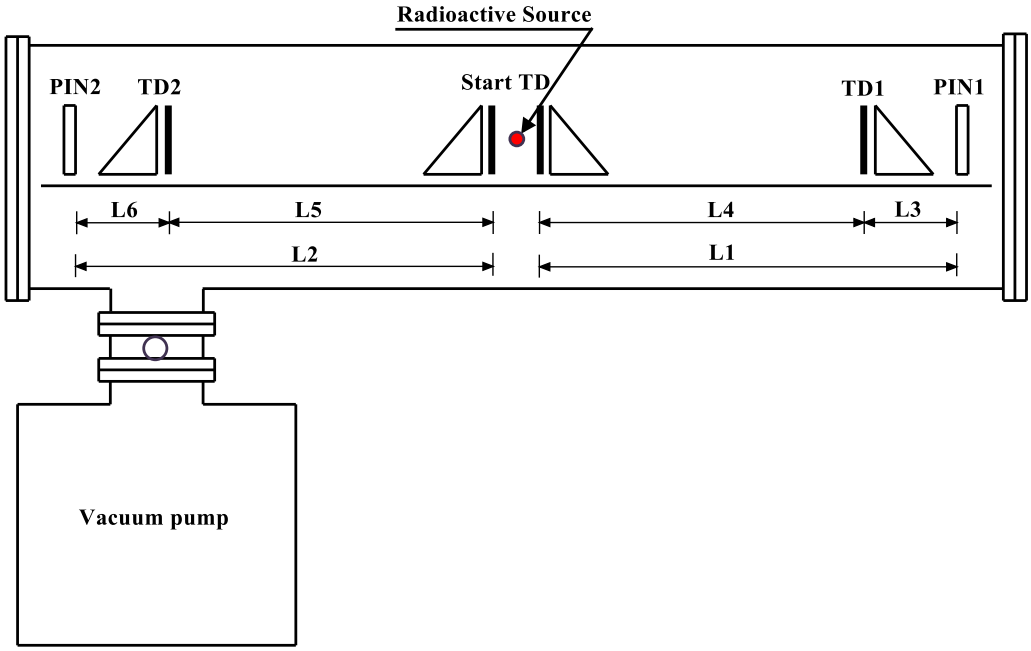

Figure 3.15: Schematic view of the LIS-SA setup.

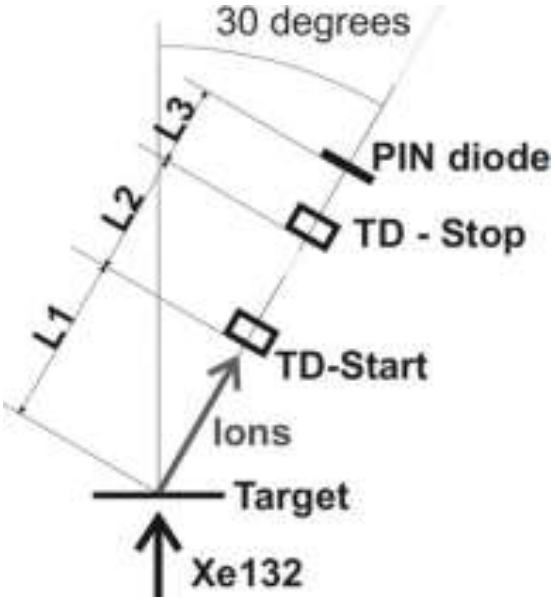

Figure 3.16: Position of the detectors in relation to the beam line. TD-Start is the Start MCP and TD-Stop is the Stop MCP detector. The distances $L1 = 500\ mm$, $L2 = 173\ mm$ and $L3 = 31\ mm$ [59].

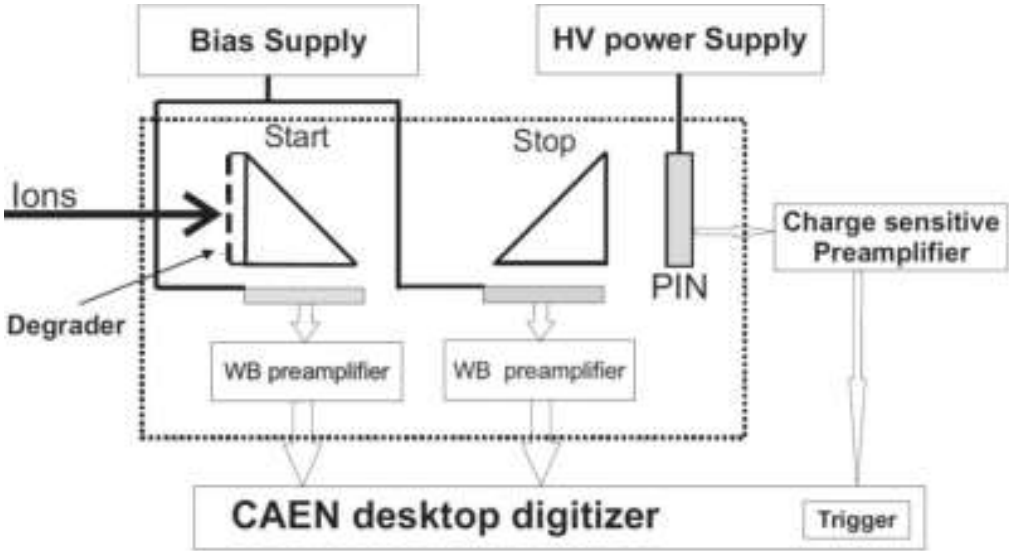

Figure 3.17: Electronics scheme of the LIS-SA setup used in the experiment where the data processing procedure was tested [59].

The aim of the experiment was to calculate the masses of the knocked out ions at different energies ranging between $7 - 115\ MeV$. To achieve the different energies, a multi-section degrader was installed in front the start detector. The aim of the degrader was to cut out the energy of the ions in sections, thus the mass of each element was calculated at different energies.

For a more efficient data acquisition process a new CAEN Desktop Digitizer DT 5742 (referred here as digitizer) has been incorporated into the electronics of the LIS-SA as the main data acquisition system. The digitizer consists of 16 and one input channels. The main reason to incorporate the digitizer is that it can convert the signals into digital values and transmit them directly into a computer. Since it has 16 inputs, one digitizer can be used in the LIS-SA for all the signal registration.

The masses of the detected ions were calculated using the procedure presented in section 3.1 (the output parameters for this procedure are shown in Table 3-5). Figure 3.18 shows the calculated masses of the detected ions at different energies. These results are also presented in [59]. The mean mass isotopes of each element are shown by vertical lines. The figure clearly shows that all the calculated mass (shown as black dots in the figure) for each element at different energies agrees very well with the expected values. This means that they all lie along the same vertical line. The procedure gives the same mass for each ion detected at different energy. The parameters for the mass reconstruction procedure applied in this experiment are shown in Table 3-5.

In this figure (Figure 3.18), there are systematic deviations from some of the experimental points from the vertical line of the Xe beam ions, which are presumably due to the random scattering of the beam. The results shown in Figure 3.18 are the expected results. This confirms that the procedure developed in section 3.1 for the reconstruction of the

fission fragment masses for the heavy ions in a wide range of mass and energy works very well for our experimental methods.

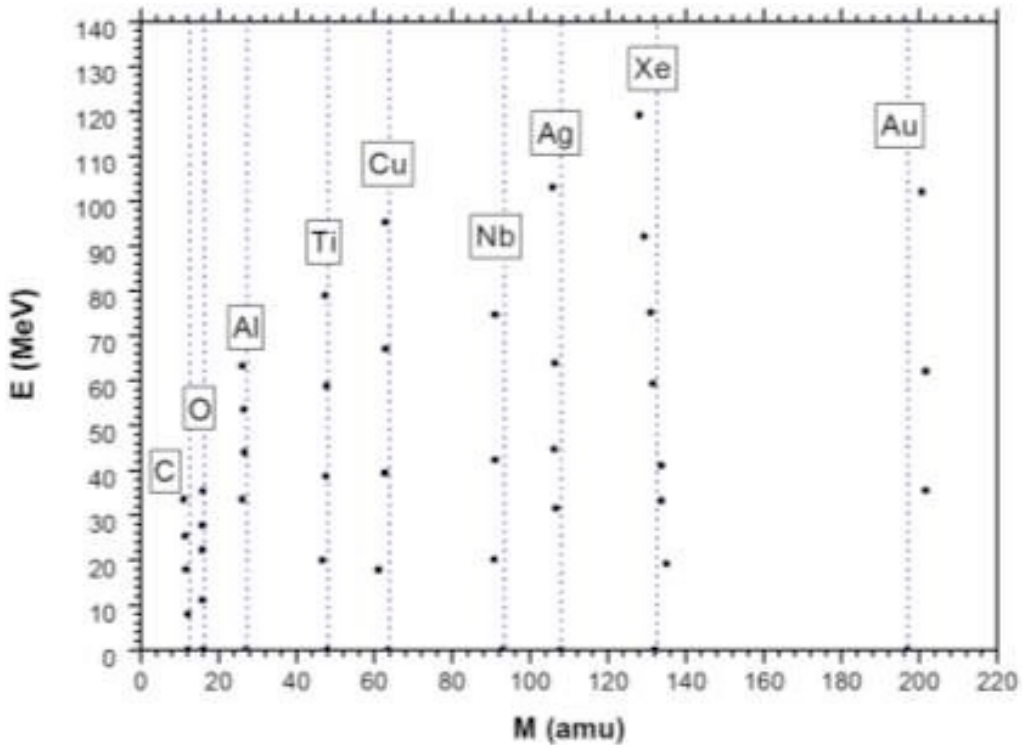

Figure 3.18: Calculated masses of different ions at different energies. The mean mass of isotopes for each element is marked by vertical line [59].

Table 3-5: Parameters for the mass reconstruction procedure for the LIS-SA experiment.

alpha	beta	lambda	phi	Gamma	kE (MeV/ch)	E0 (MeV)	Ltof (cm)	kT (ns/ch)	T0(ns)	Deg	DegM
1.4231946e-04	9.378166e-04	4.870e-01	6,985e+02	-1.41187e-01	0.000382	0.000000	10.400	0.200000	-2.00138s	0.500142	0.166680

3.4. Conclusion

The COMETA spectrometer presented in this work has been successfully used in few experiments. For future studies, the COMETA spectrometer will be the main setup for the experiments dedicated to the study of CCT. The data processing procedure presented in this chapter was first used in the early stages of the COMETA spectrometer. Since then the procedure has been greatly improved. The improvement of the procedure includes calculations (algorithms), programming codes and graphical user interface. At this stage it can be confirmed that this procedure is the most reliable procedure for the processing of experimental data from heavy ion experiments using semiconductor-based detectors such as PIN diodes. The next chapter (chapter 4) presents results obtained in an experiment performed using the COMETA spectrometer. The results are based on the investigation of the CCT outlined in chapter 1.

Chapter 4

Results and Analysis

The first results obtained from searching the new ternary decay of low excited heavy nuclei are presented in chapter 1 of this work. As discussed in the early chapters, this decay is called Collinear Cluster Tri-partition (CCT). The CCT was revealed through a particular bump corresponding to specific missing mass in the fission fragment mass distribution. The first result in which the CCT was observed from the spontaneous fission of ^{252}Cf is shown in Figure 1.2 and discussed in section 1.6.1. These results were obtained from the experiment performed using the modified-FOBOS spectrometer discussed in section 2.2.1. In these results, the CCT is observed as a 'bump' that appears in the mass-mass distribution from the side of the spectrometer that faces the source backing. The detailed study to ensure that the events appearing in the bump are real events linked to the newly observed CCT was performed and confirmation is shown in Figure 1.3, Figure 1.4, Figure 1.5 and Figure 1.6.

An experiment with neutron induced fission of ^{235}U was performed using the mini-FOBOS spectrometer (discussed in section 2.2.2.) and similar results were observed. These results are discussed in section 1.6.2. Additional results using data obtained in coincidence with neutrons from the spontaneous fission of ^{252}Cf are detailed in section 1.6.3. All these results confirmed the existence of the CCT in the framework of the

missing mass method. It was mentioned in [21], that a direct detection of all the decay partners of the CCT will be a more convincing experimental approach.

A mosaic detection system to perform the direct detection of all the decay partners of the CCT was brought into operation and has been presented in this work. This detection system is the COMETA spectrometer and was discussed in chapter 2 of this dissertation. This chapter outlines the results of the experiment that was conducted using the COMETA spectrometer installed at the FLNR at the JINR. The experiment was conducted in 2010 for a period of 9 weeks and the total statistics of binary events collected in coincidence with neutrons is about 4×10^6 events. The activity of the spontaneous ^{252}Cf source was 370 fissions per second and was deposited on the Al_2O_3 backing of 50 $\mu g/cm^2$ thickness and 18 mm in diameter.

4.1. Results from the direct detection of all the CCT partners

From the previous observations of the CCT, several decay scenarios were suggested, but the one that was more convincing is a three-body pre-scission chain reaction where a third (middle) fragment have a very low velocity. This fragment was presumed to be at rest during scission and it became an isotropic source of neutrons. The other two moving fragments will emit neutrons along their fission axis. From this idea, the COMETA spectrometer was coupled with a 'neutron-belt' (discussed in section 2.3.5) to detect neutrons in coincidence with fission fragments. This section presents the results from the COMETA spectrometer obtained with two specific conditions, namely; there are three fragments detected from three different PIN diodes of the COMETA spectrometer and the fission event is in coincidence with at least three neutrons detected by the 'neutron belt'.

Before discussing the results based on these specific conditions, consider Figure 4.1 which shows the results from the COMETA spectrometer that confirms the previously observed structures in the missing-mass method (nickel-bump). In these results, fission fragments from the spontaneous decay of ^{252}Cf were registered using the COMETA spectrometer and they were first reported in [40]. It is important to mention that the supporting structure that holds together the PIN diodes in the mosaics of the COMETA spectrometer had a bigger influence in revealing the structures shown in this figure. The fragments flying in the same direction should at least be separated by an angle larger than $\sim 1^o$ for the two fragments to be registered in the neighbouring PIN diodes (discussed in section 2.4). When the fragments are separated by $0 < \theta < 1^o$, there is a possibility for a missing-mass method. This means that one of the fragments can hit the supporting structure of the PIN diodes. In Figure 4.1 only the region of the mass-mass distribution showing the events where the Ni-bump ($M_1 = 68\,amu$ to $M_1 = 80\,amu$ and $M_2 = 128\,amu$ to $M_2 = 150\,amu$) was initially observed is shown.

In the distribution shown in Figure 4.1, some points from one of the binary fission fragments are shown but they are of no interest. The rectangular like structure below the binary fission loci bounded by the magic nuclei corresponding to Tin-128 (arrow 1 on the figure), Nickel-68 (arrow 2) and Nickel-72 (arrow 3) is observed. It is important to note that this structure is only observed in the spectrometer arm facing the source backing. There are no specific conditions applied to this data since the data from COMETA has no background due to the data acquisition procedure (mass reconstruction procedure) used.

The next feature visible in Figure 4.1 are two tilted diagonal lines marked by number 4. These lines start at the partition of $(128\,amu; 68\,amu)$ and $(134\,amu; 68\,amu)$ and corresponds to the sum of the masses $M_s = M_1 + M_2 = 196\,amu$ and $M_s = 202$ respectively. These structures are similar to the ones observed in Figure 1.3 and Figure 1.4

corresponding to $M_s = 204\ amu$, $M_s = 208\ amu$, $M_s = 212\ amu$ and $M_s = 214\ amu$ discussed in chapter 1, section 1.6.1. Note that the structures in Figure 1.3 and Figure 1.4 were revealed using a second derivative filter method [26], [33] but from the COMETA spectrometer the results are observed without any special filter method (Figure 4.1).

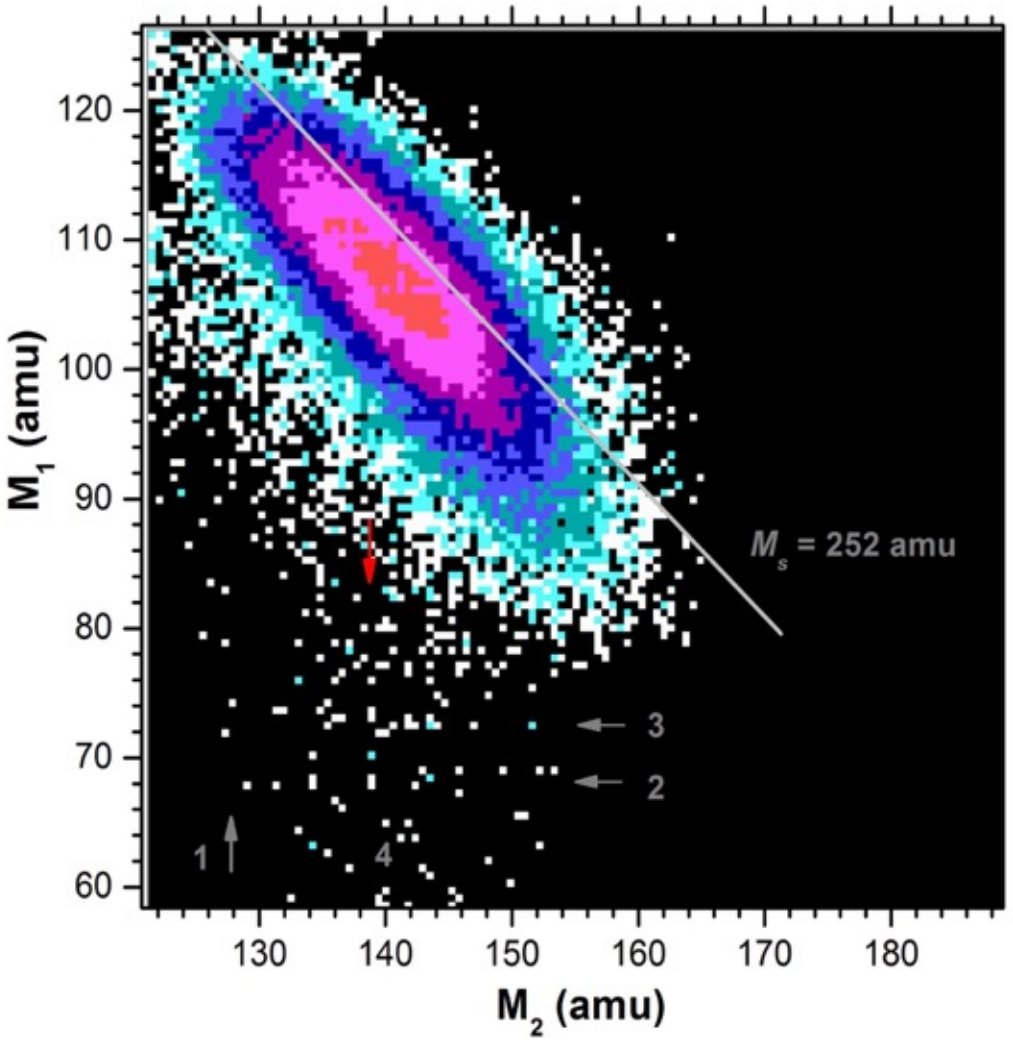

Figure 4.1: The mass-mass distribution from the COMETA setup only showing the region around where the Ni-bump was initially observed [40].

It is important to point out that the difference in the experimental yield from the results of the modified-FOBOS setup, Figure 1.2 and the COMETA spectrometer, Figure 4.1 is due to the type of the blocking medium used. The blocking medium used in the modified-FOBOS setup was the grid (mesh) shown in Figure 2.6 and the one used in the COMETA spectrometer is the supporting grid of the PIN diode detectors in the mosaics. The difference in the angular distribution of fission fragments after passing through the source backing which leads to a specific detection of the fragments by the detectors (from the two spectrometers) is also responsible for the difference in the experimental yields. The angular distribution for the modified-FOBOS is shown in Figure 2.5 and for the COMETA is shown in Figure 4.2.

Comparing the results from the modified-FOBOS and from the COMETA spectrometer confirms the existence of the tilted ridges corresponding to $M_s = const$ which are linked to magic partitions. It is important to note that the experiment performed at the modified-FOBOS and that performed at the COMETA spectrometer differs both in terms of the structure of the detectors used and the fission fragments mass calculation procedure, yet they yield comparable results. As discussed in section 2.4, the COMETA spectrometer does not only provide the direct detection, the missing-mass approach can still be applied (event marked by 1-2-3 in Figure 4.2 and section 2.4).

The region of the data shown in Figure 4.1 where the rectangular structures mentioned above are observed (shown by the red arrow) is further analysed in this chapter. These observations illustrate the fact that the CCT decay occurs in variety of modes given by the different mass combinations. Some of these decay modes will be discussed in chapter 5 of this dissertation.

4.1.1. Detection of three fragments

The COMETA spectrometer allows a detection of three fragments in-coincidence with each other from three different PIN diode detectors. The mechanism that allows the COMETA spectrometer to detect three fragments is explained in section 2.4 and illustrated in Figure 2.25 (repeated below as Figure 4.2 for ease of reference). This figure shows all the possible CCT events that can be registered by the COMETA spectrometer.

The focus of this section is on the CCT event marked by lines 1-2-5 in Figure 4.2. This is the triple detection of the CCT fragments from the COMETA spectrometer. It means that the heavy fragment flies towards one arm of the spectrometer and the two light fragments fly towards the opposite arm. The heavy fragment in this case will be the one represented by line 1 in Figure 4.2 and the two light fragments are represented by lines 2 and 5. Therefore this implies that the heavy fragment will be detected in one arm of the spectrometer in coincidence with the two light fragments detected in the other arm by two different PIN diodes. This is the direct detection of all the three fragments referred to as triple detection of the CCT fragments.

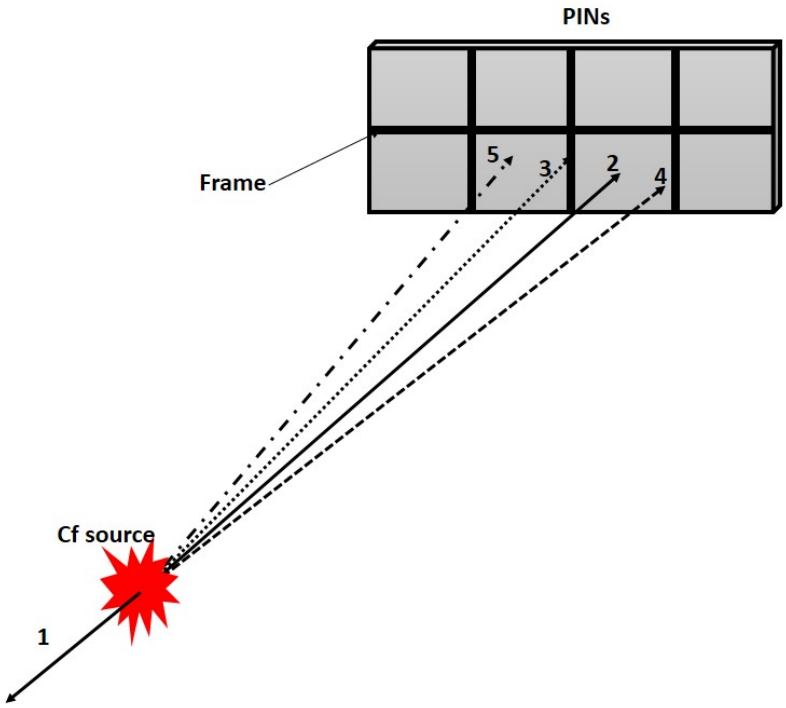

Figure 4.2: A replica of Figure 2.25 showing the different CCT events that can be registered by the COMETA Spectrometer. In this section the focus is on the event marked by lines 1-2-5, which represents the triple detection of the CCT fragments.

Figure 4.3 below shows the main results obtained from the COMETA spectrometer and they are also presented in [27] and [40]. The events shown in this figure are selected by the condition that three fragments were detected according to the triple detection explained above. It is important to note that this is a mass-mass distribution and each dot on the distribution represent three individual fragments detected from the COMETA spectrometer. The masses of the fragments are denoted by m_1, m_2 and m_3, in the order of their masses, that is, $m_1 > m_2 > m_3$. The distribution shows m_1 vs m_2, the actual value of m_3 is not shown on the distribution because the velocity of m_3, the lightest fragment, does not exceed 0.55 cm/ns and the energy does not exceed 2 MeV. The actual mass value for the m_3 was not calculated because in the mass calculation procedure presented in section 3.1.3, the energy value of 2 MeV was set as the energy threshold, this procedure could not minimize the criterion function shown in equation (3.20) for the correct value of mass at this low energy.

The events shown in Figure 4.3 represent the decay of ^{252}Cf into three fragments through the CCT channel. There are two important rectangular structures that are observed on the distribution which are formed by the line of events directly linked to the CCT decay. The first rectangular structure that can clearly be observed is bounded at the top left corner by the events representing the molybdenum-108 (^{108}Mo), shown by the horizontal line of events marking $m_2 = 108$ amu and by the events representing the tin-134 (^{134}Sn) shown by the vertical line of events marking $m_1 = 134$ amu. At the bottom, this rectangle is bounded by events representing zirconium-102 (^{102}Zr) shown by the horizontal line of events marking $m_2 = 102$ amu. The second rectangle is bounded at the top left corner by the events representing the technetium-110 (^{110}Tc) shown by the horizontal line of events marking $m_2 = 110$ amu and by the events representing the tin-128 (^{128}Sn) shown by the vertical line of events marking $m_1 = 128$ amu. This rectangle is also bounded at

the bottom left corner by events representing zirconium-102 (^{102}Zr) shown by the horizontal line of events marking $m_2 = 102\ amu$.

Below these two rectangular structures, there is a horizontal line of events marking the $m_2 = 98\ amu$, representing the deformed magic strontium-98 (^{98}Sr) (shown by arrow 3 in the figure). This horizontal line of events passes through a group of events lying in the vicinity of another deformed magic xenon-142 (^{142}Xe) (the events are marked by number 8 in the figure). These group of events represent the first fragment of mass $m_1 = 142\ amu$, which is the ^{142}Xe and the second fragment of $m_2 = 98\ amu$, which is the ^{98}Sr. The mass of the detected third fragment was not calculated due to threshold level of the data processing procedure. It is important to note that each corner (or line of events) of the rectangles represents the actual detected known nuclei with magic constituents.

Another interesting line of events to be pointed out from these results is the diagonal line cutting through the vertex of the first rectangular structure where the $^{108}Mo/^{132}Sn$ nuclei are observed. This line passes through the group of events marked by number 8 and represents the total sum of all the masses given by

$$M_s = m_1 + m_2 = 240\ amu. \tag{4.1}$$

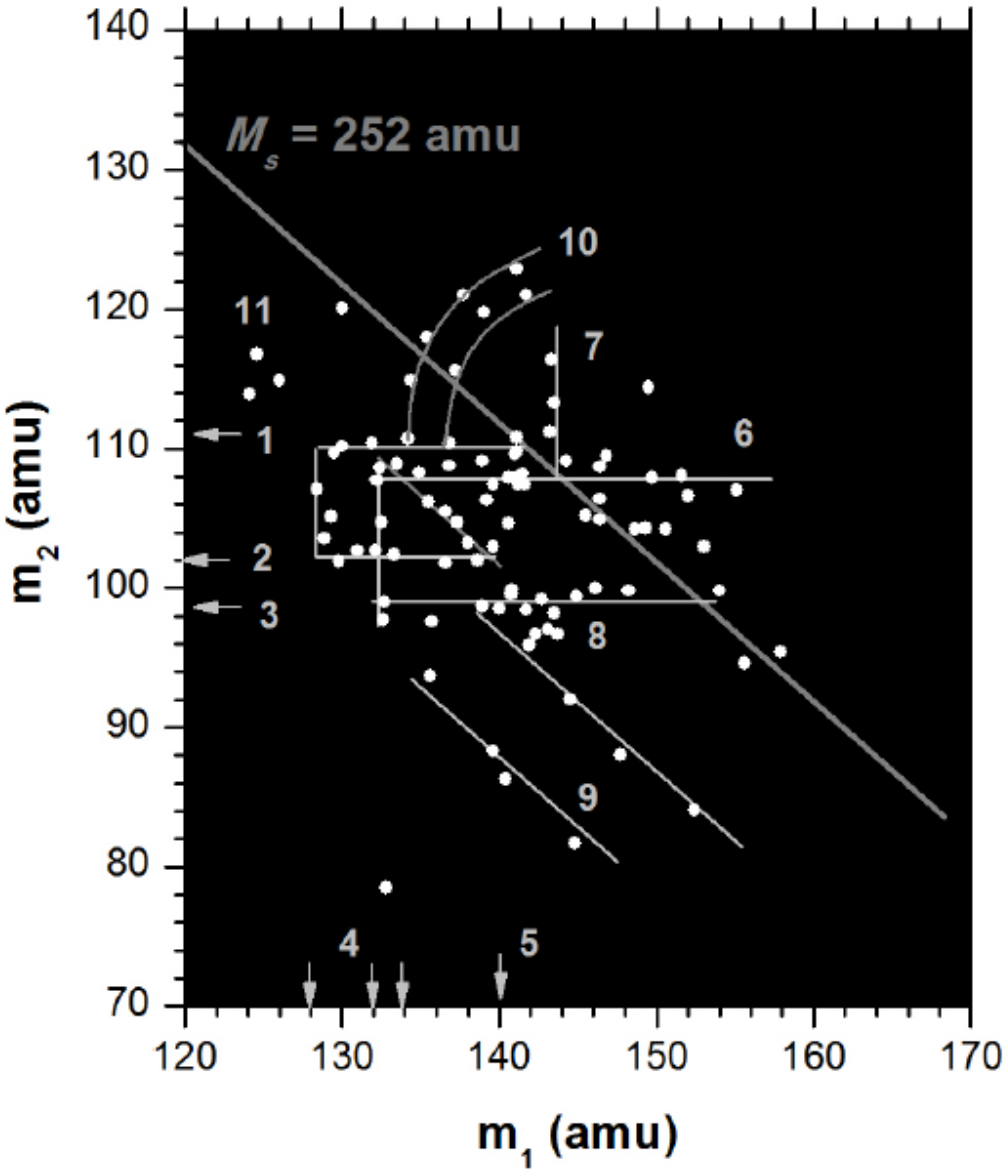

Figure 4.3: The mass-mass distribution showing the triple detection of the CCT fragments. Each event shown on this distribution represent three individual fragments registered by the COMETA with the condition that $m_1 > m_2 > m_3$. The lines, arrows and numbers on the distribution have been drawn to guide the eye (see text for discussion) [27], [40].

This diagonal line of events ($M_s = 240$) depicts that the third fragment along this line is the stable Carbon-12 (^{12}C). Two more diagonal lines of events marked by number 9 and the line above number 9, represents the lines $M_s = 228$ and $M_s = 236$, meaning the third fragment along these lines will have the masses of $m_3 = 24\ amu$ and $m_3 = 16\ amu$ respectively. It is important to note that this represents the missing mass method discussed earlier.

The group of events marked by number 11 on the distribution are of interest. These events are seen in the area where the partition of ruthenium-116 and cadmium-124 is observed. This implies that in that vicinity the fragments detected are $m_1 = 124\ amu$, the ^{124}Cd and $m_2 = 116\ amu$, ^{116}Ru. These are the magic deformed isotopes found in the minima of the C' and K' shells [34].

The points appearing above the line of $M_s = 252\ amu$ need special discussion. It should be noted that the mass of the initial nucleus used on this experiment is $M = 252\ amu$, the ^{252}Cf. The points appearing above the line $M_s = 252\ amu$ means that these are events with masses higher than the initial nucleus. The possible scenario that could lead to these events is the case where, in particular a heavy fragment such as ^{108}Mo in line 6 of the distribution detected as $m_2 = 108\ amu$. When this fragment is detected, it is followed by a slow moving light particle which hits the same PIN diode where the ^{108}Mo fragment was detected. The fast fragment amongst all of them will define the time-of-flight (based on the definition of ternary decay given in section 1.2). The energy measured from this particular PIN diode will be the sum of the two fragments that hit the detector, registered as energy for one fragment and this energy will be incorrect. Therefore, this will lead to higher values of mass which will lie above the line $M_s = 252\ amu$. The similar situation is a result of the vertical line of events linked to $m_1 = 144\ amu$, the ^{144}Ba marked by line 7 on the distribution.

It should be stressed that each event shown in the distribution represents three detected fragments. The events that appear above the diagonal line of $M_s = 252\ amu$, suggest that there is a fourth fragment hitting the same detector as one of the other three, this could be the fourth partner of the quaternary decay. The quaternary decay is not part of this study but its possibility will be outlined in the future work to be discussed in chapter 5.

The last remarkable structures here are the events forming the curved lines marked by number 10 in the distribution. These events also appear above the diagonal line of $M_s = 252\ amu$. These events suggest the possibility of the delayed sequential ternary decay. This could happen in a situation where a light particle delivers a start signal which results in populating a shape isomeric state. A delayed fission decay of the isomeric state could occur. Due to the distorted time-of-flight, two heavy fragments with higher masses (than expected) will result. The shape isomeric state and delayed fission does not form part of the scope of this work but few possibilities will be outlined in chapter 5.

4.1.2. CCT fragments in coincidence with neutrons

The COMETA spectrometer was coupled with a 'neutron belt' which can detect neutrons emitted from fission events. These neutrons are detected in coincidence with fission fragments. This means that when a fission event is registered by the mosaic detectors of the COMETA spectrometer, a gate on the neutron detectors is opened for the detection of neutrons that are in coincidence with that particular event. The neutron multiplicity and detection efficiency of the neutron belt was discussed in section 2.3.5 and outlined in [21].

Experimental results selected by the condition that at least three or more neutrons were detected by the 'neutron belt' together with the fission fragments are shown in Figure 4.4. These results were first

presented in [27] and [40]. It should be noted that the masses shown in this distribution are different from the one in Figure 4.3. In this case the M_1 represents the mean mass from arm one and the M_2 represents the mean mass from arm two. Therefore, the mass shown in this distribution is presented according to the missing mass method. The third fragment of the CCT is accounted by the fact that the selection of three or more neutrons to be detected together with fission fragments implies that there were three fragments emitted from that specific fission event.

The distribution in Figure 4.4 confirms the rectangular structures bounded by deformed magic clusters shown in Figure 4.3. Horizontal lines of events representing masses of ^{108}Mo and ^{98}Sr are clearly seen and marked accordingly on the distribution. The vertical lines of events representing masses of ^{132}Sn and ^{140}Xe are clearly seen. These lines bound the rectangular structures that are linked to the CCT decay. Moreover, these are similar structures to those that are observed in Figure 4.3 and their analysis is the same as in the above section. The difference between the two distributions is the fact that in Figure 4.4 there are no events above the diagonal line of $M_s = 252\ amu$ due to the different selection method used for this distribution.

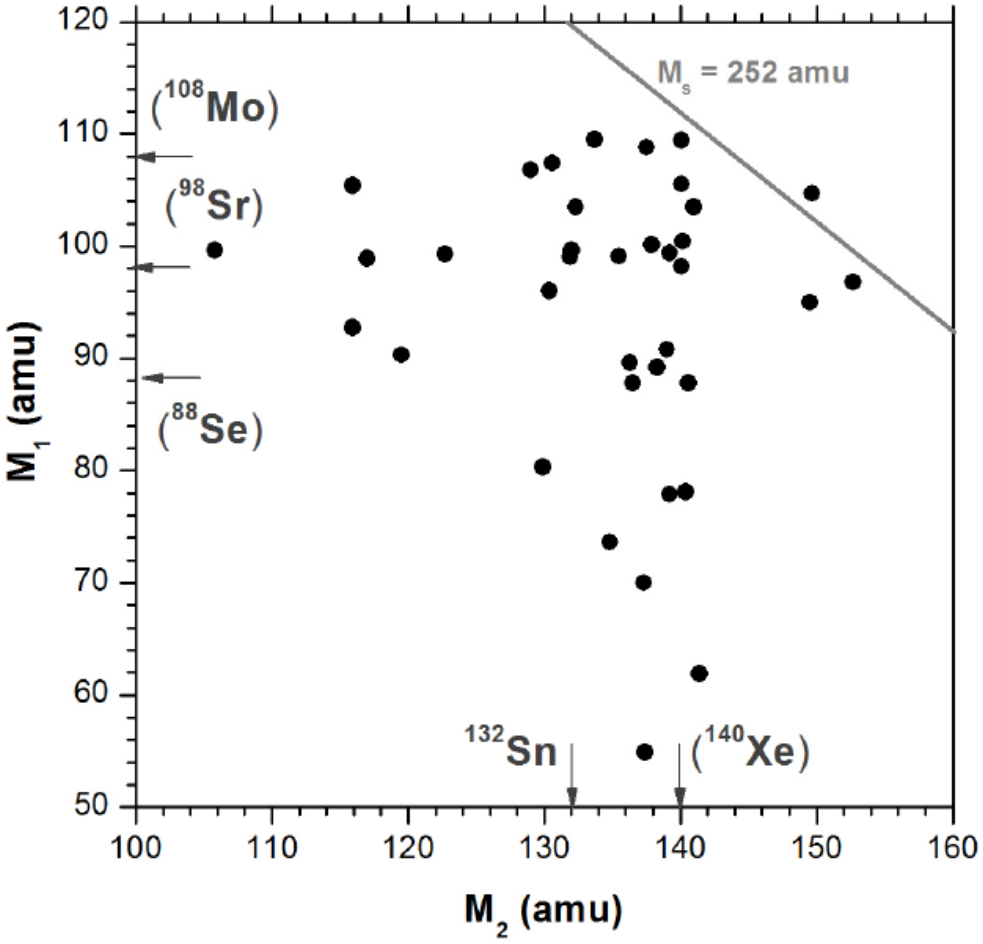

Figure 4.4: Similar events as shown in Figure 4.3 but in this distribution the events were obtained with the condition that there are three or more neutrons detected in coincidence with fragments from the fission events [27], [40].

4.1.3. Summary

Initially the CCT was observed using the missing-mass method and it manifested itself as a 'bump' that was seen in the mass-mass distributions shown in Figure 1.2 and Figure 1.7. The 'bump' was observed from the events collected from one arm of the spectrometers and this was the arm facing the source backing and the blocking medium. Further analysis of the bump revealed tilted lines of $M_s = constant$ where each line corresponded to the different combinations of two fragments detected with at least one of them having a magic nucleon number. The combinations listed in section 1.6.1 revealed that the spherical magic clusters of nickel form part of the constituents of the decay structures of the CCT.

The improved experiment from the COMETA spectrometer has revealed that not only the spherical magic cluster of Ni, but also the deformed magic clusters of ^{108}Mo and ^{98}Sr can be the constituents of the CCT decay. This has been revealed through the rectangular structures bounded by the deformed magic clusters both in the data selected by triple coincidence and neutron multiplicity (three or more neutrons in coincidence with fission events) shown in Figure 4.3 and Figure 4.4 respectively.

Based on these results, it can be concluded that the COMETA spectrometer has successfully presented an improved experimental approach in the study of multi-body decay of low excited nuclei. Not only has the COMETA spectrometer provided a more convincing approach. It successfully confirmed the existence of the CCT decay through the triple coincidence and the neutron multiplicity selection of the events from the experimental data.

4.2. Other Experiments in Searching for the CCT decay

At the same time when the work reported in this dissertation was underway, some other experiments in the study of collinear multi-body decay were performed by the colleagues and collaborators. It is worth mentioning the observations from these experiments as the techniques used were based on the similar techniques used in this work. The results obtained from these experiments confirmed the existence of the CCT and few decay scenarios of the CCT can be suggested. The decay scenarios of the CCT will be summarized in the next chapter.

Two important experiments were performed using heavy ion beams in searching for the CCT decay. The first experiment was the search for the multi-body decay in the reaction of $^{238}U + {}^{4}He(40\,MeV)$. The experimental details are fully outlined in [60]. The other experiment is the investigation of the CCT in the $^{232}Th + d(10\,MeV)$ reaction fully outlined in [61].

From these experiments, it was confirmed that the stable and strong correlations of the structures observed in the CCT decay cannot be just some random coincidences. There is a long-lived nuclear molecule, an isomer, that is formed at scission and it is based on the magic nuclear cluster. It was observed, especially in the second experiment that the pair of magic clusters from the CCT decay plays a similar role as the double magic lead (Pb) cluster in heavy decay [27]. This idea was also suggested in [62].

The main conclusion that was made, especially from the second experiment is the first observation of the true ternary fission of the ^{234}Pa from the reaction $^{232}Th + d(10\,MeV)$. This was based on the direct detection of the three coincident reaction products. The hypothesis that the lightest fragment of the ternary decay is responsible for the missing mass (in the missing mass-method) of the pairs of the magic clusters

(Ni/Sn or Ge/Sn) which could add up to the total mass of the initial nucleus was confirmed [27].

Chapter 5

Summary and Conclusion

5.1. Summary

Multiple experiments using different time-of-flight spectrometers of heavy ions led to a discovery of a new ternary decay channel involving low excited nuclei. This new channel was given the name Collinear Cluster Tri-partition (CCT) due to the features observed, that is, the decay fragments fly apart almost collinearly, one of the decaying fragments has a magic nucleon composition and it presumably decays into three fragments. The experiments were performed using double-arm time-of-flight spectrometers based on the $2V - 2E$ detection method. This means that the energy and the velocity of the fragments were measured directly from the spectrometers and the masses were calculated.

The CCT was observed for the first time in the spontaneous decay of Californium-252 (^{252}Cf) nucleus. This experiment was performed using a the modified-FOBOS spectrometer from the Flerov Laboratory of Nuclear Reactions at the Joint Institute for Nuclear Research (JINR) in Dubna, Russia. The CCT manifested itself through a particular bump in the fission fragment mass-mass distribution. The bump was linked to a magic nickel (Ni) cluster; hence it was referred to as a Ni – bump. This bump was observed using the missing-mass method, meaning only two

fragments were detected and the third one was missing. The difference in the masses of the detected fragments and the initial nucleus served as an indication of the third missing fragment. The source backing/scattering medium installed in front of the start detector and the supporting grid of the stop detectors gave rise to the missing-mass.

Further experimentation using another double arm time-of-flight spectrometer called mini-FOBOS, installed at the FLNR at the JINR in confirmed the existence of the CCT. This particular experiment involved the neutron induced fission of uranium-235 ($^{235}U(n_{th})$). A similar Ni-bump was observed in the fission fragment's mass-mass distribution.

The CCT was first revealed and confirmed in the framework of the missing-mass method. It was clear by then that the direct detection of all the decaying products of the CCT would be a more convincing experimental approach. An experimental approach that achieved the direct detection has been successfully presented in this work. This approach involves the use of a mosaic detection system. A double-arm time-of-flight spectrometer based on the mosaic detection system called the COMETA spectrometer was successfully designed and reported in this work. The COMETA spectrometer uses a mosaic of PIN-diode detectors as stop detectors in each arm to register both the energy and time signals of the fission fragments. The start signal is generated by a Micro Channel Plate (MCP) time-based detector. The scattering medium is installed as source backing facing only one arm of the spectrometer. This achieves the scattering of two light fragments flying in the same direction to be detected in two different PIN-diodes which provided the expected triple coincidence. It is worth mentioning that the missing-mass method can also be achieved in the COMETA spectrometer as one fragment could hit the supporting material of the PIN-diodes forming the mosaic array in each arm.

The COMETA registers the stop time signal and the energy signals of the fission fragments using PIN-diode detectors. This means that the

time and energy signal is registered simultaneously for each fragment reaching the detector. Measuring the time and energy of heavy fragments using silicon-based semiconductor detectors such as PIN diodes comes with two known experimental challenges. These challenges are the plasma delay associated with time measurements and the Pulse-Height Defect (PHD) associated with energy measurements. The PHD is known to have a complicated dependence on the energy and the mass of fission fragments as well as the type of detector used. This brought a challenge in the data processing for the COMETA spectrometer because the final objective is to calculate the mass of the detected fragments using their energy and velocity. A parametrization procedure for the fission fragment mass calculation that considers both the plasma delay and the PHD was successfully designed and presented in this work.

A special double arm time-of-flight experimental setup referred to as Light Ion Spectrometer for South Africa (LIS-SA) was designed to test the parametrization procedure. One arm of the LIS-SA consists of two MCP detectors and one PIN diode. One MCP detector was used as a start detector and the other as a stop detector for the first time-of-flight measurement. This time-of-flight will be free from the plasma delay effect. The other time-of-flight was measured between the start MCP detector and the stop PIN diode detector (as in the COMETA spectrometer). The ability to measure the time-of-flight of the same ion using two detector systems brought the possibility to test the parametrization procedure designed in this work. A special experiment to test the parametrization procedure using different ions with different masses at different energies was performed at the FLNR at the JINR. The results obtained from this experiment proved the procedure to be feasible for the reconstruction of the fission fragment masses. This procedure can be used in time-of-flight measurements using semiconductor-based detectors provided the detector parameters are known.

The results from the COMETA spectrometer revealed the CCT as rectangular structures bounded by the known magic clusters in the mass-mass distribution of the fission fragments. Both results from triple coincidence and neutron gated data revealed the same rectangular structures. The observed rectangular structures could be directly linked to the Ni-bump that was observed from previous experiments. Detailed analysis of these structures confirmed the CCT to be a process that takes place as a two-stage breakup of the initial three body chain-like nuclear configuration with an elongated central cluster. In-beam measurements to investigate the reactions of $^{238}U + {}^{4}He(40\,MeV)$ [60] and $^{232}Th + d(10\,MeV)$ [61] were performed independently and confirmed the CCT in a similar framework.

5.2. Suggested Decay Scenario for the CCT

One of the most pronounced CCT features reported in this work is the Nickel (Ni) bump which was first observed under the missing-mass method and later confirmed through direct detection of all the CCT partners. Similar effects of the Ni – bump was observed as the rectangular structures in the data obtained from the COMETA spectrometer. Thorough investigations of the region of the bump and the rectangular structures in the mass-mass distribution of the fission fragments were performed in order to come up with the decay scenarios that could possibly lead to the CCT. To conclude which decay scenario is associated with the CCT requires more experimental work in this field, however at this stage a few decay scenarios can be suggested.

The decay scenarios presented here are suggested based on the analysis of the results presented in chapter 1 and chapter 4. Results from the experiments mentioned in section 4.2 presented in [27] and [61] were also used. These results are generalized as the results presented in Figure 4.1 in the vicinity of the rectangular structure with its vertex

lying at (68 amu; 68 amu) and the other vertex lying at (72 amu; 72 amu). This rectangular structure is associated with the magic Ni isotope and is similar to the structures obtained from the mentioned references. It should be noted that these rectangular structures are linked to the CCT as discussed in the previous chapters.

In an experiment performed with Gammasphere using a gamma-gamma coincident technique reported in [63], two decay modes for the ^{252}Cf partition were reported. It is important to mention that these modes were reported as binary fission. In order to reproduce these modes experimentally, a cluster configuration of ^{252}Cf nucleus in the scission point was suggested by [64]. This cluster configuration is shown in row number 1 of Table 5-1. This cluster was further expanded to a binary fission of four cluster pre-scission configuration linked to the Ni isotope by [5] and is shown in row number 2 of Table 5-1.

Data from another experiment performed at the University of Jyväskylä in Finland (JYFL) in a double-arm time-of-flight spectrometer using similar techniques used in this work, revealed events where one of the missing fragments is ^{144}Ba and also where one of the detected fragments is ^{144}Ba. The details of the spectrometer and the results are outlined in [5]. In such a case, it is presumable that the pre-scission cluster configuration is similar to the one suggested in [64], shown in row 1. Specifically, for this fragmentation, the configuration is shown in row number 3 of Table 5-1. The scission scenario where ^{144}Ba is missing is shown in row number 4 and where it is detected is shown in row number 5. The missed fragment in row 4 and 5 is marked by the red cross and the sequence of ruptures are marked by the numbers. This also suggests that the true ternary fission is occuring in this scenario.

To produce the events lying in the vertex of the rectangular structure around the (72 amu; 72 amu) of Figure 4.1, the configuration and the sequence of ruptures listed in row number 6 of Table 5-1 is suggested. This configuration implies that after the first two ruptures, the residual

^{144}Ba nucleus stay almost at rest. This nucleus constitutes two ^{72}Ni clusters which will further disintegrate because it has enough interaction energy. This suggests that a quaternary decay via a 4-cluster pre-scission configuration is taking place.

The decay scenarios listed in Table 5-1 are all linked to the experimental data where the CCT was studied. It is clear that under the sequential ternary scission of 4-cluster pre-scission configuration of the mother nucleus, a quaternary decay can takes place and is illustrated in the last row of Table 5-1. Further investigations of the decay scenarios of the CCT phenomenon is part of the future work. It is worth mentioning that these scenarios could only be suggested based on the current available experimental data.

The specific CCT decay scenario presented in this work (this dissertation) gives rise to the observed Ni-bump. The rectangular structures occur as a two-stage breakup process of the initial three-body chain like nuclear configuration with an elongated central cluster. After the first scission there are two clusters, a light cluster and heavy cluster. Predominately the heavy cluster is a di-nuclear system consisting of two clusters, lighter clusters. At the touching point of these two clusters (light cluster and di-nuclear system), the deformation energy of the central cluster (formed from the di-nuclear system) allows the emission of up to four neutrons. The di-nuclear system which will then consist of a lighter cluster and the central cluster will be accelerated through the mutual Coulomb field which results in the current CCT scenario.

Table 5-1: Cluster Configurations leading to the multi-body decays of ^{252}Cf.

No	Pre-scission Cluster Configuration	Comments
1	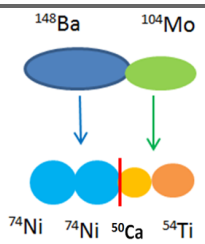	Cluster configuration suggested in [63] and [64]
2	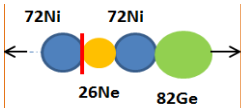	Binary fission 4 cluster pre-scission configuration suggested by [5].
3	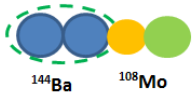	Similar configuration as suggested in row 1, with the possibility to have ^{144}Ba missing and/or detected.
4	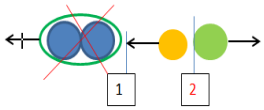	The missed fragment is marked by the red cross and the sequence of ruptures marked by the numbers.
5	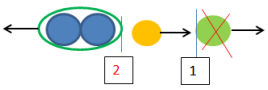	The missed fragment is marked by the red cross and the sequence of ruptures marked by the numbers.
6	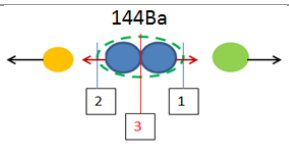	4-cluster pre-scission configuration
7	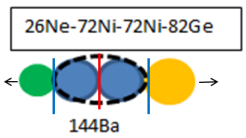	Possible quaternary decay via the 4-cluster pre-scission configuration

5.3. Conclusion

In conclusion, few concerns have been recently raised regarding the CCT phenomenon. The general concern pointed out is whether the CCT is observed in comparison with the conventional ternary fission. It was mentioned in chapter 1, the conventional ternary decay is defined as the decay where a binary fission is accompanied by an alpha particle emitted in the plane perpendicular to the fission axis. On the other hand, theoretical calculations presented in [65] agrees with the CCT phenomenon presented in this work. It is well described that the CCT is regarded as a two-step decay process of a highly deformed pre-scission nuclear configuration in the calculated valleys of the true ternary fission or in the states associated with cold deformed fission in the binary channel [65].

The potential energy of the disintegration of the ^{252}Cf nucleus that correspond to the bottoms of the potential valleys were calculated in [66]. Figure 5.1 shows these potential valleys as a function of a quantity (Q) which is proportional to the quadrupole moment. The valleys that were found connected to the CCT are denoted by numbers from 1 to 5. The shapes of the system at each point are shown in the figure.

The states of the nucleus undergoing fission found in the valley marked by number 3 in Figure 5.1 is linked to the rectangular structures revealed in the data presented in Figure 4.1. These rectangular structures consist of two distinct horizontal lines corresponding to the mass $M_1 = 68\,amu$ (arrow 2, Figure 4.1) and $M_1 = 72\,amu$ (arrow 3, Figure 4.1) and a vertical line corresponding to $M_2 = 128\,amu$ (arrow 1, Figure 4.1). The horizontal lines result in the high values of excitation energy which makes the Sn – cluster to be well preformed in the body of the mother system. Nascent deformed light clusters have enough energy to disintegrate. Predominantly the clusters Ni, Ge, Sr and Mo are formed. The horizontal line from the rectangular structures (in Figure 4.1) is linked to the low values of excitation energy. This means that the mass

of the heavy fragment shifts towards larger masses, while the lighter cluster (Ni) continues to be formed. The experimental results obtained in this work are in good agreement with theoretical calculations performed by other authors.

The results presented in this work also confirms that there is collinear kinematics in ternary decay through the CCT channel. It is important to mention that at the beginning of this work true ternary decay was considered to be undiscovered experimentally. It was only considered as a hypothesis and the collinear kinematics was concluded to be extremely unstable. The ideas of the CCT cannot be based on this concept because the scission scenarios that underlines the fact that this process is attributed by sequential disintegration have been confirmed experimentally. The fact that the di-nuclear system is formed after the first rupture and accelerated through the mutual Coulomb field concludes that the CCT is a collinear process.

The new experimental approach presented in this work (in terms of the COMETA spectrometer for the direct detection of all the CCT fragments) and the results from the other experiments performed in the search for the CCT presented in section 4.2 confirm the existence of the CCT. The discussions above and further theoretical calculations presented in [67], which agrees with the calculations from [68], are in good agreement with the observed CCT phenomenon. It is also important to point out that the CCT does not exclude the possibility of non-collinear decay pointed out in [69]. The mass spectra for CCT fragments are in good agreement with the mass spectra presented in [62] which agrees very well with the spectra presented in [70]. It should be mentioned that the question on which specific decay mode does the CCT follow remains open. This will form part of the future work on CCT.

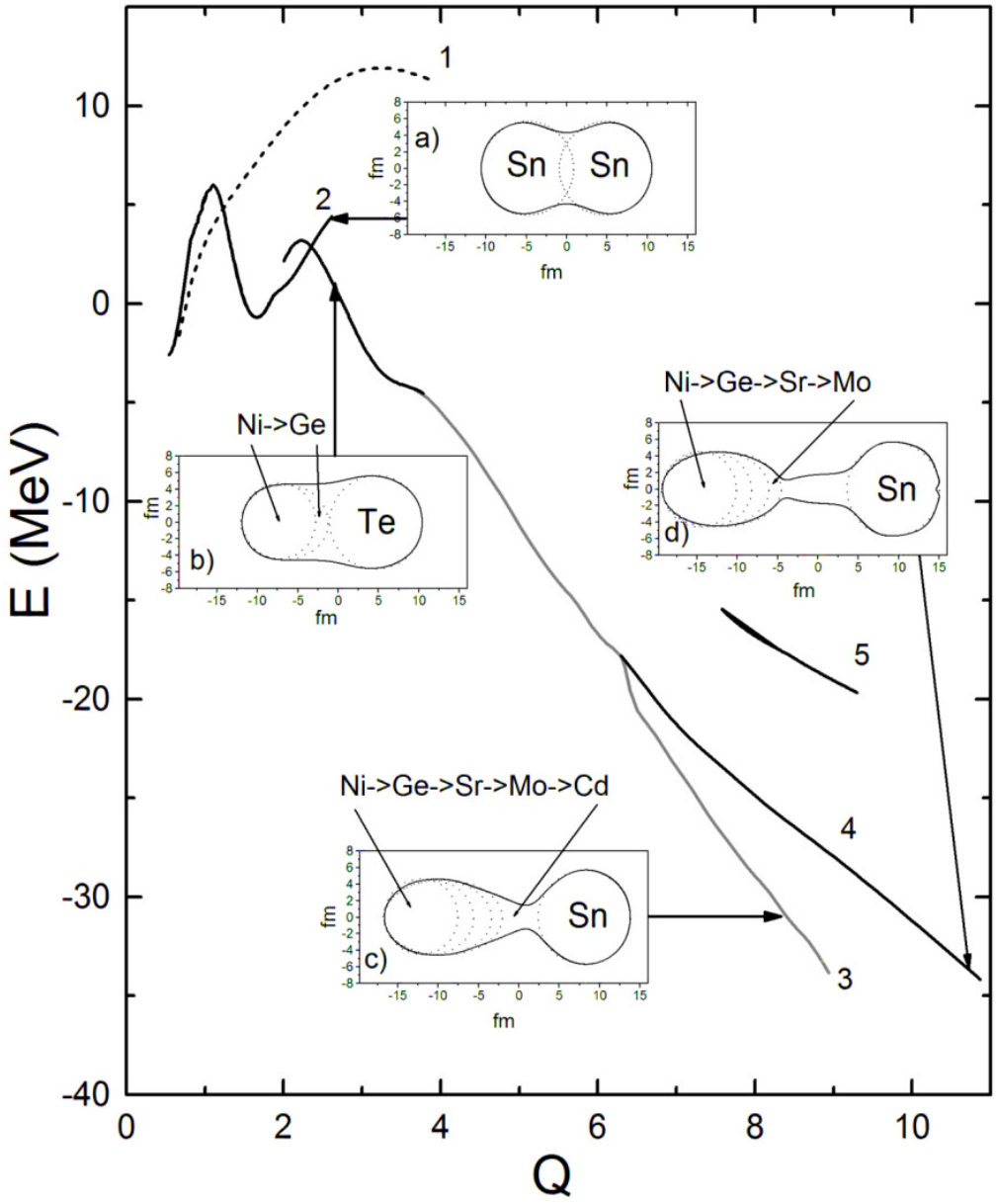

Figure 5.1: Potential energy of the disintegration ^{252}Cf nucleus corresponding to the bottoms of the valleys as a function of a parameter Q proportional to the quadrupole moment as calculated in [66].

5.4. Future work

The COMETA spectrometer presented in this dissertation was successful in confirming the existence of CCT decay. The fact that the COMETA utilised a new experimental technique as compared to the techniques used in FOBOS spectrometers made it possible to confirm the existence of the CCT. The new experimental technique brought by COMETA is the direct detection of all the decay products of the CCT.

An independent experimentation to further confirm the existence and mechanism of the CCT will be performed in near future. This experiment will involve a completely different method of detection from the one used in the COMETA. It is important to note that until recent, including this work, the CCT has been observed under the $2V - 2E$ method which was used in all the experimental setups discussed in this work. An experimental setup that involves a completely different method is the Lohengrin mass spectrometer of the Institute Laue Langevin from Grenoble, France. A series of experiments dedicated to the search for light fission fragments from the far asymmetric fission including isotopes of Ni was performed in this facility and reported in [71]. Such a facility will be used for an independent experimental verification of the CCT.

Further experimentation at the FLNR at the JINR will be performed using the COMETA spectrometer. The design of the COMETA spectrometer is flexible in such a way that it allows different experimental techniques. Some of these techniques includes the investigation of shape-isomers where degraders of different foil sizes will be installed next to the radioactive source. The COMETA spectrometer also allows investigations by in-beam measurements using the IBR-2 reactor from the Frank Laboratory of Neutron Physics at the JINR. In such a case, investigations of the reactions such as the $^{235}U(n_{th}, f)$ can be performed. Improvement of the data processing procedure where only the Desktop Digitizer will be used for data collection instead of CAMAC

modules will be investigated and implemented. The Desktop Digitizer is an electronic module that is able to convert the signals into digital values and transmit them into the computer (as discussed in section 3.3). It represents a full digital replacement of the traditional CAMAC modules. Possibilities of more research projects and collaborations linked to this facility exists.

Bibliography

[1] J. Thomson, "Cathode rays," *Philosophical Magazine,* vol. 44, p. 293, 1897.

[2] E. Rutherford, "The Structure of the Atom," *Nature,* vol. 92, pp. 402-403, 1913.

[3] N. Bohr, "On the Constitution of Atoms and Molecules," *The London Philosophical Magazine and Journal of Science,* vol. 6, pp. 1-5, July 1913.

[4] E. Schrödinger, "The Undulatory theory of the Mechanics of Atoms and Molecules," *Physical Reviews,* vol. 28, pp. 1049 - 1070, 1926.

[5] S. Yamaletdinov, "Studies of Exotic Decay Modes in Fission of Heavy Elements," PhD Dissertation, University of Jyväskylä, Jyväskylä, Finland, 2007.

[6] Fermi E, O. d'Agostino, F. Rasetti and Segre E, *Proc Roy Soc,* vol. 146, no. A, p. 483, 1934.

[7] O. Hahn and H. Strassmann, "Concerning the Existence of Alkaline Earth Metals Resulting from Neutron Irradiation of Uranium," *Die Naturwissenschaften,* vol. 27, pp. 11-15, 1939.

[8] L. Meitner and O. R. Frisch, "Disintegration of Uranium by Neutrons: a New Type of Nuclear Reaction," *Nature,* vol. 143, pp. 239-240, 1939.

[9] N. Bohr and J. Wheeler, "The Mechanism of Nuclear Fission," *Physical Review,* vol. 56, pp. 426 - 450, 1939.

[10] G. N. Flerov and K. A. Perzhak, "Spontaneous Fission of Uranium," *Physical Review,* vol. 58, p. 89, 1940.

[11] T. Michael , "Spontaneous Fission," in *The Discovery of Isotopes. A Complete Compilation*, M. Thoennessen, Ed., Switzerland, Springer, 2016, pp. 245-250.

[12] A. C. Wahl, "Nuclear-charge distribution and delayed-neutron yields for thermal-neutron-induced fission of ^{235}U, ^{233}U and ^{239}Pu and for spontaneous fission of ^{252}Cf," *Atomic Data and Nuclear Data Tables,* vol. 39, no. 1, pp. 1-156, 1988.

[13] L. L. Green and D. L. Livesey, *Nature,* vol. 195, p. 332, 1947.

[14] T. San-Tsiang, H. Zah-Wei, R. Chastel and L. Vigneron, "On the New Fission Processes of Uranium Nuclei," *Physical Reviews,* vol. 71, p. 382, 1947.

[15] F. Gonnenwein , M. Wostheinrich, M. Hesse, H. Faust, H. Fioni and S. Oberstedt, "Seminar on Fission," Belgium, 2000.

[16] E. Piasecki, M. Dakowski, T. Krogulski, J. Tys and J. Chwaszczewska, "Evidence of the Polar Emission of Alpha particles in the Thermal Neutron Fission of ^{235}U," *Physics Letters B,* vol. 33B, no. 8, pp. 568-570, 1970.

[17] E. Piasecki and J. Blocki, "Polar Emission: Tripartition or Evaporation?," *Nuclear Physics ,* vol. A208, pp. 387-408, 1973.

[18] E. Piasescki, M. Sowinski, A. Nowicki and A. Kordyasz, "Multiparameter studies of Polar Emission in ^{235}U fission," *Nuclear Physics,* vol. A255, pp. 387-404, 1975.

[19] L. Nowicki, J. Piasecki, J. Sobolewski, A. Kordyasz , M. Kisielinski, W. Czarnacki, H. Karwowski and P. Koczon, "Investigation of Polar Emission in ^{252}Cf and ^{235}U+n_{th} fission," *Nuclear Physics,* vol. A375, pp. 127-216, 1982.

[20] Y. Ronen, "The relation between ternary fission and cluster decay," *Annals of Nuclear Energy,* vol. 29, no. 8, pp. 1013-1018, 2002.

[21] V. D. Malaza, "Multi-detector Registration System for the Study of Multi-body Decay of Heavy Body Nuclei.," Master's thesis, Stellenbosch University, Stellenbosch, 2012.

[22] W. J. Swiatecki, "Theoretical and Experimental Aspects of Controlled Nuclear Fusion," in *Second UN International Confference on the Peaceful Uses of Atomic Energy*, Geneva, 1958.

[23] V. M. Strutinsky, N. Y. Lyashchenko, N. A. Popov and I. V. Kurchatov, "Symmetric shapes of equilibrium for a liquid drop model," *Nuclear Physics,* vol. 46, pp. 639 - 659, 1963.

[24] H. Diehl and W. Greiner, "Ternary Fission in the Liquid Drop Model," *Physics Letters,* vol. 45 B, pp. 35-37, 1973.

[25] H. Diehl and W. Greiner, "Theory of Ternary Fission in the Liquid Drop Model," *Nuclear Physics A,* vol. 229, pp. 29-46, 1974.

[26] Y. V. Pyatkov, V. G. Tishchenko, V. V. Pashkevich, V. A. Maslov, D. V. Kamanin, I. V. Kljuev and W. H. Trzaska, "Manifestation of fine structures in the fission fragment mass-energy distribution of the ^{233}U(n_{th},f) reaction," *Nuclear Instruments and Methods in Physics Research A,* vol. 488, pp. 381-399, 2002.

[27] D. V. Kamanin and Y. V. Pyatkov, "Clusterization in ternary fission," in *Clusters in Nuclei Volume 3*, B. Christian, Ed., Springer, 2014, pp. 2-69.

[28] K. R. Vijayaraghavan, W. von Oertzen and M. Balasubramaniam, "Kinetic energies of cluster fragments in ternary fission of ^{252}Cf," *European Physics Journal A,* vol. 48, p. 27, 2012.

[29] Y. V. Pyatkov, V. V. Pashkevich, Y. V. Penionzhkevich, V. Tishchenko and C. M. Herbach, "Collinear Tripartition of ^{248}Cm and ^{252}Cf nuclei as a probe of clustering," in *International Conference of Nuclear Physics "Nuclear Shells – 50 Years"*, Dubna, 2000.

[30] Y. V. Pyatkov, D. V. Kamanin, E. Sokol, A. A. Alexandrov, I. A. Alexandrova, S. V. Khlebnikov, S. V. Motrofanov, Y. E. Penionchkevich, Y. V. Ryabov, V. G. Tishchenko and S. R. Yamaletdinov, "Search for Collinear Tripartition of the ^{252}Cf nucleus at the modified-FOBOS Spectrometer," *World Scientific,* pp. 181 - 185, 2002.

[31] H. G. Ortlepp, W. Wagner, C. M. Herbach, A. A. Aleksandrov, I. A. Aleksandrova, M. Andrassy, A. Budzanowski, B. Czech, M. Danziger, L. Dietterle, V. N. Doronin, S. Dshemuchadse, A. S. Fomichev, W. D. Fromm, M. Gebhardt, P. Gippner, K. Heidel, S. Heinitz, H. Homeyer, S. A. Ivanovsky, D. V. Kamanin, I. V. Kolesov, A. Matthies, D. May, S. I. Merzlyakov, W. von Oertzen, Y. T. Oganessian, G. Pausch, Y. E. Penionzhkevich, Y. V. Pyatkov, S. V. Radnev, G. Renz, L. A. Rubinskaya, I. D. Sandrev, K. D. Schilling, W. Seidel, D. I. Shishikin, A. P. Sirotin, H. Sodan, O. V. Strekalovsky, V. G. Tishchenko, V. V. Trofimov, I. P. Tsurin, C. Umlauf, D. V. Vakatov, V. M. Vasko, V. A. Vitenko, E. Will, M. Wilpert, R. Yanez, V. E. Zhuchko, P. Ziem and L. Zrodlowski, "The

4pi-fragment spectrometer FOBOS," *Nuclear Instruments and Methods in Physics Research A,* vol. 403, pp. 65-97, 1997.

[32] Y. V. Pyatkov, D. V. Kamanin, W. von Oertzen, A. A. Alexandrov, I. A. Alexandrova, O. V. Falomkina, N. A. Kondratjev, Y. N. Kopatch, E. A. Kuznetsova, Y. E. Lavrova, A. N. Tyukavkin, W. Trzaska and V. E. Zhuchko, "Collinear cluster tri-partition of ^{252}Cf (sf) and in the ^{235}U(n_{th}, f) reaction," *European Physics Journal,* vol. 45, pp. 29-37, 2010.

[33] M. A. Mariscotti, "A method for automatic identification of peaks in the presence of background and its application to spectrum analysis," *Nuclear Instruments and Methods,* vol. 50, pp. 309-320, 1967.

[34] B. D. Wilkins, E. P. Steinberg and R. R. Chasman, "Scission-point model of nuclear fission based on deformed-shell effects," *Physical Review C,* vol. 14, no. 5, p. 1832, 1976.

[35] D. Rochman, I. Tsekhanovich, F. Gonnenwein, V. Sokolov, F. Storrer, G. Simpson and O. Serot, "Super-asymmetric fission in the ^{245}Cm(n_{th}, f) reaction at the Lohengrin fission-fragment mass separator," *Nuclear Physics A,* vol. 735, pp. 3 - 20, 2004.

[36] A. A. Alexandrov, I. A. Alexandrova, S. B. Borzakov, Y. N. Voronov, S. V. Denisov, G. L. Efimov, D. V. Kamanin, Y. N. Kopatch, E. A. Kuznetsova, Y. E. Lavrova, S. V. Mitrofanov, T. Panteleev, Y. V. Pyatkov, V. S. Salamantin, I. P. Tsurin, A. N. Tyukavkin and V. E. Zhuchko, "Experimental setup and Data Processing in Studying of the reaction ^{235}U(n_{th},f) at the IBR-2 beam," Dubna, 2007.

[37] Y. V. Pyatkov, D. V. Kamanin, Y. N. Kopach, A. A. Alexandrov, I. A. lexandrova, S. B. Borzakov, Y. N. Voronov, V. E. Zhuchko, E. A. Kuznetsova, T. Panteleev and A. N. Tyukavkin, "Collinear Cluster

Tripartition Channel in the Reaction $^{235}U(n_{th}, f)$," *Physics of Atomic Nuclei,* vol. 73, no. 8, pp. 1309-1316, 2010.

[38] C. Budtz-Jorgensen and H. H. Knitter, "Simultaneous investigation of fission fragments and neutrons in $^{252}Cf(sf)$," *Nuclear Physics A,* vol. 490, pp. 307-328, 1988.

[39] D. V. Kamanin, Y. V. Pyatkov, E. A. Sokol, S. V. Mitrofanov, S. R. Yamaletdinov, V. G. Tishchenko, A. N. Tyukavkin, B. V. Florko, E. A. Kuznetsova and O. Y. Gapienko, "Neutron Channel of the FOBOS Spectrometer for the Study of Spontaneous Fission," *Physics of Atomic Nuclei,* vol. 66, no. 9, pp. 1655-1658, 2003.

[40] Y. V. Pyatkov, D. V. Kamanain, W. von Oertzen, A. A. Alexandrov, I. A. Alexandrova, O. V. Folomkina, N. Jacobs, N. A. Kondratjev, E. A. Kuznetsova, Y. E. Lavrova, V. Malaza, Y. V. Ryabov, O. V. Strekalovsky, A. N. Tyukavkin and V. E. Zhuzhko, "The collinear cluster tri-partition (CCT) of $^{252}Cf(sf)$: New aspects from neutron gated data," *European Physics Journal A,* vol. 48, p. 94, 2012.

[41] D. P. Pelowitz and B. Denise, MCNPX User's Manual, version 2.6.0, United States of America: Los Alamos National Laboratory, 2008.

[42] D. V. Kamanin, Y. V. Pyatkov, A. A. Alexandrov, I. A. Alexandrova, S. B. Borzakov, M. L. Chelnokov, D. Fam Min, N. A. Kondratyev, Y. N. Kopach, E. A. Kuznetsova, T. Panteleev, Y. E. Penionzhkevich, A. I. Svirikhin, E. A. Sokol and D. Testov, ""Neutron Belt" for the COMETA," in *18th International Seminar on Interaction of Neutrons with Nuclei*, Dubna, 2010.

[43] E. A. Sokol, V. I. Smirnov, S. M. Lukyanov and Y. E. Penionzhkevich, "A detector for measuring the multiplicities and the angular correlations of neutrons," *Nuclear Instruments and Methods A,* vol. 400, no. 1, pp. 96-100, 1997.

[44] Y. V. Pyatkov, "Island of the high yields of ^{252}Cf(sf) collinear tripartition in the fragment mass space," *Romanian Reports in Physics,* vol. 59, no. 2, p. 12, 2007.

[45] D. V. Kamanin, "Experimental Evidences Of Clustering In Low Excited Heavy Nuclear Systems," *International Journal of Modern Physics E,* vol. 17, no. 10, pp. 2250-2254, 2008.

[46] W. D. Schmidt-Ott, U. Bosch and T. Mohlenkamp, "Pin-Diodes For Electron Detection," *Nuclear Instruments and Methods,* vol. 285, no. A, pp. 459-463, 1989.

[47] W. Starzecki, A. M. Stefanini, S. Lunardi and C. Signorini, "A Compact Time-Zero Detector for Mass Identification of Heavy Ions," *Nuclear Instruments and Methods,* vol. 193, pp. 499-505, 1982.

[48] J. L. Wiza, "Microchannel Plate Detectors," *Nuclear Instruments and Methods,* vol. 162, pp. 587-601, 1979.

[49] F. Busch, W. Pfeffer and B. Kohlmeyer, "A position - sensitive transmission time detector," *Neclear Instruments and Methods,* vol. 171, pp. 71-74, 1980.

[50] S. I. Mulgin, V. N. Okolovich and S. V. Zhdanov, "Two-parametric method for silicon detector calibration in heavy ion and fission fragment spectrometry," *Nuclear Instruments and Methods,* vol. A, pp. 254 - 259, 1997.

[51] H. O. Neidel, "Plasma Delay of ^{238}U ions in Surface Barrier Detectors," *Nuclear Instruments and Methods,* vol. 212, pp. 299-300, 1983.

[52] R. Schmidt and H. Henkel , "Comparison of Spontaneous Fission of ^{244}Cm and ^{252}Cf fragments masses and kinetic energies," *Nuclear Physics,* vol. A, pp. 15-28, 1983.

[53] L. Hannappel, H. Henschel and R. Schmidt, "A Direct Measurement of Plasma Delays in Surface Barrier Detectors," *Nuclear Instruments And Methods,* vol. 151, pp. 529-236, 1978.

[54] H. O. Neidel and H. Henschel, "Improved Determination of Plasma Delays of Fission Fragment and Alpha Particle Pulses in Surface Barrier Detectors," *Nuclear Instruments and Methods,* vol. 178, pp. 137-148, 1980.

[55] H. W. Schmitt, W. E. Kiker and C. W. Williams, "Precision Measurements of Correlated Energies and Velocities of ^{252}Cf Fission Fragments," *Physical Reviews ,* vol. B, no. 837, p. 137, 1965.

[56] S. B. Kaufman, E. P. Steinberg, B. D. Wilkins, J. Unik, A. J. Gorsky and M. J. Fluss, "A calibration procedure for the response of silicon surface-barrier detectors to heavy ions," *Nuclear Instruments and Methods,* vol. 115, p. 47, 1974.

[57] M. Ogihara, Y. Nagashima, W. Galster and T. Mikumo, "Systematic Measurements of Pulse-Height Defects for Heavy Ions in Surface-Barrier Detectors," *Nuclear Instruments and Methods,* vol. A, no. 251, pp. 313-320, 1986.

[58] F. James, "Minuit Function Minimization and Error Analysis, Reference Manual," CERN, Geneva, Switzerland, 1994.

[59] Y. V. Pyatkov, D. V. Kamanin, N. A. Kondratyev, A. O. Strekalovsky, S. Ilic, A. A. Alexandrov, I. A. Alexandrova, N. Mkaza, E. A. Kuznetsova, V. Malaza, O. V. Strekalovsky and V. E. Zhuchko, "Experimental testing of heavy ions mass search procedure in the measurements with PIN diodes," in *International Conference on Particle Physics and Astrophysics*, Moscow, 2016.

[60] Y. V. Pyatkov, W. Trzaska, M. Mutterer, S. Yamaletdinov, A. Tjukavkin, D. Bolgov, D. V. Kamanin, S. Khlebnikov, Y. Kopach, E. Kuznetsova, J. Lavrova, V. Lyapin, M. Sillanpaa, V. Tishchenko

and G. Tyurin, “Searching for Rare Decay Modes in the Reaction ^{238}U+^{4}He (40 MeV),” in *International Symposium on Exotic Nuclei*, Khanty-Mansiysk, 2007.

[61] D. V. Kamanin, “Preliminary Results on Collinear Cluster Tripartition in ^{232}Th + d (10 MeV) Reaction,” *Physics of Particles and Nuclei Letters,* vol. 7, no. 2, pp. 122-126, 2010.

[62] M. L. Muga, C. R. Rice and W. A. Sedlacek, “Ternary fission of heavy nuclei,” *Physical Review Letters,* vol. 18, no. 11, p. 404, 13 03 1967.

[63] S. C. Wu, R. Donangelo, J. O. Rasmussen, A. V. Daniel, J. K. Hwang, A. V. Ramayya and J. H. Hamilton, "New determination of the Ba-Mo yield matrix for Cf-252", vol. 62, Physical Review C, 2000, p. art no: 041601.

[64] T. M. Shneidman, G. G. Adamian, N. V. Antonenko, S. P. Ivanova, R. V. Jolos and W. Scheid, "Role of bending mode in generation of angular momentum of fission fragments", vol. 65, Physical Reviews C, 2002, p. art no: 064302.

[65] A. V. Karpov, "Ternary fission of a heavy nuclear system within a three-center shell model", vol. 94, Physical Review C, 2016, p. art no: 064615.

[66] Y. V. Pyatkov, V. V. Pashkevich, Y. E. Penionzhkevich, V. G. Tishchenko, A. V. Unzhakova, H. G. Ortlepp, P. Gippner, C. M. Herbach and W. Wagner, "Manifestation of clustering in the ^{252}Cf(sf) and ^{249}Cf(n_{th},f) reactions", vol. 624, Nuclear Physics A, 1997, pp. 140-156.

[67] P. Holmvall, U. Koster, A. Heinz and T. Nilsson, “Collinear Cluster Tri-partition: Kinematics constraints and stability of collinearity,” *Physical Review C,* vol. 95, p. art no: 014602, 2017.

[68] Y. V. Pyatkov, D. V. Kamanin, W. v. Oertzen, A. A. Alexandrov, I. A. Alexandrova, N. A. Kondtayev, E. A. Kuznetsova, O. V. Strekalovsky and V. E. Zhuchko, "First steps in physical treatment of the collinear cluster tri-partition mechanism," in *International Seminar on Interaction of Neutrons with Nuclei*, Ukraine, 2013.

[69] A. K. Nasirov, R. B. Tashkhodjaev and W. v. Oertzen, "Pre-scission configuration of the tri-nuclear system at spontaneous ternary fission of ^{252}Cf," *European Physics Journal,* vol. 52, p. 135, 2016.

[70] P. Schall, P. Heeg, M. Mutterer and J. P. Theobald, "On symmetric tripartition in the spontaneous fission of ^{252}Cf," *Physics Letters B,* vol. 191, no. 4, 18 06 1987.

[71] D. Rochman, I. Tsekhanovich, F. Gonnenwein, V. Sokolov, F. Storrer, G. Simpson and O. Serot, "Super-asymmetric fission in the ^{245}Cm(n_{th},f) reaction at the Lohengrin fission fragment mass separator," *Nuclear Physics,* vol. A, no. 735, pp. 3-20, 2004.

[72] K. Manimaran and M. Balasubramaniam, "Ternary fission fragmentation of ^{252}Cf for all possible third fragments," *European Physics Journal A,* vol. 45, pp. 293 - 300, 2010.

[73] R. B. Tashkhodjaev, A. K. Nasirov and W. Scheid, "Collinear cluster tripartition as sequential binary fission in the ^{235}U(n_{th},f) reaction," *European Physics Journal A,* vol. 47, p. 136, 2011.

[74] K. Manimaran and M. Balasubramaniam, "All possible ternary fragmentations of ^{252}Cf in collinear configuration," *Physical Review C,* vol. 83, p. art no: 034609, 2011.

[75] A. V. Kravtsov and G. E. Solyakin, "Search for spontaneous collinear tripartition of ^{252}Cf nuclei," *Physical Review C,* vol. 60, p. art no: 017601, 1999.

[76] V. I. Zagrebaev, V. Karpov and W. Greiner, "True ternary fission of superheavy nuclei," *Physical Review C,* vol. 81, p. art no: 044608, 2010.